Climate Change Impact and Water Resources Management of Blue Nile River Basin, Africa

by

Tebikachew Betru Tariku

A thesis submitted in partial fulfillment of the requirements for the degree of

Doctor of Philosophy

in

Water Resources Engineering

Department of Civil and Environmental Engineering

University of Alberta

Abstract

Climate change is likely one of the key challenges of the 21st Century for it could impact the livelihood, water and food security, economic growth and social well beings of countries worldwide. In recent decades the water resource of the Nile River Basin (NRB) has suffered from increasing demands from competing users, and more frequent and severe hydrologic extremes. This research addresses the climate change impact on the climate and water resources of the NRB, and to management of its water resources to mitigate such impacts.

First, the sensitivity of the Regional climate model, Weather Research and Forecasting (WRF), in regional climate modeling of NRB was investigated using 31 combinations of physical parameterization schemes of WRF. Using the ERA-Interim reanalysis data as initial and lateral boundary conditions, WRF was configured to model the climate of NRB at 36 km resolution and 30 vertical levels for 1999-2001. WRF simulated more accurate surface air temperature (T2) and downward longwave radiation than shortwave radiation and rainfall for the NRB. The simulation of rainfall is more sensitive to planetary boundary layer (PBL), cumulus and microphysics schemes, while the simulation of T2 is more sensitive to land-surface model (LSM) and radiation, than other schemes of WRF. In summary, the following schemes simulated the most representative regional climate of NRB: WSM3 microphysics, KF cumulus, MYJ PBL, RRTM longwave and Dudhia shortwave radiation schemes, and Noah LSM.

Next, WRF was used to dynamically downscale the future precipitation and temperature of NRB for the base period (1976-2005), RCP4.5 and RCP8.5 climate scenarios of four GCMs

over NRB for 2050s (2041-2070) and 2080s (2071-2100). Under these downscaled climate scenarios, the annual precipitation of Blue Nile, Atbara, and Sobat river basin, Bahar El Ghazal and Lake Victoria regions are projected to change by about [-7, 14.2], [-19, 25.3], [-7, 39], [-5.9, 23], and [3.6, 27] % in the 2050s, and [-14, 25], [-22.5, 39], [-4.7, 60.4], [-11, 31], and [11.8, 41] % in the 2080s, respectively. The mean annual air temperature for sub-basins of NRB is projected to increase by 1.67–2$^{\mathrm{o}}$C in the 2050s, 2–2.5$^{\mathrm{o}}$C in the 2080s under RCP4.5, and by 2.5–3$^{\mathrm{o}}$C in the 2050s and 3.9–4.6$^{\mathrm{o}}$C in the 2080s under RCP8.5, respectively. Since most precipitation extreme indices are projected to increase, NRB could experience more severe and frequent extreme precipitation in future. Furthermore, extreme temperature indices of NRB are projected to increase (decrease) in warm (cold) night/days.

Next, climate change impact on the mean and extreme streamflow of the Upper Blue Nile river basin (UBN) in 2050s and 2080s was projected by three hydrological models (NAM, VIC and Watflood models) driven with RCP4.5 and RCP8.5 climate scenarios of four GCMs downscaled by WRF. All hydrological models were able to accurately capture the flow dynamics in both calibration and validation periods. Mainly due to a projected increase in evapotranspiration, the median of mean annual streamflow of UBN is projected to decrease to by 7.6% with a range of -19.7 to 17.7% in the 2050s, and by 12.7% with a range of -26.8 to 31.6% in the 2080s. The ensemble mean of annual maxima (minima) of high return periods are projected to increase (decrease) in 2050s and 2080s by all hydrologic models, respectively.

To assess climate change impact on the water resource of Blue Nile River basin (BNRB), from changes in the streamflow of BNRB simulated by VIC driven by RCP4.5 and RCP8.5

climate change scenarios of four GCMs downscaled by WRF for 2050s and 2080s, the maximum, median and minimum projected changes in streamflow for BNRB were estimated. These projected changes in streamflow for BNRB were used to assess climate change impact to its future water allocations using a stochastic dual dynamic model. The results show that the outflow from the GERD reservoir, or the annual flow of BNR at Khartoum is projected to increase under maximum, but will decrease under median and minimum projected changes in streamflow for 2050s and 2080s. Since the annual net benefit is projected to increase (decrease) under the maximum (median and minimum) projected change in streamflow, the potential impact of climate change should be incorporated in the future design and development of the water resources of BNRB.

Preface

This thesis shows the possible impact of climate change on the climate and hydrologic extremes of the Nile river basin and future water allocation under future water resource development of the Blue Nile River Basin. The thesis is based on four major chapters; Chapters 2 and 3 of this thesis has published on internationally peer-reviewed scientific journals. Chapter 2 of this thesis has been published as Tariku, T. B., and Gan, T. Y., 2017, "Sensitivity of the Weather Research and Forecasting model to Parameterization Schemes for Regional Climate of Nile River Basin", Climate Dynamics, pp.1-17, doi: 10.1007/s00382-017-3870-z. Chapter 3 has been published as Tariku, T. B., and Gan, T. Y., 2018, "Regional Climate Change Impact on Extreme Precipitation and Temperature of the Nile River Basin", Climate Dynamics, pp. 1-20, doi: 10.1007/s00382-018-4092-8. For the work done in these Chapters, I was responsible for design of the research program, data collection and analysis as well as the manuscript composition. The work on Chapter 4 has been also submitted to journal of Climatic Change and is currently under review. Dr. Lie, J. and Dr. Qin, X., contributed to manuscript edits. I am also planning to submit the work done of Chapter 5 to scientific journal. Dr. Tilmant, A., assisted with data collection, developed Matlab code for stochastic dynamic programing and contributed to manuscript edits. Dr. Gan, T. Y., was the supervisory author and was involved with concept formation and manuscript composition and edits. To date my PhD study will lead to the publication of four papers on peer-reviewed scientific journals.

Tebikachew Betru Tariku
Edmonton, AB, August, 2018

Acknowledgements

Table of Contents

List of Tables

List of Figures

List of Abbreviations

BNRB	Blue Nile River Basin
CMIP5	Coupled Model Intercomparison Project phase 5
CORDEX	Coordinated Regional Climate Downscaling Experiment
CRU	Climate Research Unit
Cu	Cumulus Scheme
ENTRO	Eastern Nile Technical Regional Office
GCM	Global Climate Model
GPCC	Global Precipitation Climatology Centre
IPCC	Intergovernmental Panel on Climate Change
ITCZ	Inter Tropical Convergence Zone
LSM	Land Surface Model
LWRAD	Downward Surface Longwave Radiation
MP	Microphysics
NBI	Nile Basin Initiative
NCEP	National Centers for Environmental Prediction
NRB	Nile River basin
PBL	Planetary Boundary Layer
Ra	Radiation scheme
RCM	Reginal Climate Model
RCP	Representative Concentration Pathways
SWRAD	Downward Surface shortwave Radiation
TRMM	Tropical Rainfall Measuring Mission
WRF	Weather and Research Forecasting

Chapter 1

1.1. Introduction

Water is essential for the existence and development of a society. Typical major water users are agriculture, municipalities, and industries for economic and social developments. Water is also essential to sustain ecosystems and to maintain the biodiversity of our environment. To ensure the availability of reliable water resource for secure utilization, it will be prudent to implement an effective assessment and management of the water resources of major river basins, both the quantity and quality of water, spatially and temporarily. Water crises caused by droughts and water pollution have occurred in many regions across the world, especially in developing countries. The lack of good management and knowledge about the potential impact of climate change to the existing water resources could lead to unforeseen water crises in future. Since 1970s, observations show that hydrologic extremes (droughts and floods) have been occurring more frequently and in greater severity worldwide (Lemke et al., 2007). In the last decade, 90% of natural hazards have been related to water and they could get worse in future, such as tsunamis, floods, droughts, and storm surges that could inflict costly damages to societies, such as the 2010 flood of Pakistan and the 2012 drought of USA, which had been the worst in more than half a century, and which may be just a foretaste of more climatic extremes under a hotter and drier future in many places of the world. Many scientists and climatologists attribute the increase in occurrences of recent hydrologic extremes to the impact of climate change (e.g., Lemke et al., 2007; IPCC, 2013). According to the Clausius–Clapeyron relationship, the saturation vapor pressure increases by about 7% for every 1°K

rise in temperature. Therefore as climate warms, a warmer atmosphere has a larger capacity to hold more water vapour, which fuel more evaporation, and generate more precipitation. As a result, hydrologic cycle will accelerate which can increase the occurrences of severe climate, potentially leading to more extreme floods and droughts, which can reduce the reliability of water resources in many regions worldwide.

Africa is a relatively dry and water scare continent, with more than half Africans living in extreme poverty. In the past centuries, large-scale, severe droughts had occurred many times over Africa (Shanahan et al., 2009; Touchan et al., 2008). The droughts of Somalia in 2011, Ethiopia/Sudan in 1980s and in Sahel in 1974 had each killed and displaced several hundred thousand people. In the 5th Coupled Model Intercomparison Project (CMIP5), Sahel, West Africa, and Southern Africa are identified as climate change hotspots (Diffenbaugh & Giorgi, 2012). In the 1960s, Africa was a food exporter, but in recent years, partly because of recurrent droughts, Africa has to import about 1/3 of its grain supply. Climate change and climate variability are likely to severely compromise future agricultural production and food security in many African countries (Boko et al., 2007). Water shortages advance poverty, and in sub-Saharan Africa about 300 million people suffer from water shortages (WWAP, 2012) and water stress has been a major societal challenge, e.g., over 75% of Africans live in regions with arid and semi-arid climate, 2/3 of its population rely on limited and highly variable water resources, a significant fraction of its cropland resides in its driest regions with 40% of the irrigation non-sustainable (Vörösmarty et al., 2005). Many African countries lack the human, economic and institutional capacities to effectively develop and manage their

water resources sustainably. Prolonged over-exploitation of resources leads to land degradation, loss of biodiversity, and resource scarcity in Africa where the population had also increased several folds in the last 50 years. Therefore, threats to food security, conflicts from competing users for dwindling water supply between African nations result in growing political tension and instability in this continent.

Nile River is the longest river in the world; its water is shared by eleven countries and covers a 10% of Africa area. Countries located in the Nile River Basin (NRB) have the fastest growing population, with 54% of their total population living within the NRB. The upstream countries depend on rainfed agriculture, which is facing more and more serious water crisis. These regions also suffered from repeated droughts partly attributed to the effect of the El Niño Southern Oscillation (ENSO), which has become more severe in recent years due to the impact of climate change. Climate change and climate variability will affect the food, water and energy security of African countries. However, what are the challenges to determine the onset, extent, impact of climate change in the NRB? Because climate is a multifractal process, and hydrologic extremes are more than climate-driven, their patterns are difficult to pin down.

The Sub-Saharan Africa is the world's largest consumer of biomass energy because only one person in four in Africa has electricity (WWAP, 2012). This large consumption of biomass energy has contributed to deforestation and land degradation which further "aggravates" the hydrologic impact of climate change. The NRB has enough hydropower potential to meet the entire basin's electricity needs but such a potential has not been developed because of economic and political reasons. The water withdrawal of the river is unevenly distributed

among riparian countries. Egypt and Sudan are the largest consumers, which according to their agreement in 1959, get 55.5 billion m^3 and 18.5 billion m^3 of water per year, respectively. However, this agreement neglects upstream countries such as Ethiopia even though 85% of the Nile water comes from Ethiopian highlands. The Nile Basin Initiative launched in February 1999 by the Council of Ministers of Water Affairs of Nile Basin States, which helps to develop the river in a cooperative manner, share substantial socio-economic benefits, and promotes regional peace and security (NBI, 2015). Currently the Nile riparian countries are developing their water resources to fulfill food and energy demand due to population growth. Ethiopia has proposed four large reservoirs, hydropower stations and irrigation areas in the Blue Nile River Basin (BNRB), studied by the United States Bureau of Reclamation (USBR) in 1964 for boosting the production of hydropower and food security (Goor et.al, 2010; Block, 2007; Block and Strzepek, 2010). Given upstream developments will have both positive and negative impact on the downstream users, a proper overall planning and management of the whole NRB is recommended.

To study the regional impact of climate change to the NRB, this study will use a regional climate model, Weather Research and Forecasting (WRF) to simulate future precipitation and other climate variables. Climate data dynamically downscaled by WRF will be used to drive a physically-based (or conceptual) hydrologic model, in conjunction with a Stochastic dynamic programing model to investigate the potential impact of climate change on the hydrology, water resources management and reservoir operations of the BNRB, with the objective of optimizing water utilization across the BNRB under current and future development. This

will be useful to policy makers to execute informed prudent decisions on the planning, design and management of water resources of the BNRB.

1.2. Problem of statement

Under impending decline in water resources, increasing demand from growing population, widespread pollution, and more frequent occurrences of hydrologic extremes, upstream users of the NRB that rely on rain fed agriculture is facing worsening water crisis which will affect its food security, human health and ecosystems. There is an urgent need to better understand ongoing changes to the climatic and hydrologic regimes of the Nile, to objectively assess its vulnerability and susceptibility to hydrologic extremes especially droughts to be better prepared for potential problems associated with such natural hazards. If member countries of the NRB can better understand their vulnerability to climate change, they will be better prepared to implement effective adaptation strategies to mitigate such impacts, and to establish effective warning systems that can issue reliable warnings in a timely order. Until now, from what we know, only limited numbers of studies based on dynamic downscaling techniques have been conducted to assess climate change impact on Africa (Mohammed et al. 2005; Soliman et al. 2009; and Alemseged and Tom 2015).

Beside the potential impact of climate change, there will be new reservoirs built in the upstream parts of the NRB which could lead to water supply problem at downstream countries. It will benefit users of NRB to optimally manage water resources of the NRB under potential climate change impact and future developments. Numerous management models have been developed to assess the hydropower and agricultural irrigation potential within

Ethiopia and the whole of the NRB (Guariso and Whittington 1987; Levy and Baecher 1999; Whittington et al. 2005). These models can provide insight to develop and manage viable hydropower and irrigation projects for NRB, with potentially significant hydrologic and economic implications for the entire river basin. Reservoir operation models could provide general operation strategies to help decision makers to optimally release water based on current reservoir levels on the basis of projected inflow and water demands for different seasons. If I am not mistaken, previous studies have not included detailed climate change impact in running their reservoir operation models.

1.3. Research Objectives

The main objective of this research is to explore the potential impact of climate change to the climate and water resources of the BNRB, and to optimize the management of water resources of BNRB subjected to the impact of climate change and future water system developments.

Specific objectives

- To fine-tune the configuration and parameterization schemes of regional climate model, WRF so that it can simulate reliable regional climate of NRB using the ERA-Interim reanalysis data at 36 km resolution.

- To assess the possible impact of climate change on the extreme precipitation, temperature of the NRB based on RCP4.5 and RCP8.5 climate scenarios of four GCMs dynamically downscaled by WRF for the 2041-2070 (2050s) and 2071-2100 (2080s) relative to the 1975-2005 base period.

- To investigate the potential impact of climate change on the hydrology and hydrologic extremes of the upper Blue Nile river basin in the 2050s and 2080s based on three hydrological models (NAM, VIC and Watflood models) driven with RCP4.5 and RCP8.5 climate scenarios of four GCMs dynamically downscaled by WRF.

- To analyze the future water resource development of BNRB based on stochastic dynamic programming for jointly maximizing hydropower production and optimal allocation of water for irrigation projects in the BNRB under its present and future climatic conditions.

1.4. Organization of Thesis

The Thesis is organized into six chapters. The introduction, problem statement and research objectives are presented in Chapter 1. Chapter 2 deals with sensitivity of the WRF model to parameterization schemes for regional climate of NRB. Chapter 3 focuses on the potential impact of climate change on extreme precipitation and temperature of the NRB, while Chapter 4 presents possible impact of climate change on the hydrology and hydrologic extremes of the upper Blue Nile River basin. Chapter 5 shows potential impact of climate change on the optimal operation of a multipurpose multireservoir system in the BNRB. Finally, overall research summary, conclusions and recommendations are given in Chapter 6.

Chapter 2 Sensitivity of the Weather Research and Forecasting model to Parameterization Schemes for Regional Climate of Nile River Basin

2.1. Introduction

Global climate models (GCMs) are numerical climate models designed to simulate physical processes in the atmosphere, ocean, cryosphere and land surface at a global scale (IPCC-TGICA, 2007). GCMs are the main tools for projecting future global climate in response to rising concentrations of greenhouse gases in the atmosphere. However, usually at a spatial grid resolution of 100-300 km, and daily temporal resolutions, the output of GCMs are generally too coarse for solving basin-scale, hydrologic and water resources management problems. As a result, climate data of GCMs needs to be downscaled to produce local or regional climate at resolutions useful for hydrologic applications. Coarse resolution climate data can be downscaled by statistical procedures or dynamically using RCM to data of higher resolutions. In theory, a RCM designed to capture climate processes at basin scale can provide high resolution, representative climate data of river basins. For river basins with diversified climate and complex topography, such as the NRB with elongated ridges and escarpments parallel to faults of the East African Rift system, and the presence of large lakes such as Lake Victoria and Lake Tana (Pohl et al., 2011), high resolution climate data downscaled by a RCM from GCMs will be useful for the future management of such river basins, e.g., Mohamed et al. (2005) applied the Regional Atmospheric Climate Model (RACMO) to simulate the regional climate of the NRB. The socioeconomic activities and well-being of people living in most countries of the Nile basin are dependent on the rainfall and streamflow

of the Nile River for water supply and for sustaining the agriculture via irrigation projects and/or rain-fed mechanism. However, climate change can potentially impact the rainfall variability and streamflow of NRB which could affect the reliability of NRB's water supply to its users. Therefore, high resolution climate data for NRB downscaled by a RCM from GCMs' climate projections will be useful to assess the potential impact of climate change to the future water resources of NRB.

Various RCMs have been developed to downscale coarse resolution climate data of GCMs or reanalysis data to fine resolution data for different river basins across the world. There have been regional climate modeling studies conducted for East Africa. For example, by fine tuning the cumulus convection schemes, radiative transfer formation, surface process, boundary layer physics, and lateral boundary conditions of the study domain using the Regional Climate model, version 2 (RegCM2), Sun et al. (1999a, 1999b) simulated representative regional climate, e.g., major circulation, precipitation, temperature and water vapor patterns, of East Africa for October-December, 1988. Other studies conducted over East Africa using version 3 of the Regional Climate model (RegCM3) are such as Anyah et al. (2006); Anyah and Semazzi (2006, 2007); Segele et al. (2009a); and Diro et al. (2012). Furthermore, the RCM called WRF which has a wide range of physical parameterizations, has been applied to some parts of Africa, or the entire Africa (e.g., Pohl et al., 2011; Giorgi et al. 2009; Jones et al. 2011; Endris et al., 2013; Mooney et al., 2013; Flaounas et al., 2011). Since its development in 2000, WRF has been a popular RCM to simulate regional climate of various study sites across the world.

Pohl et al. (2011) examined WRF's simulations of the atmospheric water cycle of Equatorial East Africa using 58 combinations of physical parameterization, land-use categories, lateral forcing and the domain geometry. From the results, they found that the shortwave radiation scheme, the land surface model (LSM), the domain size, convective schemes and land-use categories play a more significant role than cloud microphysics, lateral forcing reanalysis, the number of vertical levels and planetary boundary layer (PBL) schemes in simulating reliable seasonal climate of Equatorial East Africa. The coordinated regional climate Downscaling Experiment (CORDEX) (Giorgi et al. 2009; Jones et al. 2011), initiated by the World Climate Research Program, used WRF and other RCMs to simulate high-resolution (50km) regional climate projections of different continents. Under CORDEX, Endris et al. (2013) evaluated the rainfall of East Africa simulated by 10 different RCMs (including WRF), each set up with one set of model configuration and parameterizations. They found that most of RCMs simulated a reasonable pattern of rainfall climatology over the three sub-regions but with significant biases. Mooney et al. (2013) found that WRF could simulate the 2-m surface temperature of 1990-95 over the European domain, CORDEX region-4, accurately. They found WRF to be most sensitive to LSMs, moderately sensitive to longwave radiation schemes, but not sensitive to microphysics and PBL schemes. In simulating precipitation, WRF is found to be more sensitive to LSMs in the summer than in the winter. However, precipitation simulated by WRF compared poorly with remotely sensed precipitation data.

Under CORDEX, Katragkou et al. (2015) evaluated the 1990-2008 regional climate simulated by WRF for the European domain using the ERA-Interim reanalysis data, in a multi-physics

ensemble framework with different configurations of microphysics, convection and radiation schemes. They found a systematic bias in temperature and precipitation simulated by WRF for summer and winter, an over (under) simulation of the total cloud cover (downward shortwave radiation) over northern Europe, and a strong positive bias in the downward shortwave radiation in summer over central and southern Europe. For simulating the 2006 summer West Africa monsoon, Flaounas et al. (2011) examined the sensitivity of WRF to convection and PBL schemes. They found that temperature, vertical distribution of humidity, and rainfall amount simulated by WRF is very sensitive to PBL schemes, while the dynamics and variability of precipitation simulated are sensitive to convective parameterization schemes.

WRF is computationally expensive and its optimal performance requires a tedious investigation over different combinations of parameterization schemes which vary from region to region. To the best of our knowledge, only a few RCM studies have been tested over the NRB, and as far as we know, only CORDEX has done a limited test on the performance of WRF over the whole Africa which was set up as a single domain at 50 km resolution. The objective of this study is to fine tune the configuration and parameterization schemes of WRF so that it can simulate reliable regional climate of NRB for 1999-2001 using the ERA-Interim reanalysis data at 36 km resolution.

The chapter is organized as follows: the brief description of regional climate model, configuration and study area are stated in section 2.2. In section 2.3, model verification methods for the simulated results are discussed. The results and discussions of different

evaluation are presented in section 2.4. Finally, in section 2.5, the conclusions of the study are presented.

2.2. Experimental setup

2.2.1. Model description and configuration

This study was conducted using the advanced Weather Research and Forecasting regional climate model, version WRF 3.6.1. WRF is a nonhydrostatic, primitive-equation, mesoscale meteorological model with advanced climate dynamics, physics and numerical schemes. Detailed descriptions of the WRF can be found in the model manual of Skamarock et al. (2008) and also on the WRF user Web site (http://www.mmm.ucar.edu/wrf/users). Like other RCMs, WRF tends to over or under-simulate the amount of rainfall, but it can capture essential features of storm events, such as the time of occurrence, evolution, duration and location of storms (Hong and Lee, 2009; Chen et al., 2010). Possible factors contributed to this common shortcoming of climate models are such as uncertainties of initial conditions, limited knowledge on the rainfall generation process, cloud microphysics, numerical round-off errors, etc. (Fowle and Roebber, 2003; Fritsch and Carbone, 2004). However, the selection of schemes and fine tuning of parameters for various modules of WRF, domain configurations and grid resolutions play a major role in the performance of WRF.

In the pre-processing stage of WRF, we evaluated two land use databases, sea surface temperature, setting of vertical layers and relaxation zones for lateral boundaries of the study domain. WRF was finally set up with 30 vertical pressure levels and the top level is at 50hPa. For the study period 1999-2001, the initial and lateral boundary conditions of WRF are based

on the most recent, ERA-Interim reanalysis data of the European centre for Medium Range Weather Forecasts (ECMWF) at 0.25^o x 0.25^o resolution and 6-hourly time steps. Compared with other reanalysis data, past studies show that the ERA-Interim data best represented certain aspects of the climate system, such as the air temperature (Mooney et al., 2011; Troy and wood, 2009; Screen and Simmonds, 2011).

The parameterization schemes in WRF are grouped into these modules: 1) Microphysics (MP), 2) Longwave radiation (LW), 3) Shortwave radiation (SW), 4) Land surface model, 5) Cumulus (Cu), and 6) Planetary boundary layer. Each of these modules has two or more parameterization schemes, with some schemes more applicable for climate modeling while others for weather forecasting, or both, thus making WRF a popular RCM. In fine tuning WRF, because of computational constraint, we could only test a limited combination of all available parameterization schemes, instead of testing all possible combinations. The performance of WRF for modeling the regional climate of NRB is assessed by its ability to reproduce the spatial and temporal patterns of the observed climate of NRB. 31 combinations of schemes selected to fine tune WRF over NRB are shown in Table 2.1. These schemes were selected either because they performed well in previous studies or they have not been tested before (Pohl et al., 2011; CORDEX Africa groups). Out of 31 experiments, 20 were conducted from combinations between 2 Cu, 2 PBL and 5 MP schemes, while 8 experiments were conducted from combining 2 Ra with 4 MP schemes; and 3 more experiments were conducted from combining 3 Ra schemes with 1 other LSM.

Table 2.1: The combination of Physical parameterization schemes for 31 WRF simulations

Experiment No.	Cu schemes	PBL	Microphysics	LW schemes	SW schemes	LSM
Test 1	KF	YSU	Lin	RRTM	Dudhia	NOAH
Test 2	BMJ	YSU	Lin			
Test 3	KF	MYJ	Lin			
Test 4	BMJ	MYJ	Lin			
Test 5	KF	YSU	WSM3			
Test 6	BMJ	YSU	WSM3			
Test 7	KF	MYJ	WSM3			
Test 8	BMJ	MYJ	WSM3			
Test 9	KF	YSU	WSM5			
Test 10	BMJ	YSU	WSM5			
Test 11	KF	MYJ	WSM5			
Test 12	BMJ	MYJ	WSM5			
Test 13	KF	YSU	Morrison			
Test 14	BMJ	YSU	Morrison			
Test 15	KF	MYJ	Morrison			
Test 16	BMJ	MYJ	Morrison			
Test 17	KF	YSU	WDM5			
Test 18	BMJ	YSU	WDM5			
Test 19	KF	MYJ	WDM5			
Test 20	BMJ	MYJ	WDM5			
Test 21	KF	MYJ	WSM3 WSM5 Morrison WDM5	CAM	CAM	NOAH
Test 22						
Test 23						
Test 24						
Test 25			WSM3 WSM5 Morrison WDM5	RRTMG	RRTMG	
Test 26						
Test 27						
Test 28						
Test 29	KF	MYJ	WSM3	RRTM	Dudhia	RUC
Test 30				CAM	CAM	
Test 31				RRTMG	RRTMG	

Since the dynamics and variability of precipitation are sensitive to convection parameterization schemes, two cumulus parameterization schemes, the Kain-Fritsch (KF) (Kain, 2004) and Betts-Miller-Janjic (BMJ) (Janjic, 1994) schemes were tested in this study. Even though it tends to overestimate the precipitation, the KF is the widely used cumulus parameterization scheme. Furthermore, the vertical distribution of temperature, humidity, and rainfall amount can be significantly affected by the PBL schemes. In this study, the popular Yonsei University (YSU) scheme (Hong et al., 2006) and the Mellor-Yamada-Janjic scheme (MYJ) (Janjic, 1994) were tested.

For the microphysics, the WRF single moment three-class (WSM3) scheme (Hong et al., 2004), Lin et al. (1983) scheme, WRF Single-Moment 5-class scheme (WSM5) (Hong et al., 2004), Morrison double-moment scheme (Morrison et al., 2009) and WRF Double-Moment 5-class scheme (WDM6) (Lim and Hong, 2010) were tested. The WSM3 is a simple, efficient scheme that considers ice and snow processes at mesoscale grid sizes. On the other side, WSM5 is marginally more sophisticated that also considers mixed-phase processes and super-cooled water. The radiation schemes tested were the Rapid Radiative Transfer Model (RRTM) LW scheme (Mlawer et al., 1997), Dudhia (Dudhia, 1989) SW schemes, Community Atmosphere Model (CAM) (Collins et al., 2004) and a new version of RRTM (RRTMG) (Iacono et al., 2008) for both the LW and SW radiation schemes. Lastly, the two Land surface models tested were the Noah (Ek and Mahrt 1991) and the Rapid Update Cycle (RUC) (Smirnova et al. 1997, 2000). RUC is set up to simulate soil temperature and moisture for six

layers, snow and frozen soil physics for multiple layers while the Noah LSM simulates soil temperature and moisture for four layers.

2.2.2. Domain configuration for the Nile River Basin

The Nile River is the longest river in the world with a length of 6800 km. It covers an area of about 3,400,000 km^2 and it flows over eleven countries (Burundi, DR Congo, Egypt, Eritrea, Ethiopia, Kenya, Rwanda, Tanzania, South Sudan, Sudan and Uganda). This study will focus on the Blue Nile River Basin (BNRB), which is a sub-basin of the Nile river basin. The drainage area of the BNRB approximately covers an area of 210,000 km^2, but it contributes about 60% of the average annual flows of the Nile River. NRB has different rainy seasons with diverse climatic conditions ranging from arid, semi-arid to humid regions. From north to south, there are arid, tropical, and equatorial rainfall regimes. There is virtually no precipitation in the Sahara Desert of Sudan and Egypt, but precipitation increases southward to the Ethiopian highland and Equatorial Plateaus, with the June-September rainy season over Ethiopian plateau, and two rainy seasons over the Equatorial Lakes Plateau, October-December and March-May resulted from ITCZ moving southward and northward over the region, respectively. The southern part of the Nile basin has also one rainy season from October-December (Indeje et al., 2000; Nyakwada, 2009; Endris et al., 2013). Because of different rainy seasons over the NRB, WRF was set up to perform continuous simulation over each year of the study period. WRF was set up to simulate the climate of Nile over a two-domain's configuration with one-way nesting. Domain-1 (2°E to 57°E, 20°S to 37°N) was set up for the NRB and Domain-2 (29°E to 45°E, 5°N to 17.5^{o}N) was set up for the BNRB, as

shown in Figure 2.1. First, evaluation of different parameterization schemes was based on results obtained for Domain-1 (D1) only for 1999-2001. Then, WRF was run with Domian-2 (D2) nested within D1 after we have obtained better parameterization schemes for D1, to obtain results for both domains from 1980 to 2001. However, in this paper, only results obtained from testing D1 are presented. The ERA-Interim reanalysis data were used as the lateral boundary and initial conditions for D1 with a 36-km resolution. Then, the D1 output was used as lateral and initial conditions to run the inner domain D2 with a 12 km resolution. To account for sources of moisture coming from the Atlantic and the Indian oceans, and to serve as a "spatial" spin-up, D1 was set up to be much wider than the NRB.
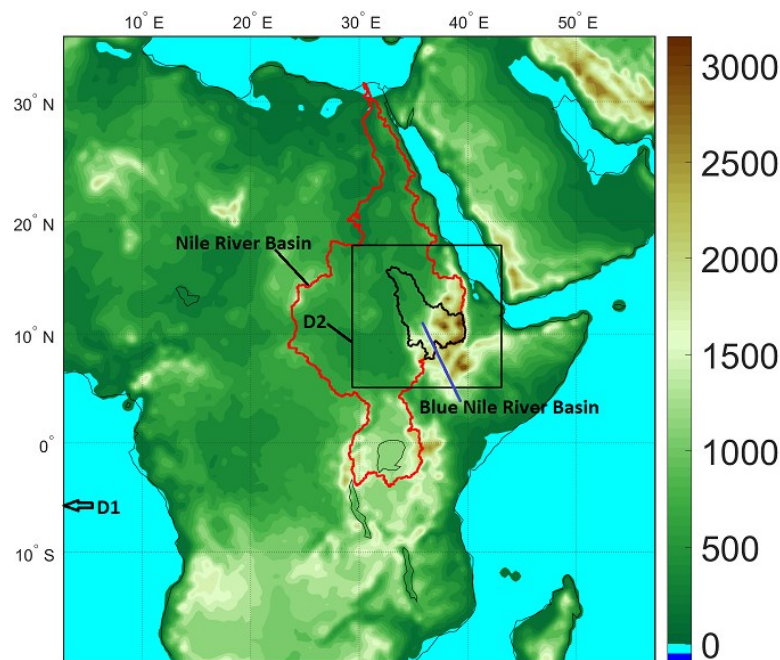
Figure 2.1: A map showing the Domain-1 and Domain-2 setup of WRF and the topography (m) of the Nile and the Blue Nile River Basin of Africa.

2.3. Model verification methods

The main problem in evaluating the performance of a RCM over Africa is a general lack of high-quality observation datasets of suitable temporal and spatial resolutions. The Tropical Rainfall Measuring Mission (TRMM 3B42 Version 6, 1998-2010) satellite based precipitation product with a 0.25^{o} spatial and daily temporal resolutions were used to assess gridded precipitation simulated by WRF. Precipitation products of TRMM have been evaluated against rain gauge data in Africa, e.g., Nicholson et al. (2003a, b); Romilly and Gebremichael (2011); Mashingia et al. (2014). Even though TRMM data agree well with gauge data for most major climatic zones of Africa in all seasons (e.g., Adeyewa and Nakamura, 2003), such satellite data have limitations, such as a lack of ability in capturing deep convective precipitation systems on daily timescales, particularly on the windward side of mountainous terrains (Dinku et al., 2008; Nair et al., 2009). In addition, two rain gauge-based datasets available at 0.5^{o} spatial and monthly temporal resolutions, the Global Precipitation Climatology Centre (GPCC version 6, 1901-2010; Schneider et.al, 2011) and the Climate Research Unit at the University of East Anglia (CRU version 3.22, 1901-2013; Harris et.al, 2014) were also used to validate the simulation of WRF. Africa has a sparse network of rain gauges, and precipitation data interpolated from a sparse network of rain gauges could lead to large errors and unrealistically smooth spatial gradients (Koutsouris et al., 2016). Therefore, we should be cautious using these widely used, gauge-based datasets. Nicholson et al. (2003a, b) used a dense network of rain gauge dataset to validate both the GPCP and the GPCC datasets for 1988-94 and for 1998 over West Africa. They found that the mean precipitation

fields derived from the dense gauge network, the GPCC and the GPCP are remarkably similar. However, they found that both GPCP and GPCC datasets compare well with the rain gauge data at seasonal but not at monthly time scales. The air temperature at 2m (T2) simulated by WRF was evaluated against the CRU data; downward short- and Longwave radiation at the surface simulated by WRF was evaluated against the National Centers for Environmental Prediction (NCEP) Climate Forecast System Reanalysis (CFSR) data (Saha et al, 2010). The reanalyses data are climatological data generated from applying data assimilation schemes on available observed data into a climate model. Zhang et al. (2013) found that the latest reanalysis dataset called CFSR yields the best results in the precipitation mean and variability over South Africa when compared with the CRU data. In this study, the above observed and reanalysis data were re-gridded to the resolution of D1 to facilitate comparison with WRF's simulations. Some errors are expected in the re-gridding process, but the error introduced should not be significant, which will partly depend on the spatial variability of data and partly on the re-gridding algorithms used. The performance of WRF is assessed using statistics such as the root mean square error (RMSE), the mean error (ME) and the standard deviation (SD) calculated from all the simulations of WRF for each grid point of D1 over the study period; and the correlation coefficients between simulated and observed monthly climate variables. The spatial plots are used to evaluate the ability of WRF to capture the spatial distribution and the bias of WRF's simulations over the basins. These plots show different bias of WRF in different areas, but it is difficult to conclude if the overall bias for the entire basin is positive or negative. The time series of WRF's grid-based simulations for the BNR are spatially

averaged and analysed to assess the ability of WRF to capture the rainfall seasonality of the BNR basin.

2.4. Results and discussions

2.4.1. Rainfall climatology

Figure 2.2 and Figure 2.3 show the mean annual rainfall bias in mm/day for all model configurations of WRF tested with respect to the TRMM datasets over the 1999-2001 period. We chose TRMM instead of GPCC data for comparison partly because TRMM datasets are of daily rainfall while GPCC are monthly rainfall data. Figure 2.2 presents the results using different combinations of WRF's parameterization schemes, which are cumulus parameterization (KF and BMJ), planetary boundary layer (YSU and MYJ) and microphysics (Lin, WSM3, WSM5, Morrison and WDM6); to determine which set of schemes can simulate the most representative rainfall of NRB, e.g., the depth and variability of rainfall. From these two figures, it seems that WRF simulated representative rainfall over the NRB in all parameterization schemes tested, but more schemes over-simulated while a few under-simulated the rainfall of Ethiopian highlands and the Congo basin, but most schemes under-simulated the rainfall over the Lake Victoria area. Other studies such as Endris et al., (2013) also encountered this over-simulation problem over the Congo basin and Ethiopian highlands. The parameterization schemes considered consists of two cumulus parameterizations which controls the dynamics and variability of rainfall regimes are shown in columns 1 and 2 under the YSU PBL scheme; and columns 3 and 4 under the MYJ PBL scheme. Overall, KF tends to over-simulate rainfall while the BMJ scheme tends to under-simulate. Our results are

consistent with that of Pohl et al. (2011), who also found KF to simulate a wetter climate than the BMJ scheme for East Africa. Figure 2.2 also shows that under KF combined with the YSU PBL scheme, WRF consistently over-simulated the rainfall of the Indian Ocean and the eastern Congo Basin. Further, under a given set of PBL and Cu, the double-moment MP scheme would lead to more simulated rainfall than the single-moment MP, especially if KF is the cumulus scheme selected. In contrast, under the BMJ cumulus scheme, the effect of changing MP on the amount of rainfall simulated tends to be negligible. On a whole, the Morrison double-moment scheme is associated with more simulated rainfall, which also agrees with results of Pohl et al. (2011). The BMJ scheme is a moist convective adjustment scheme, where the thermodynamic profile is adjusted toward an observed reference profile in a quasi-equilibrium state. The BMJ scheme is triggered when the parcel is warmer than the environment determined by the Convective Available Potential Energy (CAPE). The scheme favors activation in cases with significant amounts of moisture at low and mid-levels and positive CAPE (Pohl et al., 2011). In contrast, KF, as a low-level control convective scheme, rearranges air mass in a column using the updraft, downdraft, and environmental mass fluxes until at least 90% of CAPE is removed (Kain, 2004). The predominance of a strong convective regime over the Indian Ocean leads to over-simulation of rainfall.
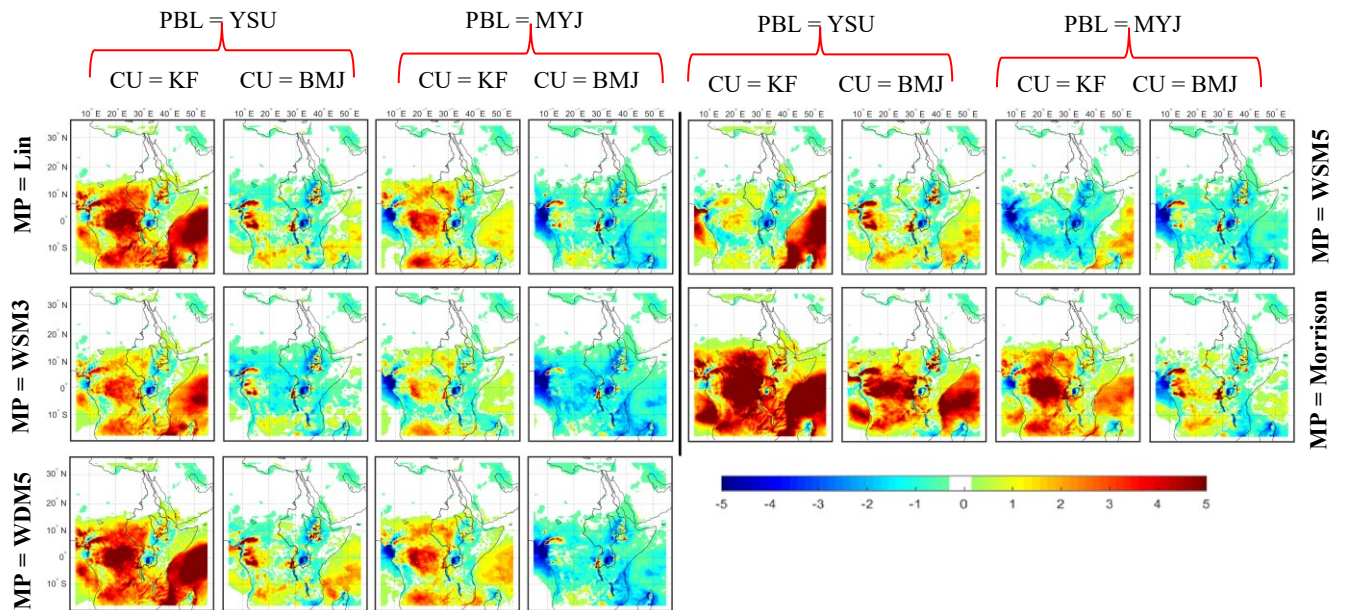
Figure 2.2: Differences between observed (TRMM) and WRF's simulated annual mean rainfall (mm/day) over the Nile river basin under different MP, CU and PBL schemes, fixed RRTM, Dudhia Ra schemes and NOAH LSM.
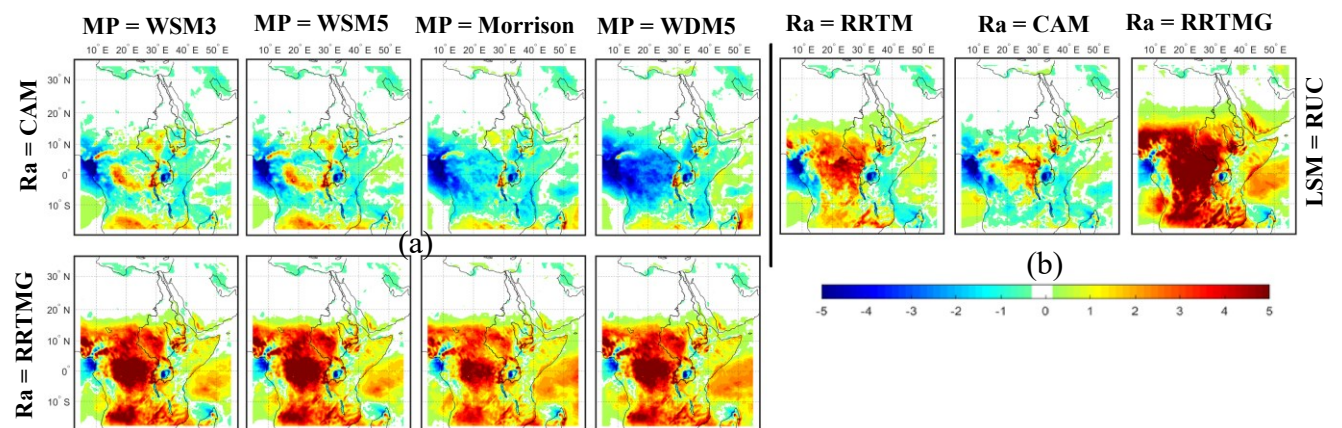
Figure 2.3: Differences between observed (TRMM) and WRF's simulated annual mean rainfall (mm/day) over the Nile river basin under different combinations of (a) Ra and MP, with fixed MYJ and KF schemes, and NOAH LSM, and (b) Ra with fixed WSM3, MYJ, KF schemes, and RUC LSM.

Beside the cumulus scheme, by mixing and the transfer of surface water vapour to higher layers, PBL also plays a significant role in the amount of rainfall simulated. For example, the positive bias of KF over the Congo basin, Indian and Atlantic Ocean has been mostly corrected by changing the YSU PBL to the MYJ PBL scheme as shown in column 1 (YSU) and 3 (MYJ) of Figure 2.2 under the KF Cu scheme. However, under MYJ, the rainfall of the West Coast of Africa/Cameroon tends to be under-simulated. In addition, combining MYJ PBL with the BMJ Cu scheme favours the simulation of a much drier climate compared with combining YSU PBL with BMJ Cu, which agrees with other studies, e.g., Evans et al. (2012) also found that YSU PBL tends to induce more convection in the KF scheme which leads to an over-simulation of precipitation. The MYJ (Mellor and Yamada, 1982) tends to simulate a drier climate because it is a local closure PBL scheme reported to produce insufficient mixing in the convective boundary layer (Brown, 1996), for a weaker vertical mixing would transfer less surface water vapour to higher layers (HU et al, 2010). In contrast, YSU (Hong et al. 2006) is a non-local closure PBL scheme that produces a well-mixed boundary layer profiles. This is likely a key reason why YSU favours a wetter simulation as compared with MYJ.

Besides PBL and Cu, the effect of different radiation schemes, which provides the atmospheric heating and the ground heat budget, over the amount of rainfall simulated, is shown in Figure 2.3a. Figure 2.3a is presented with respect to different combinations of WRF's parameterization schemes, namely, radiation schemes (CAM and RRTMG) and microphysics (WSM3, WSM5, Morrison and WDM6) under KF and MYJ as the Cu and PBL schemes, respectively. Apparently, changing the radiation scheme than the MP scheme has a

relatively larger effect on the amount of rainfall simulated, given that the RRTMG scheme generally leads to a wetter climate than other radiation schemes, especially the CAM scheme which tends to produce lesser rainfall.

Lastly, the LSM which interacts with the lower atmosphere also plays a role in the amount of moisture fluxes, the outgoing short- and longwave radiation and sensible heat fluxes simulated, which are partly absorbed by the cloud. This is because heat and moisture fluxes simulated by the LSM over the land surface will be used as the lower boundary conditions for computing the vertical transport in the PBL scheme (Skamarock et al., 2008). However, changing the LSM between Noah and RUC shows little effects over the amount of rainfall simulated as shown in Figure 2.3b, even though RUC LSM marginally simulates more rainfall than the NOAH LSM (as shown in column-1 of Figure 2.3a, and row-2 vs column-3 of Figure 2.2).

The annual cycles of mean monthly rainfall for all test cases over the BNRB are shown in Figure 2.4. Compared with TRMM, CRU or GPCC dataset, more test cases show positive than negative bias during the May-September rainy season, but the simulations of WRF have generally captured the monthly rainfall variation of BNRB/Ethiopian highland for the rainy season. As explained earlier, compared with the other parameterization schemes of WRF, under the KF cumulus with YSU PBL scheme, WRF tends to over-simulate the rainfall of BNRB. A Taylor diagram is used to evaluate the agreement between the simulated and observed monthly rainfall using statistics such as the Pearson correlation, RMSE, and standard deviation for each simulation over the BNRB as shown in Figure 2.14a. The plot

shows a relatively high correlation between simulated and TRMM data in monthly time step, but the standard deviations normalized by the standard deviation of TRMM tend to be larger than one, which means rainfall simulated by WRF show larger variabilities than satellite data. The RMSE of WRF's simulations range between 0.45 and 8.04 mm/day where higher RMSE represents simulations coming from WRF based on WSM3 MP, RRTMG radiation scheme, and RUC LSM.
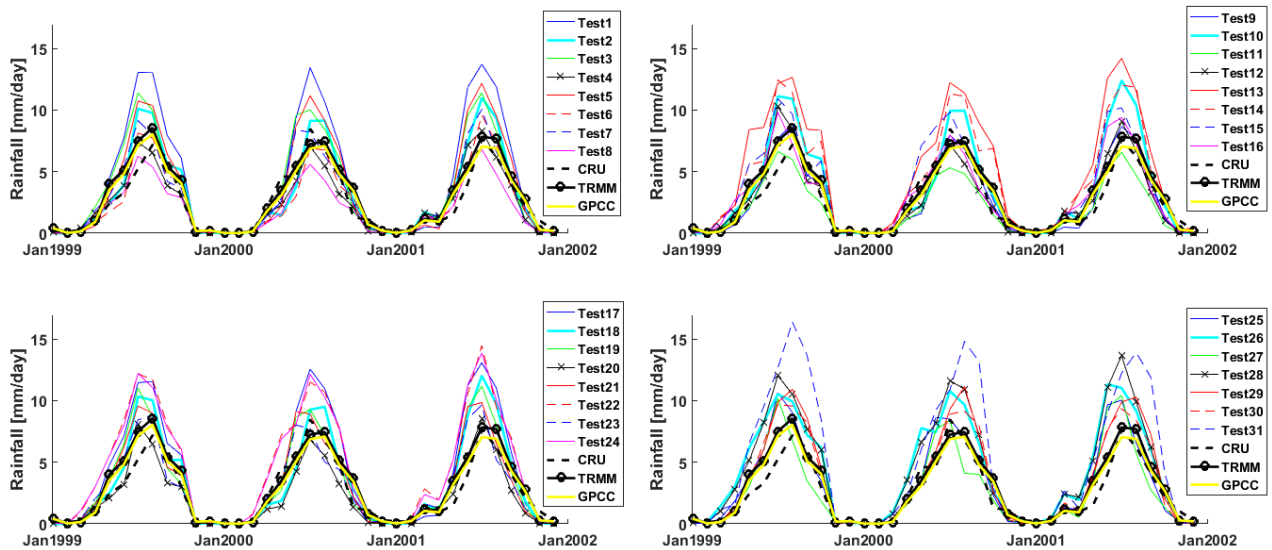
Figure 2.4: Comparison of mean monthly rainfall (mm/day) simulated by WRF for Blue Nile River with observed data of CRU, TRMM, and GPCC.

2.4.2. Surface temperature at 2m

Biases of the mean annual 2m air temperature simulated by WRF under different parameterization schemes with respect to observed data of CRU are shown in Figure 2.5. The results show that spatial patterns of temperature simulated by WRF generally agree well with observed data with reasonable discrepancies. Even though the maximum cold bias can be -

7°C and the maximum warm bias can be 8°C at some places, the mean bias ranges from -3°C to 0.5°C. WRF clearly under-simulated the temperature of the Sahara Desert when the Noah LSM was used, and even the NCEP reanalysis data is also too cold for the Sahara Desert when compared with the CRU data (not shown here). As a result, we cannot objectively assess the bias of temperature simulated by WRF under certain selected parameterization schemes with default parameters built into WRF, for as expected, observed data such as CRU also has uncertainties.
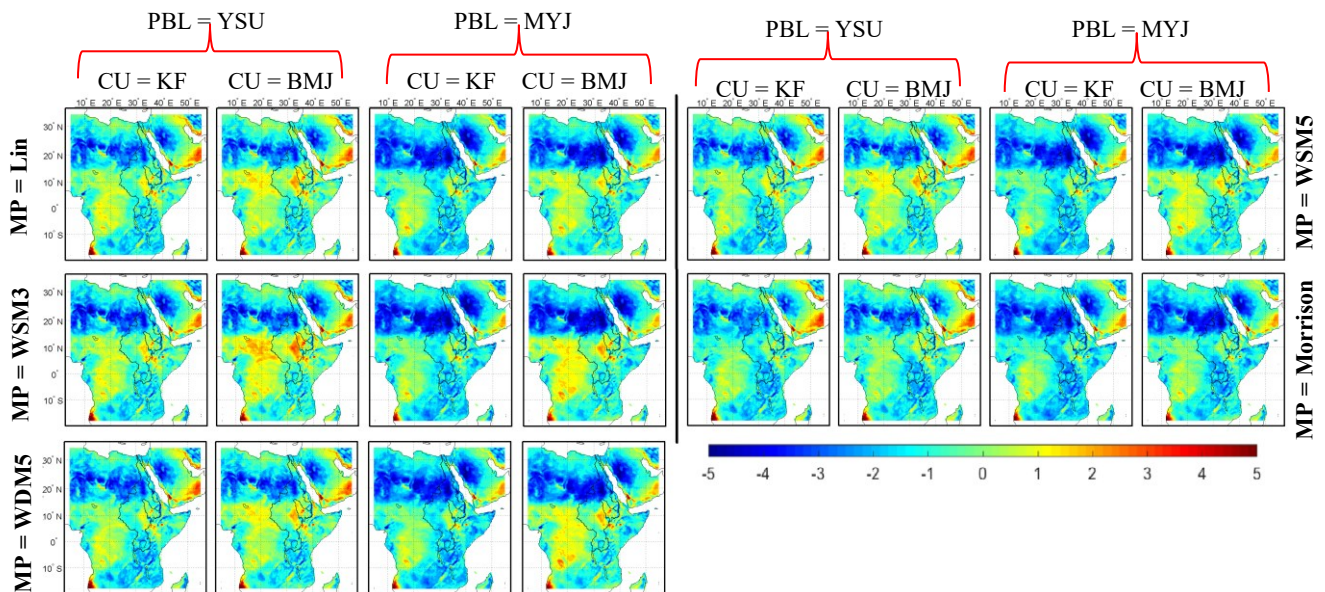
Figure 2.5: Differences between observed (CRU) and WRF's simulated annual mean Temperature (°C) over the Nile river basin under different combinations of MP, CU and PBL schemes, fixed RRTM, Dudhia Ra schemes and NOAH LSM.

On the basis of differences between WRF's simulations and the CRU annual mean Temperature (°C) over the NRB for different combinations of MP, Cu and PBL schemes, it

seems these schemes have marginal influence on the temperature simulated by WRF as shown in Figure 2.5. On the other hand, LSM and Ra schemes which simulate the radiation forcing and heat exchanges between the land surface and the atmosphere exert stronger impact on air temperature simulated by WRF as shown in Figure 2.6. Temperature biases over the Sahara Desert were partly corrected by changing either the LSM or the Ra scheme. The RRTMG combined with Noah LSM simulated more accurate air temperature compared to other radiation schemes as shown in Figure 2.6a, while the CAM scheme resulted in a large negative temperature bias over the whole domain set up for the NRB. Also, using the RUC LSM resulted in a higher simulated temperature than the Noah LSM as shown in Figure 2.6b. Similarly, Mooney et al. (2013) also found the summer surface temperature of Europe simulated by WRF was mostly controlled by the selection of land surface models (LSMs) and radiation schemes but less sensitive to MP and PBL. In their study, they found the NOAH LSM simulated surface temperature that better agree with the observed data than the RUC LSM, even though under NOAH the surface temperature tends to be under-simulated, especially when combining NOAH with the CAM radiation scheme.

Figure 2.7 shows the mean monthly, areally averaged 2m air temperature of BNRB simulated by WRF for all the test cases to generally capture the characteristic of observed temperature of BNRB, with lower air temperature during rainy seasons than dry seasons. Among all test cases considered, the CAM radiation scheme combined with WDM6 MP (designated as Test 27) resulted in simulated air temperature that on a whole is colder than all other test cases conducted in this study. The RMSE of WRF's simulated temperature ranges from 0.27 to 4

^{o}C, has a correlation with the observed temperature higher than 0.8, and the normalized standard deviation is closed to one as shown in Figure 2.14b of the Taylor diagram.
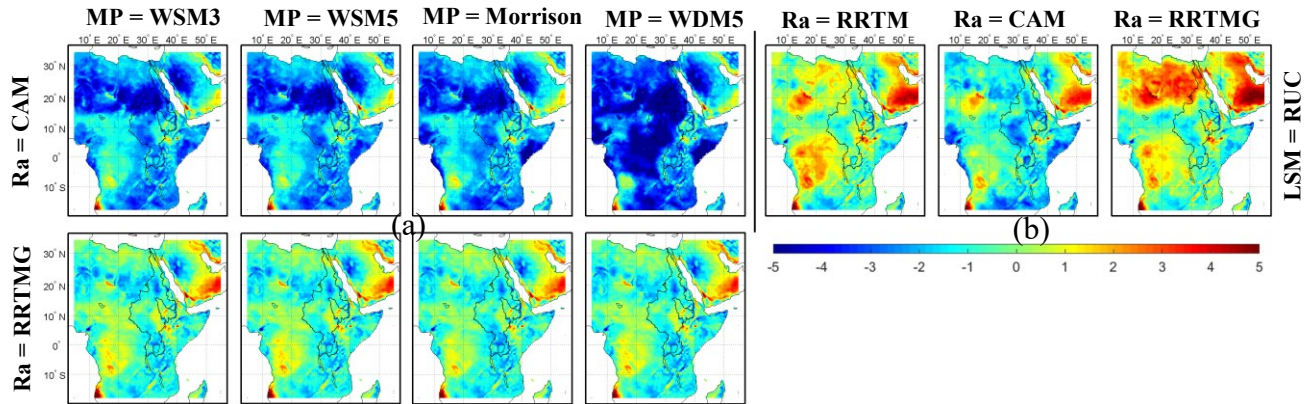
Figure 2.6: Differences between observed (CRU) and WRF's simulated annual mean temperature (^{o}C) over the Nile river basin under different combinations of (a) Ra and MP, with fixed MYJ and KF schemes, and NOAH LSM, and (b) Ra with fixed WSM3, MYJ, KF schemes, and RUC LSM.
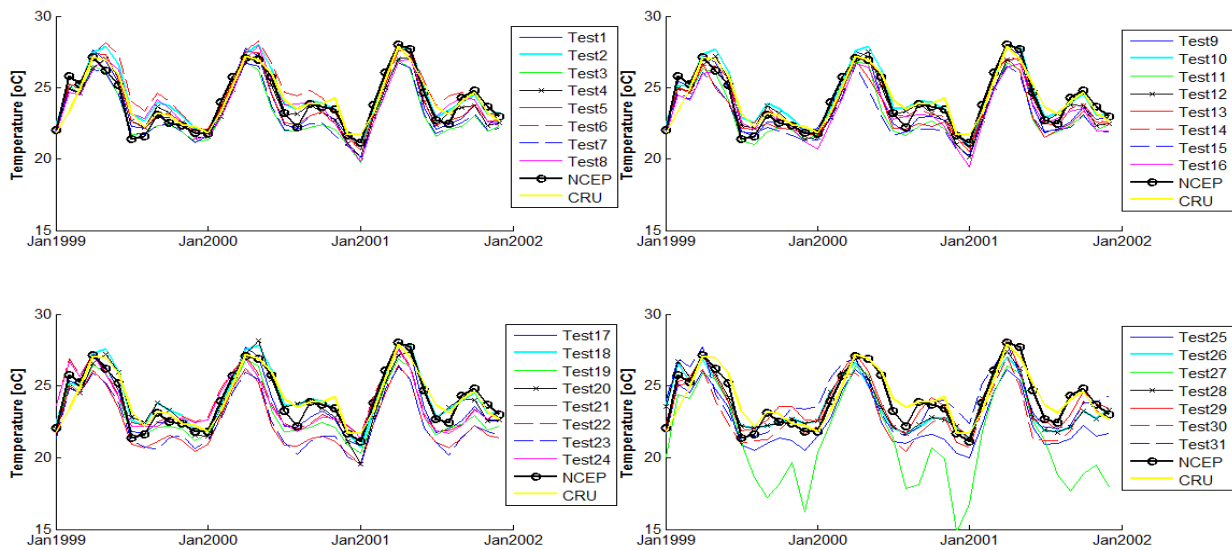
Figure 2.7: Comparison of mean monthly 2m temperature (^{o}C) simulated by WRF for Blue Nile River with observed data of CRU and NCEP.

2.4.3. Downward longwave radiation at the surface (LWRAD)

Figure 2.8 and Figure 2.9 show the mean annual surface downward longwave radiation bias (W.m^{-2}) for all model configurations of WRF tested with respect to NCEP reanalysis data. The LWRAD is less sensitive to Cu and MP schemes, but slightly more sensitive to Ra, LSM and PBL schemes as shown in Figure 2.8 and Figure 2.9. Under the YSU PBL scheme, RRTM simulated more LWRAD than under the MYJ PBL scheme. Further, under the double-moment MP scheme RRTM simulated more LWRAD than under the single-moment MP, especially if YSU is the PBL scheme selected, e.g. the Morrison double-moment MP with YSU schemes lead to more LWRAD simulated than under other combination of MP and PBL schemes, resulting in higher rainfall simulated, as discussed in Section 2.4.1. Furthermore, in addition to Ra schemes, the selection of LSM also plays an important role in the amount of LWRAD as shown in Figure 2.9. The figure shows that RUC LSM and RRTMG simulated larger LWRAD than other parameterization schemes of WRF considered in this study, while the CAM radiation scheme under-simulated LWRAD across the entire study domain. The discrepancy between WRF's simulated LWRAD and that of NCEP reanalysis data under different combinations of parameterization schemes can range from -60 to 30 W.m^{-2}, and with a mean bias ranging from -25 to 3 W.m^{-2}, a RMSE ranging from 6.4 to 29.9 W.m^{-2}, and a standard deviation from 26.7 to 33.53 W.m^{-2}.
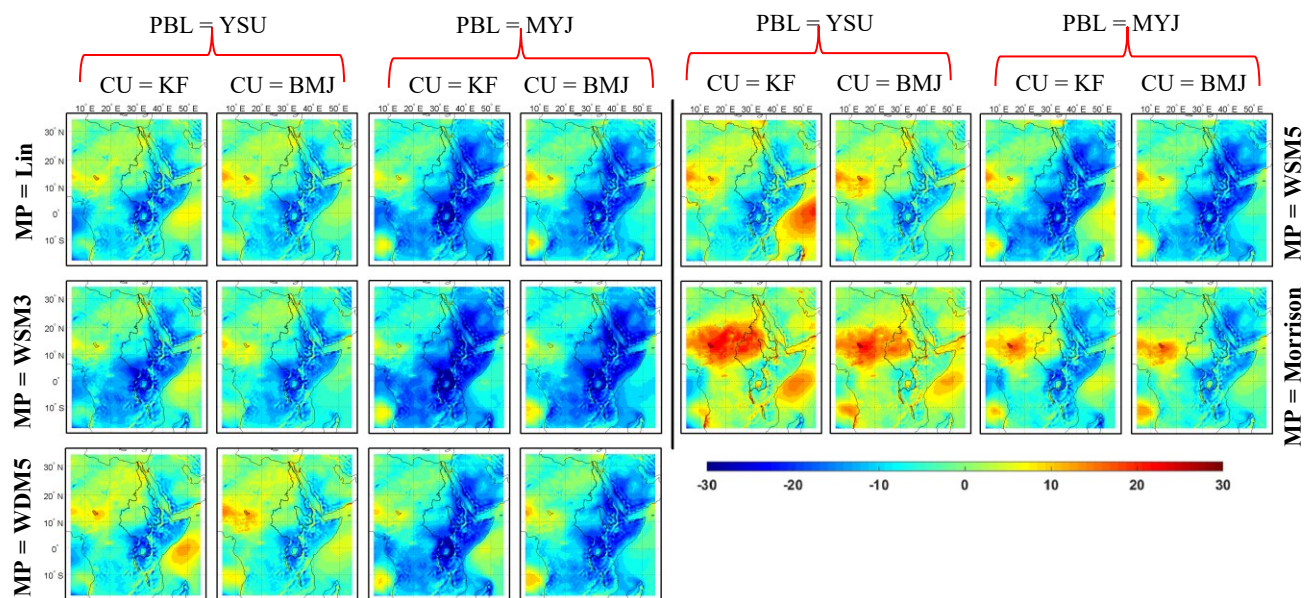
Figure 2.8: Difference between NCEP reanalysis data and WRF`s simulated annual mean LWRAD (W.m^{-2}) over the Nile river basin for different combinations of MP, CU and PBL schemes, fixed RRTM, Dudhia Ra schemes and NOAH LSM.
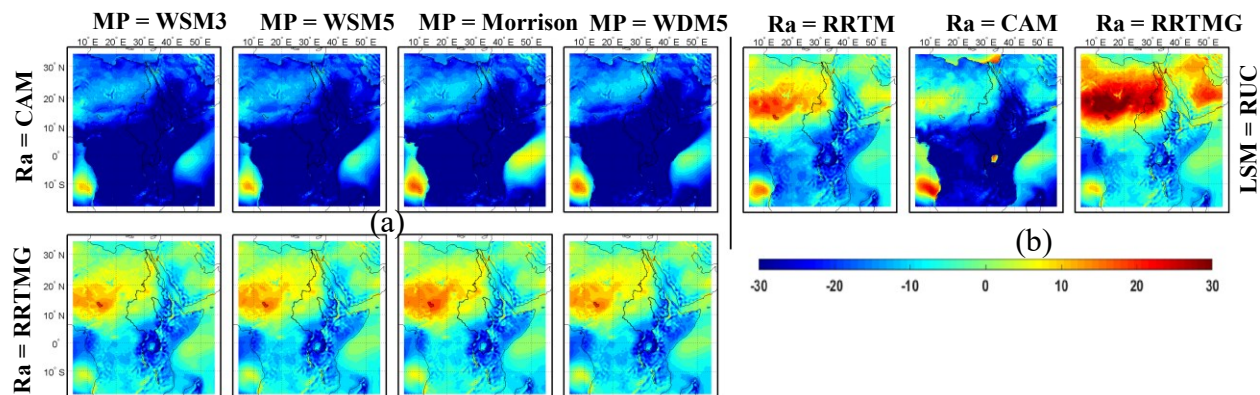
Figure 2.9: Differences between annual mean LWRAD (W.m^{-2}) of NCEP reanalysis data and that simulated by WRF over the Nile river basin for different combinations of (a) Ra and MP, with fixed MYJ and KF schemes, and NOAH LSM, and (b) Ra with fixed WSM3, MYJ, KF schemes, and RUC LSM.

Figure 2.10 shows that in comparison to the NCEP data, the mean monthly, areally averaged LWRAD for the BNRB simulated by WRF for all test cases suffers a systematic under-simulation, especially under the CAM radiation scheme. As shown in the Taylor diagram in Figure 2.14c, the RMSE between the LWRAD of WRF and that of NCEP ranges from 25 to 134 W.m^{-2}, but their correlation is above 0.95, which demonstrates that the LWRAD simulated by WRF for the BNRB with an acceptable uncertainty.
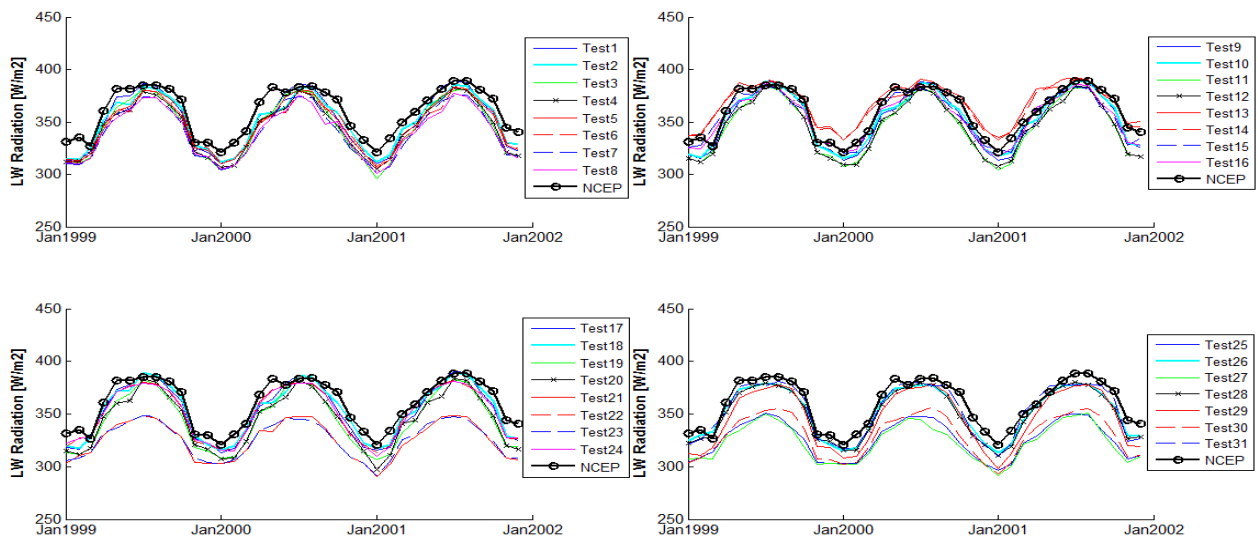
Figure 2.10: Comparison of mean monthly LWRAD (W.m^{-2}) simulated by WRF for Blue Nile River with NCEP reanalysis data.

2.4.4. Downward shortwave radiation at the surface (SWRAD)

The downward shortwave radiation flux is dependent on the solar zenith angle which affects the path length. Further, while penetrating through the atmosphere, the SWRAD is attenuated by cloud covers, scattered by aerosols and dust particles, and also absorbed by atmospheric

water-vapour. Besides SWRAD, the atmospheric cloud cover plays a critical role in the simulation of rainfall and LWRAD which are interconnected to each other. For example, more cloud cover means more rainfall but less SWRAD passing through the cloud which emits more LWRAD to the surface. Therefore, as shown in the figures, when LWRAD is under-simulated, rainfall is also expected to be under-simulated while SWRAD over-simulated, and vice versa, but this will also depend on the cloud type and size, and the composition of water droplets and/or ice particles that form the cloud.

Biases in the mean annual SWRAD simulated by WRF with respect to the NCEP data are shown in Figure 2.11 and Figure 2.12. The annual rainfall of the Equatorial area, where SWRAD is mostly over-simulated by WRF, is higher than surrounding regions. Under the Dudhia shortwave radiation scheme, the simulation of SWRAD is less sensitive to Cu, PBL scheme and LSM, but very sensitive to the MP scheme. The higher the rainfall, the lesser will be the SWRAD simulated because of a higher absorption by cloud or water particles in the atmosphere. Compared with other MP schemes, the Morrison scheme is associated with over-simulated rainfall (Section 2.4.1) but the SWRAD simulated agrees better with the NCEP reanalysis data, while Lin and WSM3 MP schemes are associated with more bias in the SWRAD simulated. In terms of the radiation schemes, RRTMG and CAM generally simulate higher amount of SWRAD than the Dudhia scheme as shown in Figure 2.12. On the other hand, in contrary with the Dudhia shortwave radiation scheme (shown in Figure 2.11), under CAM and RRTMG radiation schemes, the effect of MP schemes on the simulation of SWRAD is relatively marginal. Compared with the NCEP reanalysis data, WRF generally

shows more over than under-simulation of SWRAD, with a discrepancy ranging from -120 to 160 W.m^{-2}; and a mean bias ranging from 3.9 to 45.53 W.m^{-2}. Between WRF's simulation and the NCEP data, the RMSE ranges from 19.3 to 51.8 W.m^{-2} and the standard deviation from 25.2 to 44.6 W.m^{-2}. From the mean monthly surface downward shortwave radiation average over BNRB shown in Figure 2.13, there is a systematic over-simulation of SWRAD over the BNRB except when WRF was under the Morrison or the WSM5 microphysics schemes combined with the KF, RRTM, and YSU schemes. The Taylor diagram of Figure 2.14d shows that the correlation between WRF's simulation and the NCEP reanalysis data ranges from 0.45 to 0.9, and the RMSE from 22 to 60 W.m^{-2}.
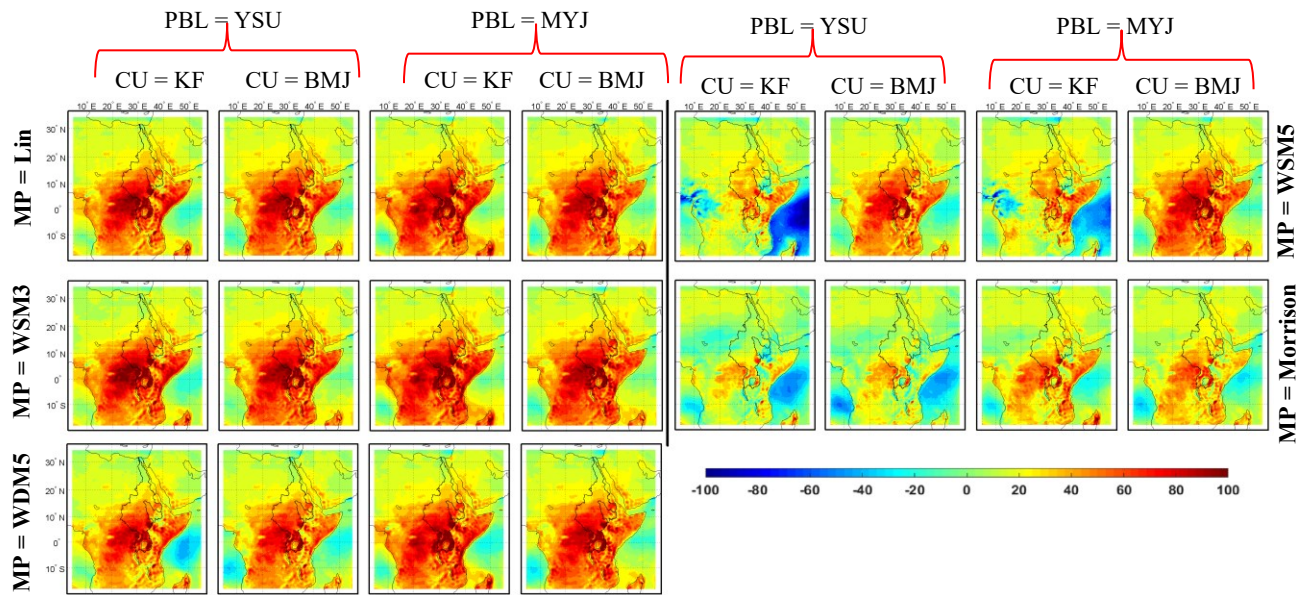
Figure 2.11: Differences between NCEP reanalysis data and WRF`s simulated annual mean SWRAD (W.m^{-2}) over the Nile river basin under different combinations of Cu, MP and PBL, fixed RRTM, Dudhia Ra schemes and NOAH LSM.
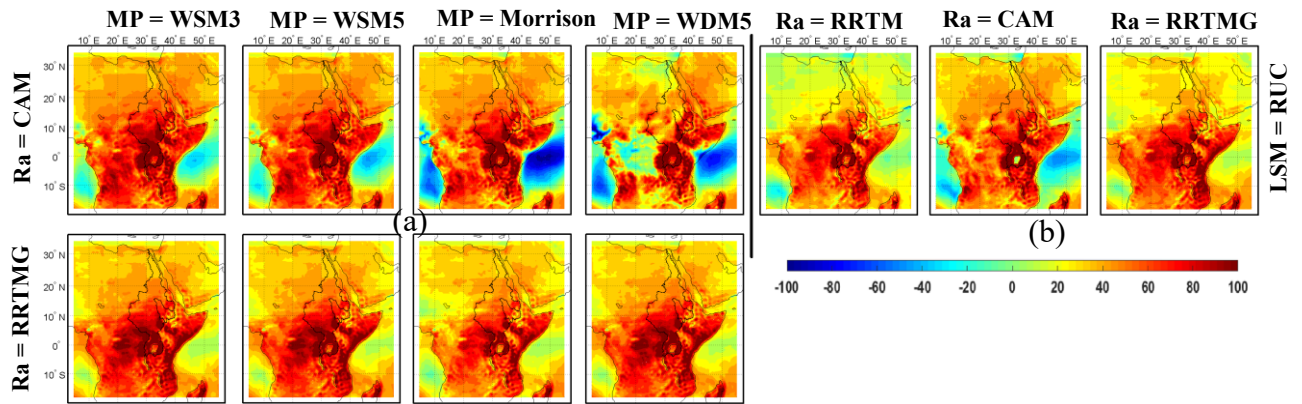
Figure 2.12: Differences between NCEP reanalysis data and WRF's simulated annual mean SWRAD (W.m^{-2}) over the Nile river basin under different combination of (a) Ra and MP, with fixed MYJ and KF schemes, and NOAH LSM, and (b) Ra with fixed WSM3, MYJ, KF schemes, and RUC LSM.
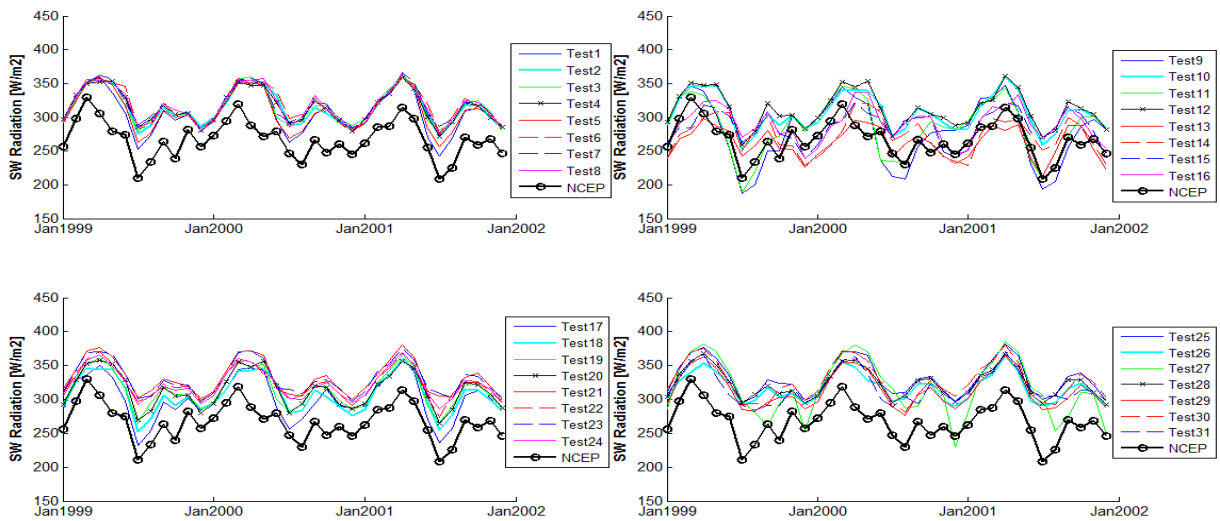
Figure 2.13: Comparison of mean monthly SWRAD (W.m^{-2}) simulated by WRF for Blue Nile River with NCEP reanalysis data.
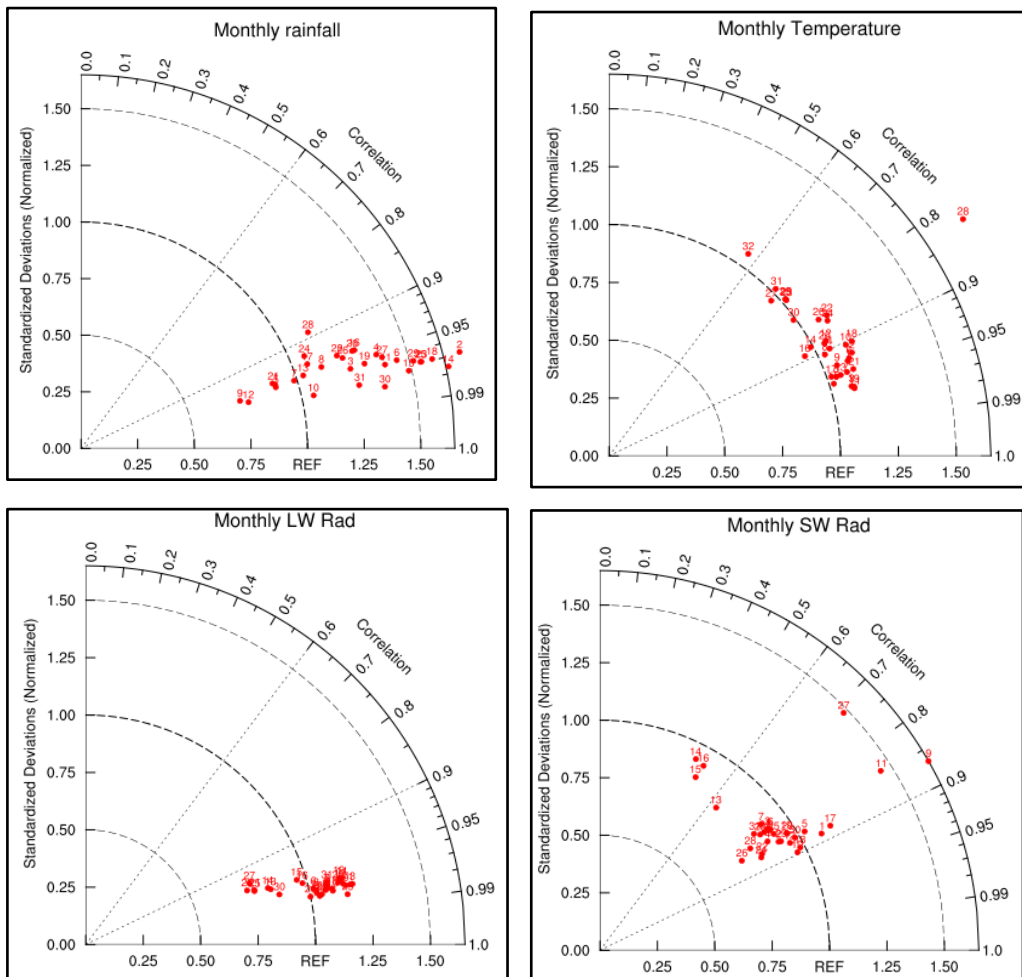
Figure 2.14: Taylor diagram showing correlation coefficient and standard deviation of (a) mean monthly rainfall, (b) surface air temperature, (c) longwave radiation, and (d) shortwave radiation relative to observed and reanalysis data for the 31 WRF simulations over Blue Nile river basin.

2.4.5. Multi-year regional climate simulation of WRF

From the above analysis of results, it seems that WRF can achieve modeling more representative regional climate of NRB by using the WSM3 microphysics, KF cumulus, MYJ PBL, RRTM longwave radiation, and Dudhia shortwave radiation schemes and coupled to the

Noah LSM than other schemes coupled to Noah or other land surface schemes. The above configuration of WRF calibrated from using the 1999-2001 data was further tested to see if WRF-Noah can simulate representative, long-term regional climate of NRB over 1980-2001 which include a combination of wet and dry years. The mean annual difference between observed and WRF simulated rainfall, temperature, long- and shortwave radiation are shown in Figure 2.15. The results confirm that the configured WRF-Noah can simulate the climate of NRB accurately, with a RMSE between simulated and observed data of 1.1mm/day, 2.4^{o}C, 13.2 W.m^{-2}, and 40.7 W.m^{-2}; and a mean error of 0.27mm/day, -2°C, -10.5 W.m^{-2}, and 31.3 W.m^{-2}; and the spatial correlation of 0.89, 0.92, 0.97 and 0.61 for rainfall, temperature, longwave and shortwave radiation, respectively. Similar to results obtained for the 1999-2001 calibration experience, WRF over-simulated the rainfall in the Congo basin, under-simulated the temperature in the Sahara Desert, under-simulated the longwave radiation and over-simulated the shortwave radiation in NRB marginally. The long-term simulation of WRF was compared against NCEP reanalysis data for long- and shortwave radiation, and GPCC and CRU data for rainfall and temperature, respectively.
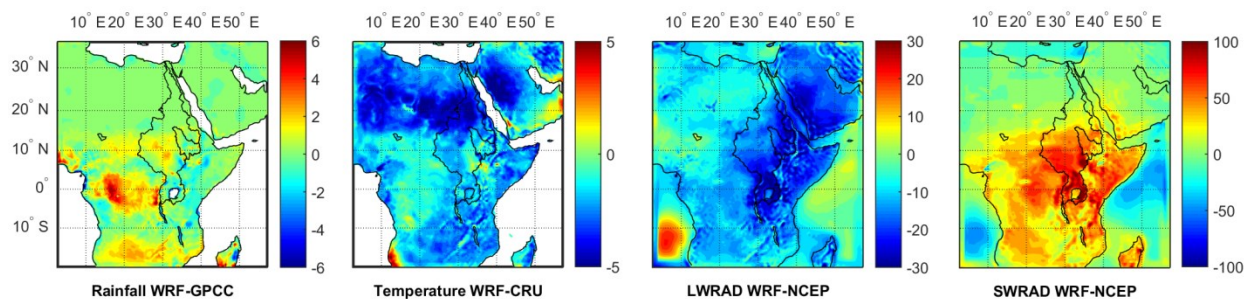
Figure 2.15 Differences between observed GPCC, CRU, reanalysis NCEP data and WRF's simulated mean annual (1980-2001) rainfall (mm/day), temperature (^{o}C), longwave and shortwave radiation (W.m^{-2}) over the Nile river basin.
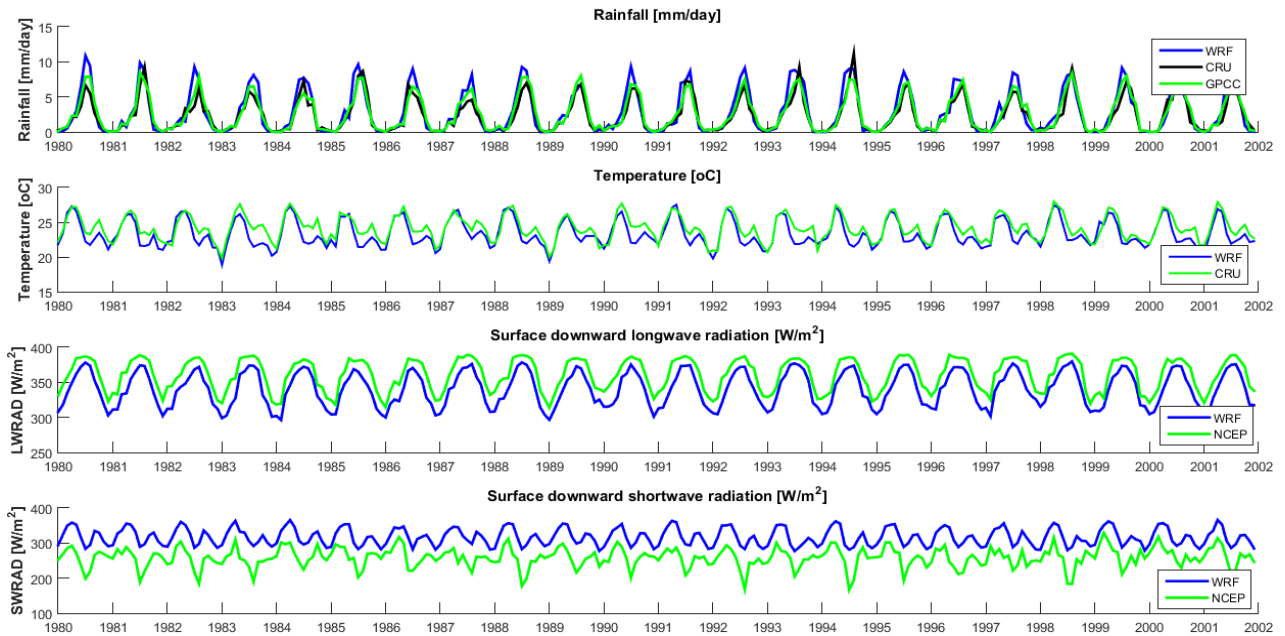
Figure 2.16: Comparison of mean monthly rainfall, temperature, longwave, and shortwave radiation simulated by WRF for Blue Nile River with observed GPCC, CRU and NCEP radiation data.

Figure 2.16 shows that the mean monthly, areally averaged rainfall, 2m air temperature, long-, and shortwave radiation of BNRB simulated by WRF for 1980-2001 generally captured the observed climate variables of BNRB reasonably well, even though the rainfall of BNRB was over-simulated during rainy season, and WRF consistently over- and under simulated the short- and longwave radiation of BNRB, respectively. Comparing the rainfall, temperature, longwave and shortwave radiation simulated by WRF for BNRB with the observed data, the correlations are 0.94, 0.91, 0.97, and 0.73; the RMSE are 1.14mm/day, 1.13^{o}C, 21.4 W.m^{-2} and 61.5 W.m^{-2}; and the Mean error are 0.29 mm/day, -0.82^{o}C, -20.4 W.m^{-2} and 58.3 W.m^{-2},

respectively. The above statistics between WRF's simulation with the observed climate data over the 1980-2001 period show that the configuration chosen for WRF coupled to the Noah LSM can reasonably simulate the long-term regional climate of BNRB over both dry and wet years.

2.5.   Summary and Conclusions

In this study, WRF model was carefully configured to select the best optimal combination of parameterization schemes to simulate representative, 1999-2001 climate of the NRB using ERA interim data as the boundary condition. As expected, no one parameterization scheme is consistently superior over other schemes under different evaluation criteria. In most RCM studies, the configuration and parameterization of a RCM is evaluated in terms of the accuracy of precipitation and temperature simulated only, which has its drawback because the results could be good even though the model configuration chosen may not be optimal for modeling a climatic regime. In this study using WRF as the RCM to model the regional climate of the NRB, the performance of WRF was also evaluated in terms of energy fluxes simulated, which should be more comprehensive than just evaluating WRF in terms of only precipitation and temperature simulated.

Overall, with reference to NCEP reanalysis and CRU climate data, the T2 and LWRAD simulated are generally more accurate than precipitation and SWRAD data for all WRF parameterization schemes tested in this study. The simulation of rainfall is more sensitive to the choice of PBL, Cu and MP schemes than other schemes of WRF. For example,

combining the KF convective scheme with the YSU PBL scheme tends to simulate rainfall with significant bias over the NRB, while by combining KF with the MYJ PBL scheme, WRF simulated better rainfall than all other combinations of Cu and PBL schemes. T2 is more sensitive to LSM and Ra than to Cu, PBL and MP schemes selected for NRB. The surface air temperature simulated using Noah as the LSM agrees better with observed data (e.g., small negative bias) than that simulated using RUC as the LSM which has a high positive bias. From testing several radiation schemes with Noah as the LSM, the simulated T2 tends to have a negative bias with CAM as the radiation scheme, a positive bias with RRTMG as the radiation scheme, and has a negative bias over the Sahara Desert while using other radiation schemes. The SWRAD simulated by WRF is generally more dependent on MP and Ra schemes than Cu, LSM and PBL schemes. While most SWRAD simulated by WRF tends to have a positive bias, SWRAD simulated from combining the Morrison MP scheme with the Dudhia radiation scheme tends to be more accurate than other combination of schemes, e.g., SWRAD simulated from CAM and RRTMG schemes have more positive bias than that simulated using the Dudhia scheme. Finally, LWRAD simulated by WRF is highly sensitive to LSM, Ra and PBL schemes, but less sensitivity to Cu and MP schemes. On a whole, RUC, RRTMG and YSU schemes tend to result in simulating LWRAD with a positive bias than other schemes. Furthermore, with a strong positive bias in SWRAD, WRF tends to simulate low rainfall and low longwave radiation, and vice versa. Therefore, a careful selection of the configuration and physical parameterization schemes for WRF is essential to simulate representative key climate variables such as T2, precipitation, SWRAD and LWRAD. From a

tedious effort calibrating WRF with the objective of simulating representative regional climate of NRB, we found the following combination of schemes to be more comprising than other schemes: the Single-moment WSM3 microphysics, KF cumulus, MYJ PBL, RRTM longwave radiation scheme, Dudhia shortwave radiation scheme, and Noah LSM. In addition, these selected schemes are also efficient in terms of computation time as compared with other WRF parameterization schemes tested in this study. Lastly, the above configuration of WRF coupled to the Noah LSM has been shown to simulate representative regional climate of NRB over 1980-2001 which include a combination of wet and dry years of the NRB.

References

Adeyewa ZD, and Nakamura K. (2003) Validation of TRMM Radar Rainfall Data over Major Climatic Regions in Africa. J. Appl. Meteorol. 42: 331–347, doi: 10.1175/1520-0450(2003)042<0331:VOTRRD>2.0.CO;2.

Anyah RO, and Semazzi FHM. (2006) Climate variability over the Greater Horn of Africa based on NCAR AGCM ensemble. Theor. Appl. Climatol., 86, 39-62, doi:10.1007/s00704-005-0203-7.

Anyah RO, and Semazzi FHM. (2007) Variability of East African rainfall based on multiyear RegCM3 simulations. Int. J. Climatol., 27:357–371, doi:10.1002/joc.1401.

Anyah RO, Semazzi FHM, Xie L. (2006) Simulated physical mechanisms associated with multiscale climate variability over Lake Victoria Basin in East Africa. Mon. Weather Rev., 134, 3588–3609, doi:10.1175/MWR3266.1.

Brown, A.R. (1996) Evaluation of parametrization schemes for the convective boundary layer using large-eddy simulation results. Bound.-Layer Meteor., 81, 167-200, doi:10.1007/BF00119064.

Chen C.-S., Lin Y.-L., Peng W.-C., Liu C.-L. (2010) Investigation of a heavy rainfall event over southwestern Taiwan associated with a subsynoptic cyclone during the 2003 Mei-Yu season. Atmos. Res., 95, 235–254, doi:10.1016/j.atmosres.2009.10.003.

Collins, W. D., et al. (2004) Description of the NCAR Community Atmosphere Model (CAM3.0). Technical Note TN-464+STR, National Center for Atmospheric Research, Boulder, CO, 214 pp.

Dinku T, Chidzambwa S, Ceccato P, Connor SJ, Ropelewski CF. (2008) Validation of high resolution satellite rainfall products over complex terrain. Int. J. Remote Sens. 29: 4097–4110.

Diro, G. T., Grimes D., and Black E. (2012) Dynamical downscaling of ECMWF Ensemble seasonal forecasts over East Africa with RegCM3. J Geophys Res 117:D16103. doi: 10.1029/2011JD016997.

Dudhia J. (1989) Numerical study of convection observed during the winter experiment using a mesoscale two-dimensional model. J. Atmos. Sci., 46, 3077–3107, doi: 10.1175/1520-0469(1989)046<3077:NSOCOD>2.0.CO;2.

Ek, M., and Mahrt L. (1991) OSU 1-D PBL model user's guide, version 1.04. Department of Atmospheric Sciences, Oregon State University, 120 pp.

Endris H.S., Omondi P., Jain S., et al. (2013) Assessment of the Performance of CORDEX Regional Climate Models in Simulating East African Rainfall. J. Climate, 26, 8453-8475, doi:10.1175/JCLI-D-12-00708.1.

Evans J.P., Ekström M., and Ji F. (2012) Evaluating the performance of a WRF physics ensemble over South-East Australia. Clim. Dynam., 39, 1241–1258, doi:10.1007/s00382-011-1244-5.

Flaounas E, Bastin S, and Janicot S. (2011) Regional climate modelling of the 2006 West African monsoon: sensitivity to convection and planetary boundary layer parameterisation using WRF. Clim. Dyn., 36, 1083-1105, doi:10.1007/s00382-010-0785-3.

Fowle M.A., Roebber P.J. (2003) Short-range (0-48 h) numerical prediction of convective occurrence, mode, and location. Wea. Forecasting, 18, 782–794, doi: 10.1175/1520-0434(2003)018<0782:SHNPOC>2.0.CO;2.

Fritsch J.M., Carbone R.E. (2004) Improving quantitative precipitation forecasts in the warm season: a USWRP research and development strategy. Bull. Amer. Meteor. Soc., 85, 955–965, doi: 10.1175/BAMS-85-7-955.

Giorgi F., Jones C., and Asrar G.R. (2009) Addressing climate information needs at the regional level: The CORDEX framework. WMO Bull., 58 (3), 175–183.

Harris I., Jones P.D., Osborn T.J., and Lister D.H. (2014) Updated high-resolution grids of monthly climatic observations – the CRU TS3.10 Dataset. Int. J. Climatol., 34, 623–642. doi: 10.1002/joc.3711.

Hong SY, Lee JW (2009) Assessment of the WRF model in reproducing a flash-flood heavy rainfall event over Korea. Atmos Res 93:818–831. doi: 10.1016/j.atmosres.2009.03.015.

Hong, S.Y., Dudhia J., and Chen S. H. (2004) A revised approach to ice microphysical processes for the bulk parameterization of clouds and precipitation. Mon. Wea. Rev., 132, 103–120, doi: 10.1175/1520-0493(2004)132<0103:ARATIM>2.0.CO;2.

Hong, S.Y., Noh Y., and Dudhia J. (2006) A new vertical diffusion package with an explicit treatment of entrainment processes. Mon. Wea. Rev., 134, 2318–2341, doi: 10.1175/MWR3199.1.

Hu X.M., Nielsen-Gammon J.W., and Zhang F. (2010) Evaluation of three planetary boundary layer schemes in the WRF model. J. Appl. Meteor. Climatol., 49, 1831–1844, doi: 10.1175/2010JAMC2432.1.

Iacono M.J., Delamere J.S., Mlawer E.J., Shephard M.W., Clough S.A., and Collins W.D. (2008) Radiative forcing by long-lived greenhouse gases: Calculations with the AER radiative transfer models. J. Geophys. Res., 113, D13103, doi:10.1029/2008JD009944.

Indeje, M., Semazzi H. M. F., and Ogallo J. L. (2000) ENSO signal in East African rainfall seasons. Int. J. Climatol., 20, 19–46, doi:10.1002/(SICI)1097-0088(200001)20:1<19::AID-JOC449>3.0.CO;2-0.

IPCC-TGICA, (2007) General Guidelines on the Use of Scenario Data for Climate Impact and Adaptation Assessment. Version 2. Prepared by T.R. Carter on behalf of the Intergovernmental Panel on Climate Change, Task Group on Data and Scenario Support for Impact and Climate Assessment, p. 66.

Janjic Z.I. (1994) The step-mountain eta coordinate model: further developments of the convection, viscous sublayer, and turbulence closure schemes. Mon. Wea. Rev.,122,927–945,doi: 10.1175/1520-0493(1994)122<0927:TSMECM>2.0.CO;2.

Jones C. G., Samuelsson P. and Kjellström E. (2011) Regional climate modelling at the Rossby Centre. Tellus A, 63, 1–3. doi:10.1111/j.1600-0870.2010.00491.x

Kain J.S. (2004) The Kain–Fritsch Convective Parameterization: An Update. J Appl. Meteor., 43,170–181, doi: 10.1175/1520-0450(2004)043<0170:TKCPAU>2.0.CO;2.

Katragkou E., Garcia-Diez M., Vautard R., Sobolowski S., Zanis P., Alexandri G., Cardoso R. M., Colette A., Fernandez J., Gobiet A., Goergen K., Karacostas T., Knist S., Mayer S.,

Soares P. M. M., Pytharoulis I., Tegoulias I., Tsikerdekis A., and Jacob D. (2015) Regional climate hindcast simulations with EURO-CORDEX: evaluation of a WRF multi-physics ensemble. Geosci. Model Dev., 8, 603-618, doi:10.5194/gmd-8-603-2015.

Koutsouris, A. J., Chen, D. and Lyon, S. W. (2016) Comparing global precipitation data sets in eastern Africa: a case study of Kilombero Valley, Tanzania. Int. J. Climatol., 36: 2000–2014. doi:10.1002/joc.4476.

Lim K.-S. S., and Hong S.-Y. (2010) Development of an Effective Double-Moment Cloud Microphysics Scheme with Prognostic Cloud Condensation Nuclei (CCN) for Weather and Climate Models. Mon. Wea. Rev., 138, 1587–1612, doi: 10.1175/2009MWR2968.1.

Lin Y.L., Rarley R.D., Orville H.D. (1983) Bulk parameterization of the snowfield in a cloud model. J. Climate Appl. Meteor., 22, 1065–1092, doi: 10.1175/1520-0450(1983)022<1065:BPOTSF>2.0.CO;2.

Mashingia F, Mtalo F, Bruen M. (2014) Validation of remotely sensed rainfall over major climatic regions in Northeast Tanzania. Phys. Chem. Earth, Parts 67–69: 55–63, doi: 10.1016/j.pce.2013.09.013.

Mellor GL, Yamada T. (1982) Development of a turbulence closure model for geophysical fluid problems. Rev Geophys., 20,851–875, doi:10.1029/RG020i004p00851.

Mlawer E.J., Taubman S.J., Brown P.D., Iacono M.J., and Clough S.A. (1997) Radiative transfer for inhomogeneous atmosphere: RRTM, a validated correlated-k model for the long-wave. J. Geophys. Res., 102, 16663–16682, doi:10.1029/97JD00237.

Mohamed Y. A., van den Hurk B.J.J.M., Savenije H. H. G., and Bastiaanssen W. G. M. (2005) Hydroclimatology of the Nile: results from a regional climate model. Hydrol. Earth Syst. Sci., 9, 263–278, doi:10.5194/hess-9-263-2005.

Mooney P. A., Mulligan F. J., and Fealy R. (2011) Comparison of ERA-40, ERA-Interim and NCEP/NCAR reanalysis data with observed surface air temperatures over Ireland. Int. J. Climatol., 31, 545–557, doi:10.1002/joc.2098.

Mooney P.A., Mulligan F.J., and Fealy R. (2013) Evaluation of the sensitivity of the Weather Research and Forecasting Model to parameterization schemes for regional climates of

Europe over the period 1990–1995. J. Climate, 26, 1002–1017, doi:10.1175/JCLI-D-11-00676.1.

Morrison H., Thompson G., and Tatarskii V. (2009) Impact of cloud microphysics on the development of trailing stratiform precipitation in a simulated squall line: comparison of one-and two moment schemes. Mon. Wea. Rev., 137, 991–1007, doi: 10.1175/2008MWR2556.1.

Nair S, Srinivasan G, Nemani R. (2009) Evaluation of multi-satellite TRMM derived rainfall estimates over a western state of India. J. Meteorol. Soc. Jpn. 87: 927–939, doi: 10.2151/jmsj.87.927.

Nicholson SE, Some B, McCollum J, Nelkin E, Klotter D, Berte Y, Diallo BM, Gaye I, Kpabeba G, Ndiaye O, Noukpozounkou JN, Tanu MM, Thiam A, Toure AA, Traore AK. (2003a) Validation of TRMM and Other Rainfall Estimates with a High-Density Gauge Dataset for West Africa. Part I: Validation of GPCC Rainfall Product and Pre-TRMM Satellite and Blended Products. J. Appl. Meteorol. 42: 1337–1354, doi: 10.1175/1520-0450(2003)042<1337:VOTAOR>2.0.CO;2.

Nicholson SE, Some B, McCollum J, Nelkin E, Klotter D, Berte Y, Diallo BM, Gaye I, Kpabeba G, Ndiaye O, Noukpozounkou JN, Tanu MM, Thiam A, Toure AA, Traore AK. (2003b) Validation of TRMM and other rainfall estimates with a high-density gauge dataset for West Africa. Part II: validation of TRMM rainfall products. J. Appl. Meteorol. 42: 1355–1368, doi: 10.1175/1520-0450(2003)042<1355:VOTAOR>2.0.CO;2.

Nyakwada, W. (2009) Predictability of East African seasonal rainfall with sea surface temperature gradient modes, Ph.D. dissertation, University of Nairobi, 265 pp.

Pohl B., Cretat J., and Camberlin P. (2011) Testing WRF capability in simulating the atmospheric water cycle over Equatorial East Africa. Clim. Dyn., 37, 1357-1379, doi: 10.1007/s00382-011-1024-2.

Romilly TG, Gebremichael M. (2011) Evaluation of satellite rainfall estimates over Ethiopian river basins. Hydrol. Earth Syst. Sci. 15:1505–1514, doi: 10.5194/hess-15-1505-2011.

Saha, S., et al. (2010) NCEP Climate Forecast System Reanalysis (CFSR) 6-hourly Products, January 1979 to December 2010. Research Data Archive at the National Center for Atmospheric Research, Computational and Information Systems Laboratory. http://dx.doi.org/10.5065/D69K487J. Accessed† 20 Jul 2015.

Schneider U., Becker A., Finger P., Meyer-Christoffer, A., Rudolf B., Ziese M. (2011) GPCC Full Data Reanalysis Version 6.0 at 0.5°: Monthly Land-Surface Precipitation from Rain-Gauges built on GTS-based and Historic Data. DOI: 10.5676/DWD_GPCC/FD_M_V6_050.

Screen J. A., and Simmonds I. (2011) Erroneous Arctic temperature trends in the ERA-40 reanalysis: A Closer Look. J. Climate, 24, 2620–2627, doi: 10.1175/2010JCLI4054.1.

Segele, Z.T., Leslie L.M., and Lamb P.J. (2009a) Evaluation and adaptation of a regional climate model for the Horn of Africa: Rainfall climatology and interannual variability. Int. J. Climatol., 29, 47–65, doi:10.1002/joc.1681.

Skamarock W.C., Klemp J.B., Dudhia J., Gill D.O., Barker D.M., Duda M., Huang X.Y., Wang W., Powers J.G. (2008) A description of the advanced research WRF version 3. NCAR technical note, NCAR/TN\u2013475?STR, 123 pp.

Smirnova, T. G., Brown J. M., and Benjamin S.G. (1997) Performance of different soil model configurations in simulating ground surface temperature and surface fluxes. Mon. Weather Rev., 125, 1870–1884, doi: 10.1175/1520-0493(1997)125<1870:PODSMC>2.0.CO;2.

Smirnova, T. G., Brown J. M., Benjamin S.G., and Kim D. (2000) Parameterization of cold season processes in the MAPS land surface scheme. J. Geophys. Res., 105, 4077–4086, doi:10.1029/1999JD901047.

Sun L, Semazzi FHM, Giorgi F, Ogallo L (1999a) Application of the NCAR regional climate model to eastern Africa: 1. Simulation of the short rains of 1988. J Geophys Res 104(D6):6529–6548. doi: 10.1029/1998JD200051.

Sun L, Semazzi FHM, Giorgi F, Ogallo L (1999b) Application of the NCAR regional climate model to eastern Africa: 2. Simulation of interannual variability of short rains. J Geophys Res 104(D6):6549–6562. doi: 10.1029/1998JD200050.

Troy, T. J., and Wood E. F. (2009) Comparison and validation of gridded radiation products across northern Eurasia. Environ. Res. Lett., 4, 045008, doi:10.1088/1748-9326/4/4/045008.

Zhang Q, Körnich H, Holmgren K. (2013) How well do reanalyses represent the southern African precipitation? Clim. Dyn. 40: 951. doi: 10.1007/s00382-012-1423-z.

Chapter 3 Regional Climate Change Impact on Extreme Precipitation and Temperature of the Nile River Basin

3.1. Introduction

Possible impact due to climate change and climate variability will likely affect future agricultural production and food security in many African countries significantly (Boko et al., 2007; Gan et al., 2015). In Sub-Saharan Africa about 300 million people suffer from water shortages (WWAP, 2012), and water shortages promote poverty (Gizaw and Gan, 2016). Water stress has been a major societal challenge in Africa, e.g., over 75% of Africans live in regions with arid and semi-arid climate, 2/3 of its population rely on limited and highly variable water resources, a significant fraction of its cropland resides in its driest regions with 40% of the irrigation non-sustainable (Vörösmarty et al., 2005). The threats to food security, conflicts from competing users for dwindling water supply between African nations result in growing political tension and instability in this continent (Dodo, 2014). Our climate will likely continue to change in the coming decades, both as a result of natural factors that affect the climate system and anthropogenic greenhouse gases emissions to the atmosphere. These will change the regional and local temperature and precipitation patterns in Africa and globally.

NRB is the longest river in the world and it is under pressure from both anthropogenic (i.e., growing population that leads to increase in water demands for domestic, agricultural and hydroelectric power water usage) and natural factors (i.e., climate variability and change that

promote hydrologic extremes such as droughts). Climate change affects many climate sensitive sectors, such as agriculture, livestock, water resources and health (IPCC, 2014). NRB is vulnerable to climate change impact because of the dominance of rain-fed rather than irrigated agriculture for food production, and limited water availability and the increasing water demand (Swain, 2011). There is an urgent need to better understand the possible climate change impact over the future water resources of NRB which may decrease or increase because of rising temperature which enhances evaporation loss, reduced precipitation and changes to precipitation patterns. Given the possible impact of climate change varies widely across the world (IPCC, 2007), it is essential to conduct a vigorous regional analysis of climate change impact to NRB.

Large scale climate patterns that affect the rainfall variability of NRB or Eastern Africa are the Inter-Tropical Convergence Zone (ITCZ) and El Nino Southern Oscillation (ENSO) (Ntale and Gan, 2004). ITCZ is formed when dry northeast Trade winds meet the wet southwest Trade winds, forcing the moist air to rise and causing water vapour to condense (Mohamed et al., 2005). Moist air from the Atlantic and the Indian Oceans that flows towards a low pressure zone north of the Equator is the main sources of atmospheric moisture over NRB. The seasonal migration of the ITCZ is latitudinal and towards the area of most solar heating or warmest surface temperature (Schneider et al., 2014). Therefore, it moves toward the Southern Hemisphere from September through February and reverses direction towards the Northern Hemisphere during summer. As a result, there is one rainy season in southern and northern Africa, or a dual rainy season in equatorial Africa. Other than ITCZ, past studies

show that flooding and droughts in NRB are strongly linked to Sea surface temperature (SST) of Atlantic and Indian Oceans (Sun et al. 1999a; Diem et al. 2014), and also to ENSO events (e.g. Eltahir, 1996; Indeje et al. 2000; Segele and Lamb, 2005; Ntale and Gan, 2004; Siam and Eltahir, 2017). Eltahir (1996) found that 25% of the natural variability of the Nile River is associated with ENSO. El Nino (La Nina) events generally result in drier (wetter) than normal conditions in the BNRB (Zaroug et al., 2014; Block and Rajagopalan, 2007), e.g., many major droughts occurred in Africa were partly caused by ENSO events (Shanahan et al., 2009), such as the 2011, Somalia drought, and droughts of Ethiopia/Sudan in the 1980s that killed many people. Mwale and Gan (2005) found that East Africa suffered a total of 12 droughts between 1965 and 1997.

Given the spatial and temporal resolutions of GCMs are generally very coarse, it is necessary to apply statistical or dynamical downscaling methods to downscale climate projections of GCMs to regional or local scales in order to adequately assess the hydrologic impact of climate change to small or mid-size river basins. Statistical downscaling methods empirically relate large scale climate variables (predictors) such as GCM models outputs (temperature, humidity, sea-level pressure, geopotential height, etc.) to local climate (predictands). Past climate change research conducted in NRB using the statistical downscaling techniques are such as Elshamy et al. (2009) and Beyene et al. (2010).

Regional Climate Models are commonly used to dynamically downscale climate projections of GCMs because RCMs can produce more plausible, regional scale climate change scenarios for regional studies than statistical downscaling methods (Fowler et al., 2007). The key

disadvantage of RCMs is that in general they are computationally expensive and in the past teleconnection models have been developed to predict seasonal rainfall, e.g., Ntale et al. (2003) used the canonical correlation analysis to predict the seasonal rainfall of East Africa. There have been studies conducted using RCMs for the entire Africa or some parts of Africa, using either reanalyses data or GCMs' output (e.g. Anyah et al. 2006; Anyah and Semazzi, 2007; Segele et al. 2009; Diro et al. 2012). The coordinated regional climate Downscaling Experiment (CORDEX) (Giorgi et al. 2009), initiated by the World Climate Research Program, has developed high-resolution (50km) regional climate projections for different regions using a RCM. Endris et al. (2013) compared the performance of 10 RCMs in simulating the rainfall of East Africa. They found some RCMs could simulate reasonable rainfall climatology for East Africa but most RCMs' simulations suffer significant biases. Mohamed et al. (2005), who was among the first to apply a RCM to simulate the regional climate of the Nile Basin, used a modified version of the Regional Atmospheric Climate Model (RACMO). Their results obtained for NRB are satisfactory given they agree with the observed extremely low runoff coefficients of NRB. From the CORDEX dataset, Alemseged and Tom (2015) evaluated historical rainfall simulations of eight GCMs downscaled by a RCM called RCA4 for the Upper BNRB of Africa. They found that nearly all GCMs underestimated the mean annual and dry season rainfall (1.4 to 50%) of the upper BNRB. The GCMs' bias exceeded the interannual rainfall variability and is highly dependent on the terrain elevation with the largest bias over high elevation areas. Among the 8 GCMs, MPI-ESM-LR performed the best in terms of rainfall bias, coefficient of variation and root mean

square error. CanESM2 performed best in terms of the correlation coefficient between gauged and simulated annual rainfall amounts. MIROC5 is superior to the other models in terms of capturing rainfall anomaly; i.e., occurrence of wet and dry years. Mariottie et al. (2011) investigated climate change impact to the entire Africa using both the A1B climate change scenario of raw ECHAM5 GCM output and the output that was downscaled by RegCM3 for the late 21st century relative to the base period, 1980-2000. They projected the temperature of Africa will increase by 5°C, precipitation over the equatorial Africa will increase moderately in DJF season, while most of West Africa and the Sahel will experience a reduction in precipitation, in the late 21st century. Soliman et al. (2009) also used RegCM3 to downscale the ECHAM5 GCM A1B scenario over the BNRB. RegCM3 projected the precipitation to decrease by 5% over the Mendaya sub-catchment of Blue Nile, and to increase by 7% over the Border sub-catchment.

Many RCMs have been developed but to the best of our knowledge, only few RCMs have been used to study the regional climate change impact over sub-basins of the NRB. Climate projections over Africa are characterized by high level of uncertainties partly because the climate of Africa is not well understood, and partly because of the limitations of RCMs and GCMs (e.g. Mariotti et al., 2014; Lucas-Picher et al., 2008). As an effort to address uncertainties associated with long-term climate projections, an ensemble of climate change scenarios of IPCC (2013) were used in this study to estimate the possible range of climate change impact on NRB so that appropriate adaptation, preparedness and mitigation strategies may be developed to minimize the impact. In particular, the objective is to evaluate climate

change impact on extreme precipitation and temperature of NRB using WRF to downscale RCP4.5 and RCP8.5 climate scenarios of four GCMs (CanESM2, GFDL-ESM2M, MPI-ESM-LR and ACCESS1-3) of CMIP5 for the 2050s and 2080s.

The chapter is organized as follows: brief description of WRF, its configurations, study site, description of extreme climate indices and bias correction method are presented in section 3.2, discussions of results in section 3.3, and summary and conclusions are in section 3.4.

3.2. Methodology

3.2.1. Model Configuration

Climate scenarios of selected GCMs were dynamically downscaled using the advanced Weather Research and Forecasting (WRF) numerical climate model, version of WRF 3.6.1 of NCAR (National Center for Atmospheric Research). Detailed descriptions of WRF can be found in Skamarock et al. (2008) and also in the WRF user Web site (http://www.mmm.ucar.edu/wrf/users). In this study, the study site domain is set at 36 km resolution and WRF is configured with 30 vertical pressure levels such that the top level is at 50hPa. Out of many configurations tested for WRF, the final selected configurations for WRF consists of *WRF Single-Moment 3-class microphysics scheme* (Hong et al., 2004)*, NOAH land surface scheme* (Ek and Mahrt 1991)*, MYJ planetary boundary layer* (Janjic, 1994)*, Eta similarity surface layer (Janjic, 1994), and Dudhia* (Dudhia, 1989)*, and RRTM atmospheric radiation schemes* (Mlawer et al., 1997). Further, among many cumulus parameterization schemes available in climate models (e.g., Kerkhoven et al., 2006), the *Kain-Fritsch cumulus parameterization* (Kain, 2004) together with the above configurations

were chosen after extensive testing of WRF using ERA-Interim reanalysis data as the initial and lateral boundary conditions (Tariku and Gan, 2017).

First, WRF simulated 30 years of the baseline (1976-2005) climate condition, using one-way nesting with 2-domain configuration, and the outputs of 4 GCMs as initial and lateral boundary conditions for the outermost domain (D1) at 36km resolution. The D1 output was used as lateral boundary conditions for the second domain (D2) of 12 km resolution but, only two GCMs were downscaled into D2 to reduce the amount of computation, and in this paper, only results obtained from D1 are presented. The climate projections of newest generation in the Coupled Model Intercomparison Project (CMIP5) of four selected GCMs (CanESM2 of Canada, ACCESS1-3 in Australia, GFDL-ESM2M of USA and MPI-ESM-LR of Germany) for two RCP (Representative Concentration Pathways) climate scenarios (i.e. RCP4.5 and RCP8.5) over 2041-2100 have been applied to simulate the possible range of future climate of NRB. These GCMs are chosen because of their good performance in the baseline case, their projections cover a wide range of future climate scenarios, and these GCMs have been used in other climate change studies (Bhattacharjee and Zaitchik, 2015; McSweeney et al., 2015). The base period precipitation and 2m surface air temperature of NRB simulated by WRF were evaluated against the Global Precipitation Climatology Centre (GPCC version 6, 1901-2010; Schneider et.al, 2011) and the Climate Research Unit at the University of East Anglia (CRU version 3.22, 1901-2013; Harris et.al, 2014) gauge-based datasets with 0.5^{o} spatial and monthly temporal resolutions, respectively.

3.2.2. Study Area

The study area is the Nile River basin covers an area of about 3.35×10^6 km^2 (Swain, 2011) and shared by eleven countries (Burundi, DR Congo, Egypt, Eritrea, Ethiopia, Kenya, Rwanda, Tanzania, South Sudan, Sudan and Uganda). Its drainage area covers a 10% of Africa's landmass; and the NRB countries have the fastest growing population, with 54% of their total population living within the NRB (Swain, 2011). This study will focus on the BNRB (2) which is the main sub-basin of NRB, but the Atbara (1) and Sobat (4) river basin, Bahar El Ghazal (from now on El Ghazal) (3) and Lake Victoria (5) regions are also considered for climate change impact assessment as shown in Figure 3.1a. The irregular shapes of the five sub-basins were used for analyzing climate change impact at sub-basin scales. BNRB approximately covers an area of 210,000 km^2, which contributes 60% of the average annual flow of the Nile River (Senay et al., 2014). Under a two-domain framework, D1 (2^oE to 57^oE, 20^oS to 37^oN) was set up for NRB at 36 km resolution, and D2 (29^oE to 45^oE, 5^oN to 17.5^oN) was set up for BNRB at 12km resolution, as shown in Figure 3.1b. D1 is much wider than NRB to adequately account for the source of moisture to the basin (i.e. Atlantic and Indian Ocean) and as spatial spin-up.

There are different rainy seasons over NRB, with diverse climate conditions ranging from arid, semi-arid to humid conditions. For example, virtually no precipitation falls in the Sahara Desert of Sudan and Egypt, and little precipitation in the Sahel region of Sudan, but precipitation increases southward to the Ethiopian highland and Equatorial Plateaus, where June-September is the rainy season over the Ethiopian highland. The Equatorial plateaus have

two rainy seasons, October-December and March-May, resulted from the southward and northward movement of ITCZ over the region, respectively. The southern part of NRB also has one rainy season, October-December (Indeje et al., 2000; Endris et al., 2013). Because of the diverse climatic condition, WRF was set up for full-year simulation to account for variations in rainfall pattern over the entire NRB. The mean total annual rainfall for NRB based on the GPCC dataset from 1980-2000 is shown in Figure 3.1b. The mean annual temperature of NRB ranges widely, from 45°C to 16°C (Figure 3.1c), according to the dataset of CRU. The Sahel region has relatively higher temperature, while the Ethiopian highland and Equatorial Plateaus have colder temperature.
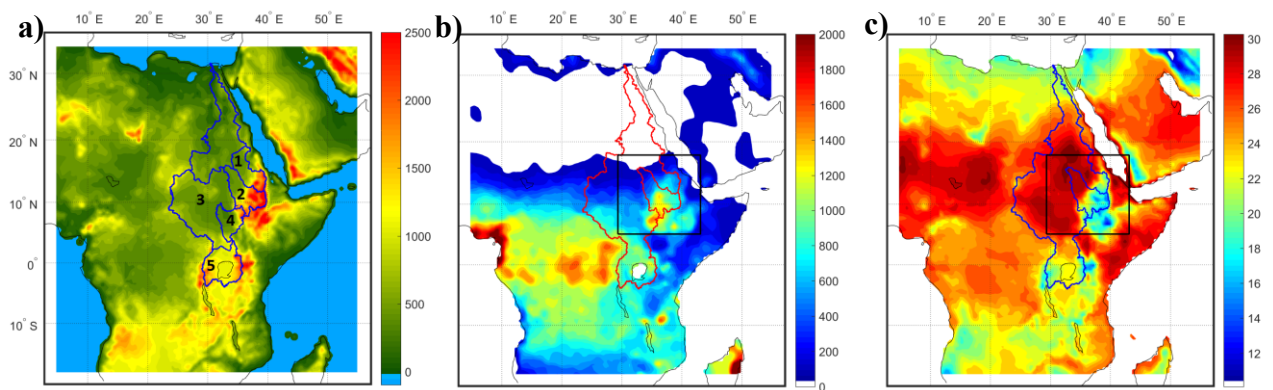
Figure 3.1: (a) The sub-basins considered for this study and the topography in m above sea-level, (b) the two domains configured for WRF (a box in black) and mean annual rainfall distribution over the basin in mm (GPCC data using 1976-2005), and (c) mean annual temperature in $^{\circ}$C (CRU 1976-2005)

Table 3.1: List of indicators considered for this study devised by the ETCCDI (see section 3.2.3). T_{max} and T_{min} refer to daily maximum and minimum temperature, respectively.

ID	Index	Definition	Unit
TX90p	Warm days	number of days in a year with daily T_{max} >90th percentile	days
TN90p	Warm nights	number of days in a year with daily T_{min} >90th percentile	days
TX10p	Cold days	number of days in a year with daily T_{max} <10th percentile	days
TN10p	Cold nights	number of days in a year with daily T_{min} <10th percentile	days
WSDI	Warm spell duration index	number of days in a year with daily T_{max} >90th percentile for six consecutive days	days
CSDI	Cold spell duration index	number of days in a year with daily T_{min} <10th percentile for six consecutive days	days
R20mm	Very heavy precipitation days	Number of days where daily precipitation >20 mm	days
R95p	Very wet days	Annual total precipitation derived from days >95th percentile	mm
R99p	Extremely wet days	Annual total precipitation derived from days >99th percentile	mm
RX1day	Max 1 day precipitation	Annual maximum 1-day precipitation	mm
RX5day	Max 5 day precipitation	Annual maximum consecutive 5-day precipitation	mm

3.2.3. Extreme climate indices

Climate extremes have impacts on the economic, political and well-being of any society. For example, temperature extremes can affect human health, agriculture, and increase forest fire hazards, while precipitation extremes could overwhelm urban drainage systems, cause flooding and costly damage to cities (Patz et al., 2005; Rosenberg et al. 2010; and Anyamba et al., 2014). Using GCMs' RCP climate scenarios that have been dynamically downscaled by WRF, we project future temperature and precipitation extremes of NRB. A list of extreme

indices in Table 3.1 taken from the Expert Team on Climate Change Detection and Indices (ETCCDI) was selected to assess projected changes on future extreme precipitation and temperature events (Klein Tank et al., 2009; Frich et al., 2002; and Alexander et al., 2006). These ETCCDI indices and have been used in other climate change studies (e.g., Gizaw and Gan, 2015; Sillmann et al., 2013a).

3.2.4. Bias correction

RCMs' simulation of temperature and precipitation often show significant biases which need to be corrected. To reduce biases of precipitation and temperature extremes simulated by WRF, quantile-based and linear scaling bias correction methods are applied to reduce the bias, respectively (Teutschbein and Seibert, 2012). Daily precipitation of NRB simulated by WRF was bias corrected using the Climate Hazards Group Infrared Precipitation with Stations (CHIRPS version 2.0, 1981-2005; Funk et al., 2014) datasets of 0.05^o spatial and daily resolutions. The quantile-based bias correction method involves matching the cumulative distribution function (CDF) of the RCM's simulation to the CDF of the observed rainfall. First, the CDF of observed (CHIRPS) and simulated (WRF) precipitation data exceeding 10 mm day^{-1} is developed using a generalized extreme value (GEV) distribution (Equation (3.1)).

$$F(x) = exp\left\{-\left[1 + k\left(\frac{x-\mu}{\alpha}\right)\right]^{-1/k}\right\} \tag{3.1}$$

$$P_c^*(d) = F^{-1}(F(P_c(d)|\alpha_{c,m}, k_{c,m}, \mu_{c,m})|\alpha_{o,m}, k_{o,m}, \mu_{o,m}) \tag{3.2}$$

$$P_s^*(d) = F^{-1}(F(P_s(d)|\alpha_{c,m}, k_{c,m}, \mu_{c,m})|\alpha_{o,m}, k_{o,m}, \mu_{o,m}) \tag{3.3}$$

Using WRF and CHIRPS daily precipitation time series (1981-2005) exceeding 10 mm day^{-1}, the k (shape), α (scale), and μ (location) parameters of a GEV distribution were derived. *c* represents the control period, *o* the observed and *s* the scenarios periods, *d* the day of *P* and *m* the monthly parameters of P. Then, the quantile of the simulated precipitation *P* obtained from the CDF of WRF's simulated precipitation is used to identify the corresponding precipitation (P*) of the CDF of observed precipitation with the same quantile. Therefore, P* is the bias corrected precipitation using this quantile approach represented by Equation (3.2) for control period and Equation (3.3) for projected period.

On the other hand, WRF's daily simulated temperature, $T_c(d)$ or $T_s(d)$, was corrected by a simple, linear scaling approach by adding the difference between the monthly long-term mean observed CRU temperature of 1976-2005 and the corresponding monthly mean of WRF's simulation as represented by Equations (3.4) and (3.5) for the control period and future scenarios, respectively. In this approach, we assume the applied addends are the same between the control and the scenario periods (Teutschbein and Seibert, 2012).

$$T_c^*(d) = T_c(d) + \mu_m\big(T_o(d)\big) - \mu_m(T_c(d)) \tag{3.4}$$

$$T_s^*(d) = T_s(d) + \mu_m\big(T_o(d)\big) - \mu_m(T_c(d)) \tag{3.5}$$

Where, μ_m is the long-term monthly mean temperature of observed and control period data.

3.3. Results and discussions

3.3.1. Validation of WRF model

Figure 3.2 compares the spatial distributions of average annual precipitation difference between observed GPCC data, and that of four GCMs downscaled by WRF (Figure 3.2a), and GCM's raw output data (Figure 3.2b) for 1976-2005. On a whole, GCMs' output downscaled by WRF agrees better with GPCC data (smaller difference) than GCMs' raw output, even though the GCM output of the four GCMs downscaled by WRF still suffers over-simulation for the Congo Basin and the southern boundary, and under-simulation for NRB using the output of ACCESS1-3, in contrast to the raw output of ACCESS1-3 which over-simulated NRB's rainfall.
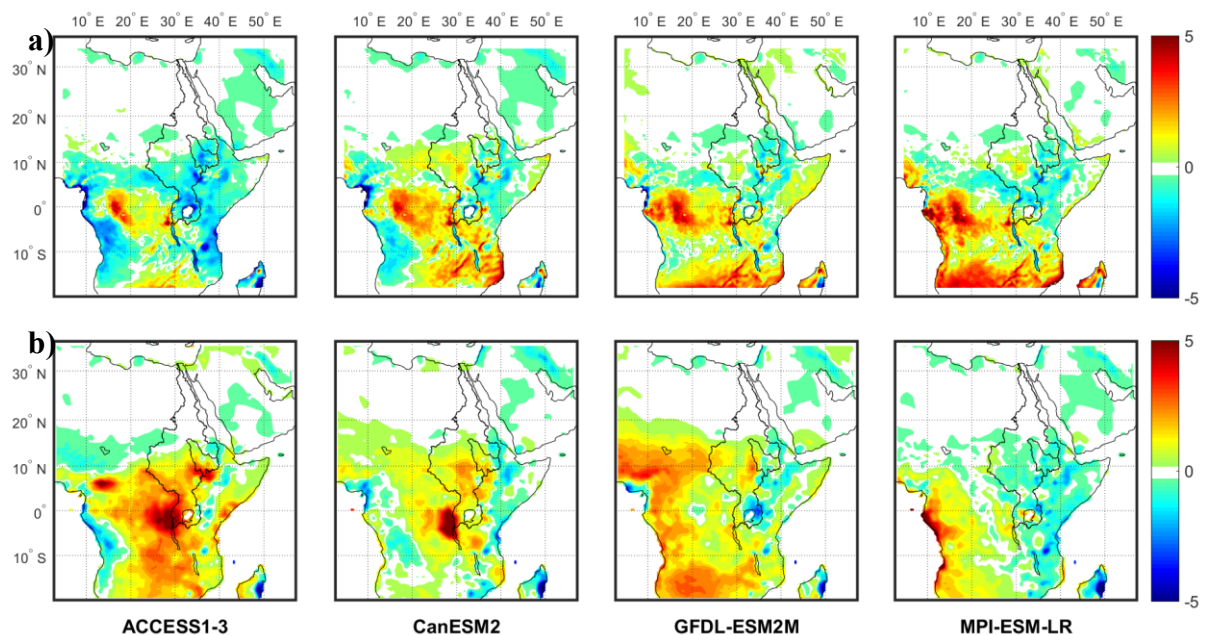
Figure 3.2: Difference in mean annual precipitation (mm/day) between observed GPCC data, and (a) that of four GCMs downscaled by WRF, and (b) GCM's raw output data for 1976-2005.

Figure 3.3 compares the difference between mean annual surface air temperature of the observed CRU data, and that of four GCMs downscaled by WRF (Figure 3.3a), and GCM's raw output data (Figure 3.3b) for 1976-2005. The figure shows that all the GCM's raw output temperature data, except that of ACCESS1-3, agree better with CRU observed surface air temperature than that downscaled by WRF, but the warm biases are very large in some places. In contrast, by downscaling GCMs' raw output, WRF coupled with Noah LSM under-simulated the historical surface air temperature over the Sahara Desert, similar to WRF's simulation when it downscaled the ERA-Interim data over the Sahara Desert (Tariku and Gan, 2017). On the other hand, the NCEP reanalysis data is also similar to WRF's simulation under-simulated the historical surface air temperature over the Sahara Desert when compared with CRU data. Therefore we cannot objectively conclude whether the under-simulation of temperature by WRF over the Sahara Desert is caused by the limitation of WRF or the accuracy of the CRU or NCEP datasets. Even though WRF also under-simulated the temperature over the entire NRB when it downscaled the raw output of GFDL-ESM2M and MPI-ESM-LR, the degree of under-simulation is relatively modest except in the northern part of NRB. In addition, WRF did not under-simulate the raw output of the other two GCMs over NRB. Therefore, unlike the Sahara Desert and the northern part of NRB, WRF can generally simulate the air temperature of NRB reasonably well. However, this systematic temperature bias over the Sahara Desert can still somewhat affect the regional climate simulated by WRF over the northern part of NRB.
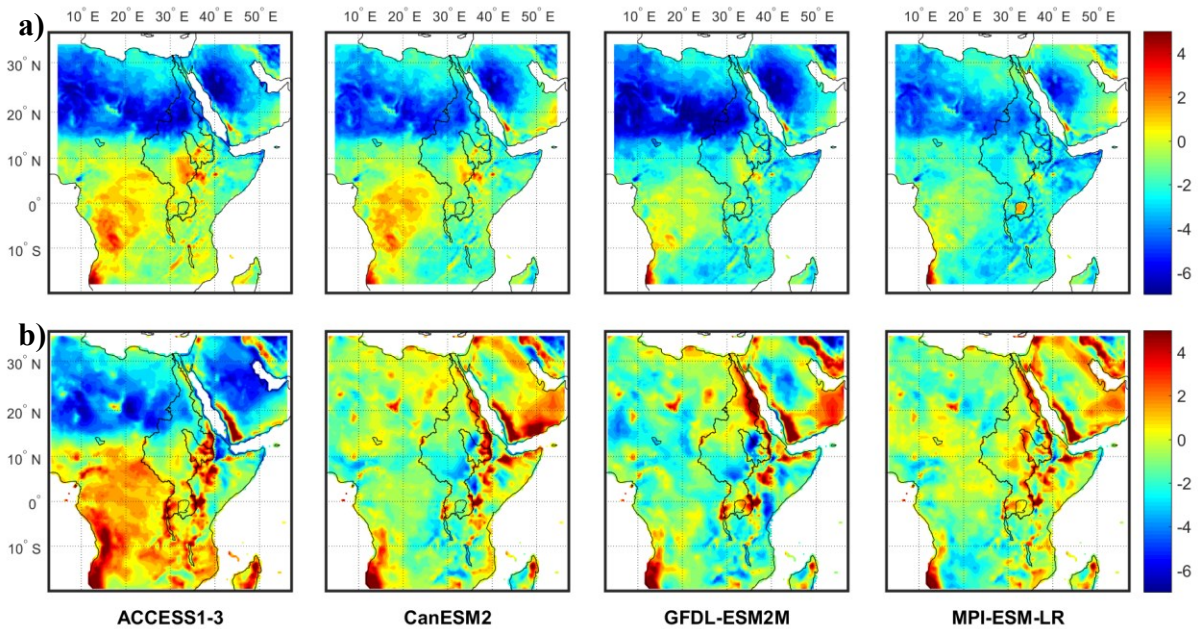
Figure 3.3: Mean annual surface air temperature difference (^{o}C) between CRU data, and (a) that of four GCMs downscaled by WRF, and (b) GCM's raw output data for 1976-2005.

3.3.2. Future mean climate change projections

i. Precipitation change

Figure 3.4 shows the spatial distributions of projected precipitation changes in % for 2050s (climatological mean of 2041-2070 minus the mean of 1976-2005 and divided by the mean of 1976-2005) based on the RCP4.5 (Figure 3.4a) and RCP8.5 (Figure 3.4b) climate scenarios of four GCMs downscaled by WRF. As shown in the figure, results for different GCMs downscaled by WRF are different from each other, sometimes with opposite projected changes over different places of NRB. For instance, the precipitation of NRB is projected to increase when WRF downscaled the RCP 4.5 and 8.5 climate scenarios of ACCESS1-3 and CanESM2. Similarly, a small increase in precipitation in southern NRB is projected when

WRF downscaled climate scenarios of GFDL-ESM2M and MPI-ESM-LR, but the precipitation over northern NRB is projected to decrease. The projected changes in precipitation pattern over the simulation domain under both RCP4.5 and RCP8.5 climate scenarios are relatively consistent, but as expected, projected precipitation changes under RCP8.5 are larger than that under RCP4.5. By 2050s, the annual precipitation of BNRB, *Atbara*, and Sobat river basin, *El Ghazal* and Lake Victoria regions are projected to change by a range of about [-7, 14], [-19, 25.3], [-4, 37], [-5.9, 19.5], and [3.6, 22.4] for RCP4.5 scenarios, and [-6.3, 14.2], [-16.7, 25], [-7, 39], [-4.9, 23], and [4.6, 27] for RCP8.5 scenarios, respectively. Overall, the ranges of projected change in precipitation over each sub-basin are almost the same under RCP4.5 and RCP8.5.
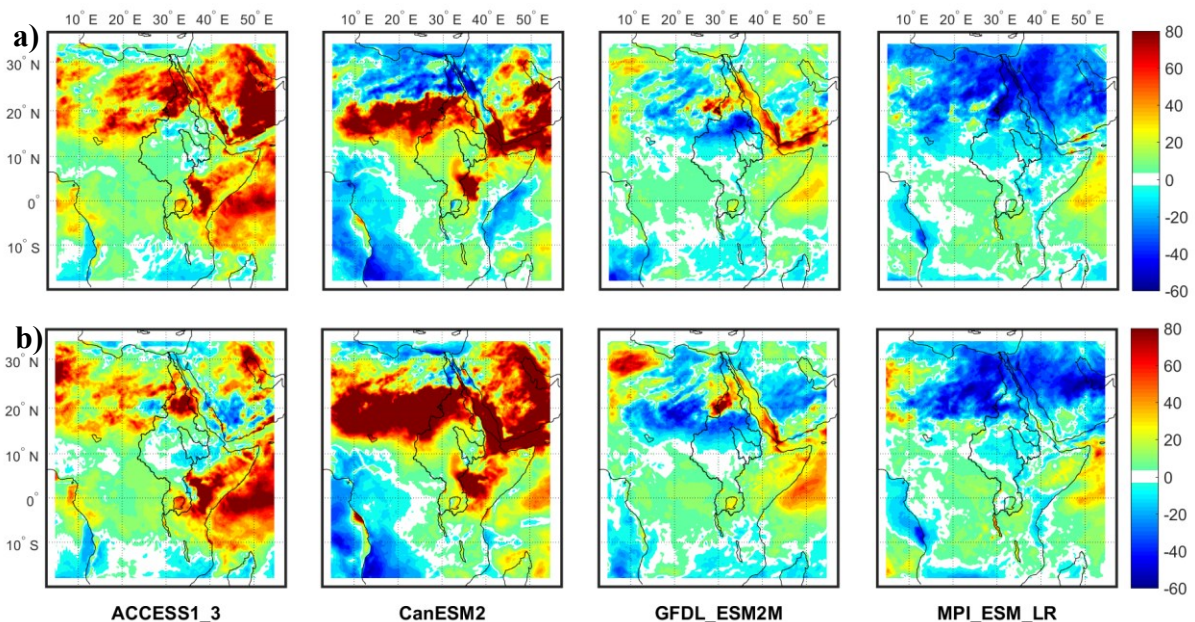
Figure 3.4: Projected precipitation change in % (mean of 2041-2070 minus the mean of 1976-2005 and divided by the mean of 1976-2005) based on (a) RCP 4.5 and (b) RCP 8.5 climate scenarios of four GCMs downscaled by WRF.

The projected precipitation changes in % over NRB for 2080s (mean of 2071-2100 minus the mean of 1976-2005 and divided by the mean of 1976-2005) downscaled by WRF from four GCMs under RCP4.5 and RCP8.5 climate scenarios are shown in Figure 3.5a and Figure 3.5b, respectively. As shown in Figure 3.5, the projected precipitation change is generally higher in 2080s as compared to the 2050s. However, projected changes in precipitation patterns over the simulation domain as well as discrepancies between GCM's projections remain similar between 2050s and 2080s. Overall, the mean precipitation of NRB is projected to increase over the southern basin, such as the Equatorial Plateau regions, and either a decrease or no change over the Sahel region of NRB, but the projected change will be larger in the 2080s as compared to the 2050s. By 2080s, the annual precipitation of BNRB, *Atbara*, and Sobat river basin, *El Ghazal* and Lake Victoria regions are projected to change by a range of about [-9, 18.6], [*-20.7, 34.6]*, [0, 41.3], [*-7.3, 24.7]*, and [5.6, 26.8] for RCP4.5 climate scenarios, and [-14, 25], [*-22.5, 39]*, [-4.7, 60.4], [*-11, 31]*, and [11.8, 41] for RCP8.5 scenarios, respectively. On a whole, the Lake Victoria regions will most likely experience an increase in precipitation under both climate scenarios but other regions could experience a wide range of change from a decrease to a major increase in precipitation. The projected changes in precipitation over each sub-basin of NRB between the four GCMs downscaled by WRF for 2050s and 2080s periods under RCP4.5 and RCP8.5 climate scenarios are presented in Figure 3.8, where the median shows a projected increase in precipitation all sub-basins of NRB.
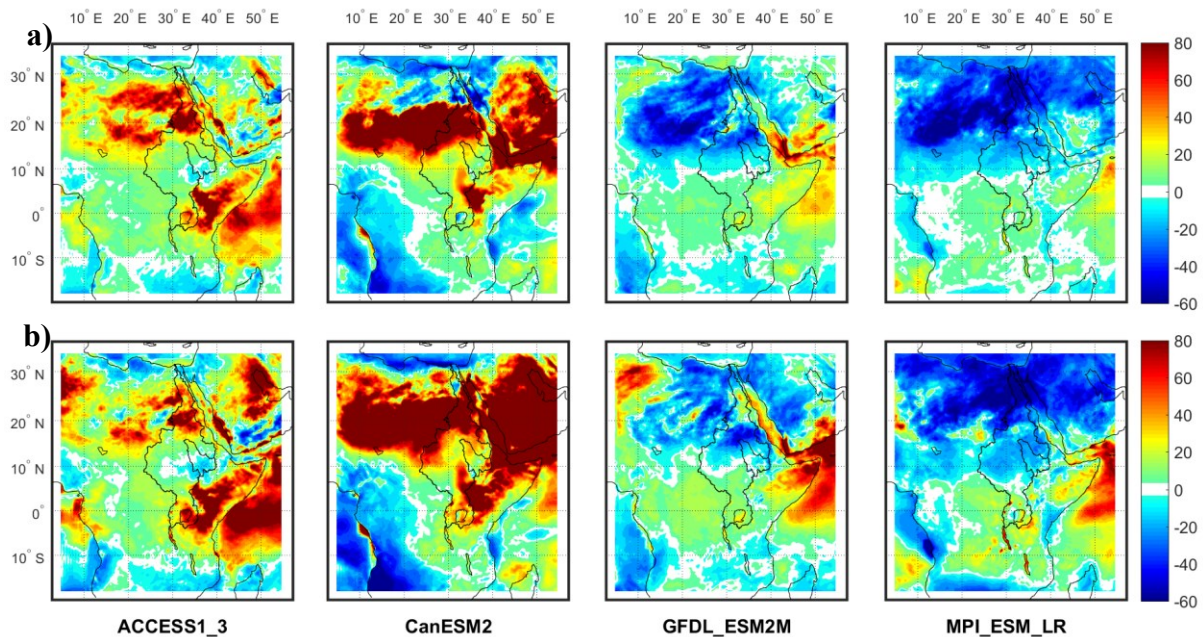
Figure 3.5: Projected precipitation change in % (mean of 2071-2100 minus the mean of 1976-2005 and divided by the mean of 1976-2005) based on (a) RCP 4.5 and (b) RCP 8.5 climate scenarios of four GCMs downscaled by WRF.

Previous climate change studies on the seasonal precipitation of NRB or its sub-basins based on SRES (Special Report on Emission Scenarios) climate scenarios also find the projections of GCMs to differ from each other in terms of directions and magnitudes of precipitation change, such as Kim et al. (2009), and Beyene et al. (2010). The projected changes in precipitation of NRB in this study based on RCP scenarios of four GCMs are similar with that of Beyene et al. (2010) even though they used SRES climate scenarios (A2 and B1) of 11 GCMs of the 4th IPCC (2007) assessment report for NRB. These 11 GCMs projected a wide range precipitation change in terms of magnitude, direction, and seasons, e.g., the DJF precipitation change ranges from -40 to 18%, and JJA precipitation change ranges from -42 to

15% in 2080s relative to 1950-1999 baseline for the entire NRB under A2 emissions scenario. Using six GCMs' output under A2 emission scenarios for 2050s relative to the 1961-1990 baseline, Kim et al. (2009) found projected changes in the mean annual precipitation over the upper BNR range between -11% and 44% with an average change of 11%. Elshamy et al. (2009) also found no consensus on the direction of projected precipitation change between 17 GCMs under the A1B scenario for 2081-2098 compared to the1961-1990 baseline over the upper BNR, e.g., the projected change in annual precipitation range between -15% and 14%, with 10 GCMs projected a decrease while 7 GCMs projected an increase in precipitation, of which 6 GCMs projected small changes within 5%.

ii. Change in temperature

The projected change in the mean surface air temperature based on RCP4.5 and RCP8.5 climate scenarios of four GCMs downscaled by WRF are shown in Figure 3.6 and Figure 3.7 for 2050s (2080s) which are mean of 2041-2070 (2071-2100) minus the mean of 1976-2005, respectively. Both figures show that the surface air temperature is projected to increase across the simulation domain in both RCP4.5 and RCP8.5 climate scenarios for 2050s and 2080s, and as expected, the projected temperature changes are higher under RCP8.5 than under RCP4.5 scenarios, and also higher in the 2080s than 2050s. Furthermore, the projected temperature changes over the NRB are more significant when WRF downscaled climate scenarios of ACCESS1-3 and CanESM2 than other two GCMs. However, spatial patterns of projected changes in surface air temperature are similar over the NRB under both climate scenarios.
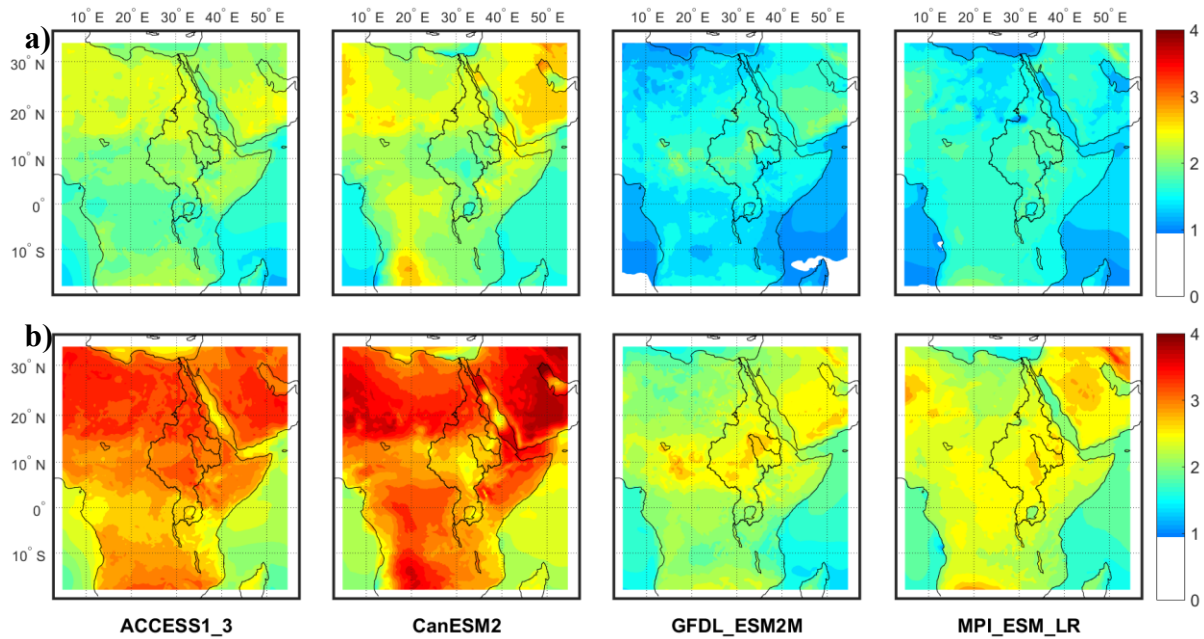
Figure 3.6: Projected mean surface air temperature change in °C (mean of 2041-2070 minus the mean of 1976-2005) based on (a) RCP 4.5 and (b) RCP 8.5 climate scenarios of four GCMs downscaled by WRF.
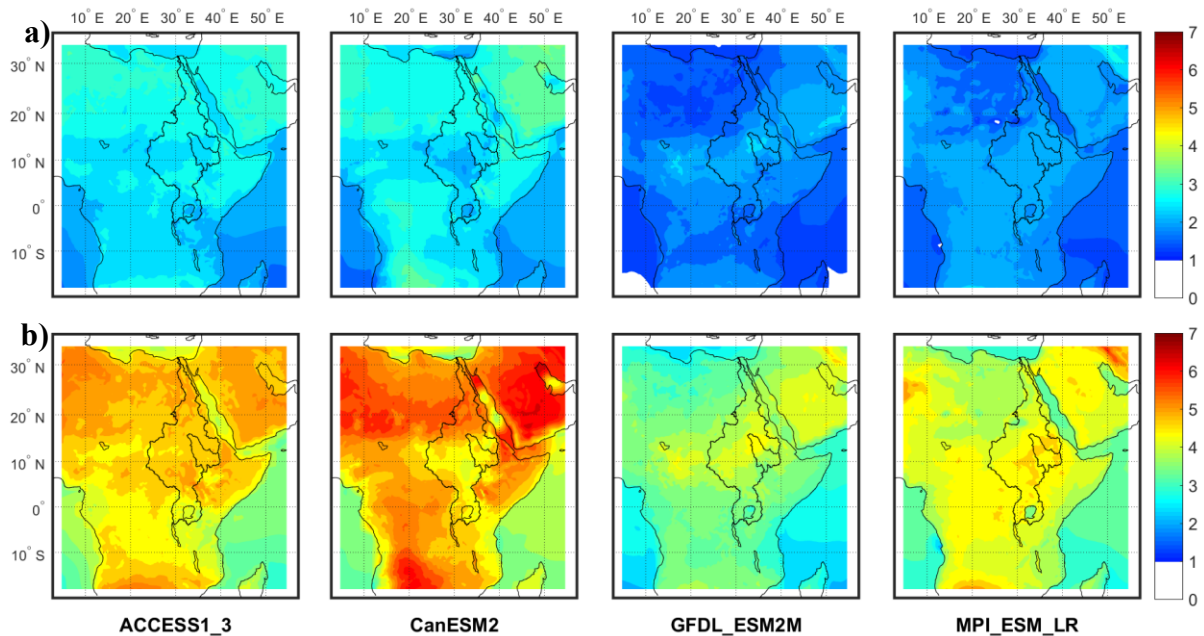
Figure 3.7: Projected mean surface air temperature change in °C (mean of 2071-2100 minus the mean of 1976-2005) based on (a) RCP 4.5 and (b) RCP 8.5 climate scenarios of four GCMs downscaled by WRF.

According to RCP4.5 climate scenarios, the air temperature of the five sub-basins of NRB are projected to increase by about 1.67 – 2°C for 2050s and 2 – 2.5^{o}C for 2080s, while under the RCP8.5 climate scenarios, it is projected to increase by about 2.5 – 3°C and 3.9 – 4.6^{o}C in the 2050s and 2080s, respectively. The results are consistent with that of previous studies, such as Beyene et.al. (2010) who from using 11 GCMs' output found a projected temperature increase by 3.4 – 5.9^{o}C and 3 – 4.1^{o}C across the NRB in the late 21st century (2070-2099) relative to the 1950-1999 for A2 and B1 scenarios, respectively. Kim et al. (2009) projected the mean annual temperature to increase from 1.4^{o}C to 2.6^{o}C with an average change of 2.3^{o}C over the upper BNR for 2050s relative to the 1961-1990 for A2 emission scenario. Elshamy et al. (2009) also projected the annual surface temperature to increase over the upper Blue Nile of 2°C to 5°C at the end of the 21st century under the A1B scenario compared to the1961-1990 baseline. IPCC (2014) also concluded that the projected surface temperature is very likely to rise by 3°C - 6°C across the different regions of Africa by the end of the 21st century under RCP8.5 relative to the 1986-2005 baseline. Furthermore, Figure 3.8 show the projected changes in the surface air temperature over sub-basins of NRB based on RCP4.5 and RCP8.5 climate scenarios of four GCMs downscaled by WRF for 2050s and 2080s periods are consistent across the basins, that the surface air temperature is expected to increase in all sub-basins.
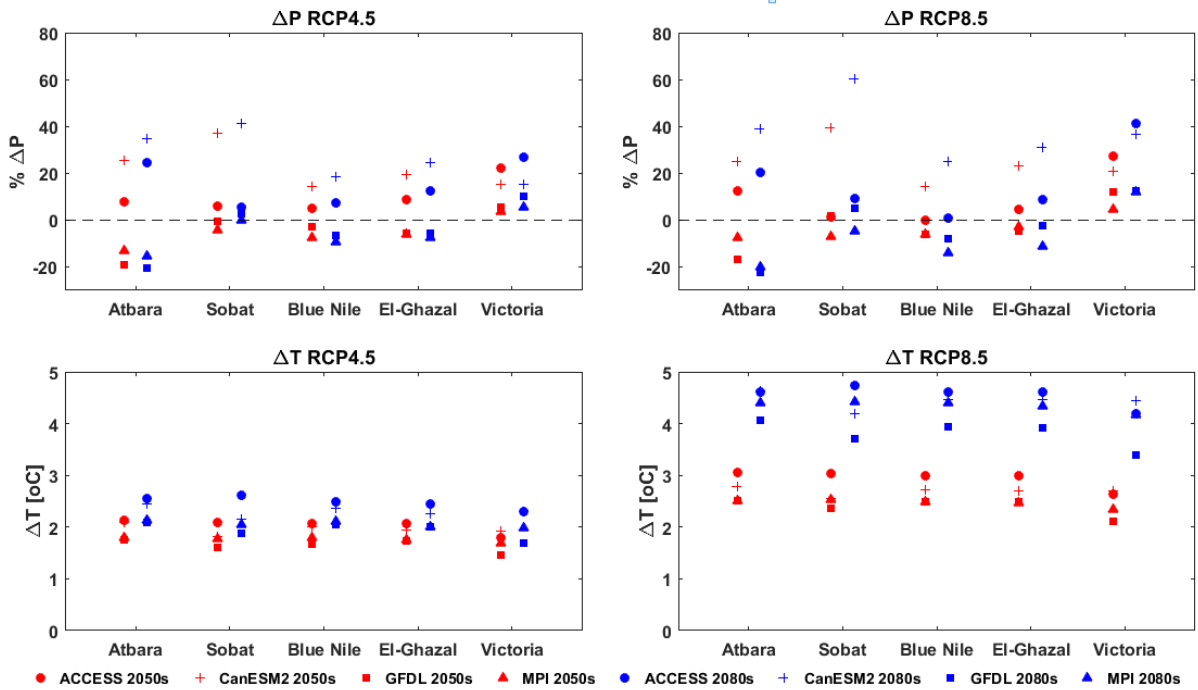
Figure 3.8: The projected changes to annual total rainfall and surface air temperature of Atbara, Sobat, and Blue Nile river basin, and EL Ghazal and Lake Victoria regions with respect to the base period (1976-2005) derived from the projections of RCP4.5 and RCP8.5 climate scenarios of four GCMs downscaled by WRF.

The above comparison shows differences between the future precipitation and temperature of NRB downscaled by WRF from the same climate scenarios of different GCMs, and from the same GCMs for different climate scenarios. These results also show that projections of precipitation are more uncertain than temperature projections.

3.3.3. Change in precipitation extremes

a. R20mm index

The R20mm index is the number of days in a given period that the daily precipitation exceeded 20mm. As shown in Table 3.2, the ensemble mean and standard deviation of the change in R20mm index computed from four GCMs under RCP4.5 and RCP8.5 for 2050s and 2080s relative to the control period downscaled by WRF vary widely. For most of NRB's sub-basins, the R20mm index is projected to increase in two GCMs (ACCESS1-3 and CanESM2) but decrease in the other two GCMs (GFDL-ESM2M and MPI-ESM-LR). However, on a whole the ensemble mean under RCP4.5 and RCP8.5 scenarios of all GCMs analysed compared with the control period, the annual R20mm is projected to increase by a range of 2.5–77.5% for all sub-basin in the 2050s and 2080s, except for the Atbara river basin where it is projected to decrease by 0.8–1.9% in 2050s and then to increase by 0.9–1.4% in 2080s. The Lake Victoria region is projected to undergo a larger change in the R20mm, ranging from 36 up to 77.5% as compared with other basins. The R20mm index is projected to be higher under RCP8.5 than under RCP4.5 scenarios in both 2050s and 2080s, and higher in the 2080s than in the 2050s. Overall, NRB is projected to experience more very heavy precipitation in the mid-and late 21st century. The standard deviations of regional projections of R20mm index for the sub-basins are much higher than their mean projected changes, which show a large variation in very heavy precipitation projections among the GCMs.

Table 3.2: The projected mean and standard deviation changes (%) to the R20mm, RX5day and P30yr index of Atbara, Sobat, and Blue Nile river basin, and El Ghazal and Lake Victoria regions with respect to the base period (1976-2005) derived from four GCMs under the RCP4.5 and RCP 8.5 scenarios downscaled by WRF

	R20mm				RX5day				P30yr			
	RCP4.5		RCP8.5		RCP4.5		RCP8.5		RCP4.5		RCP8.5	
	2050	2080	2050	2080	2050	2080	2050	2080	2050	2080	2050	2080
Atbara												
Mean	-1.9	1.4	-0.8	0.9	-0.3	8.8	5.6	10.8	15.3	27.8	19.7	40.7
STD	20.7	21.5	16.5	26.3	12.0	8.0	3.4	14.7	4.9	2.5	6.9	13.1
Median	**-3.4**	0.7	-1.1	-1.1	0.3	**7.7**	7.0	7.1	14.8	**28.7**	17.8	**36.6**
Sobat												
Mean	18.4	22.6	18.8	40.4	10.5	9.7	12.8	27.3	27.8	44.9	27.0	53.2
STD	32.5	37.0	39.9	57.2	5.7	22.4	27.6	37.1	9.6	12.6	10.9	18.8
Median	4.5	5.4	1.7	**13.6**	11.5	5.2	0.8	**12.7**	24.1	**42.4**	25.8	**47.4**
Blue Nile												
Mean	3.3	3.8	2.4	6.0	3.4	6.3	6.2	14.0	17.2	28.2	18.3	35.7
STD	14.0	16.6	17.0	26.6	8.4	10.6	7.1	9.6	4.5	10.0	7.7	13.4
Median	-0.04	-2.89	-4.59	**-5.04**	1.0	4.4	6.2	**15.0**	16.5	27.1	18.9	**34.6**
El Ghazal												
Mean	13.0	19.0	15.8	27.8	3.0	9.4	13.5	15.3	22.6	41.0	26.7	47.2
STD	29.7	30.6	27.5	39.9	15.9	17.5	24.3	21.0	9.5	18.5	16.2	27.0
Median	3.4	8.7	3.3	**12.7**	6.5	6.4	**8.7**	6.7	22.7	**38.8**	22.4	**37.9**
Lake Victoria												
Mean	36.1	44.1	45.8	77.7	14.4	16.0	19.5	28.2	28.8	48.0	34.7	59.7
STD	20.1	23.7	20.9	36.1	10.4	12.7	9.0	10.2	12.2	23.7	12.8	18.5
Median	37.6	44.1	47.3	**76.8**	12.5	11.6	17.6	**29.5**	23.8	38.5	29.8	**53.7**

* Values in bold show significant changes compare to the base period

b. R95p and R99p indices

R95p and R99p are the annual total amount of precipitation for days when the daily precipitation is greater than the 95th and the 99th percentile precipitation, respectively. Figure 3.9 shows that median values of R95p and R99p of four GCMs under RCP4.5 and RCP8.5 downscaled by WRF are projected to increase in the 2050s and 2080s, relative to the base period for all sub-basins, but the mean projected change varies between the sub-basins. There is a large discrepancy between GCMs' downscaled projections for R95p and R99p. For most sub-basins, a decrease in R95p and R99p is projected by downscaled climate scenarios of MPI-ESM-LR (except Lake Victoria region) and GFDL-ESM2M (except Sobat and Lake Victoria regions), but an increase based on downscaled projections of CanESM2 and ACCESS1-3 (except BNRB). The range of mean projected change in R95p and R99p for all sub-basins considered is 0.75 – 55% and -13 – 90%, respectively. R95p and R99p of the Sobat river basin are projected to increase more than other sub-basins, by 21-55% and 29-90% for both 2050s and 2080s, respectively. This means that extreme precipitation events occurring in very wet and extremely wet days could be substantially more intensive over NRB in 2050s and 2080s.
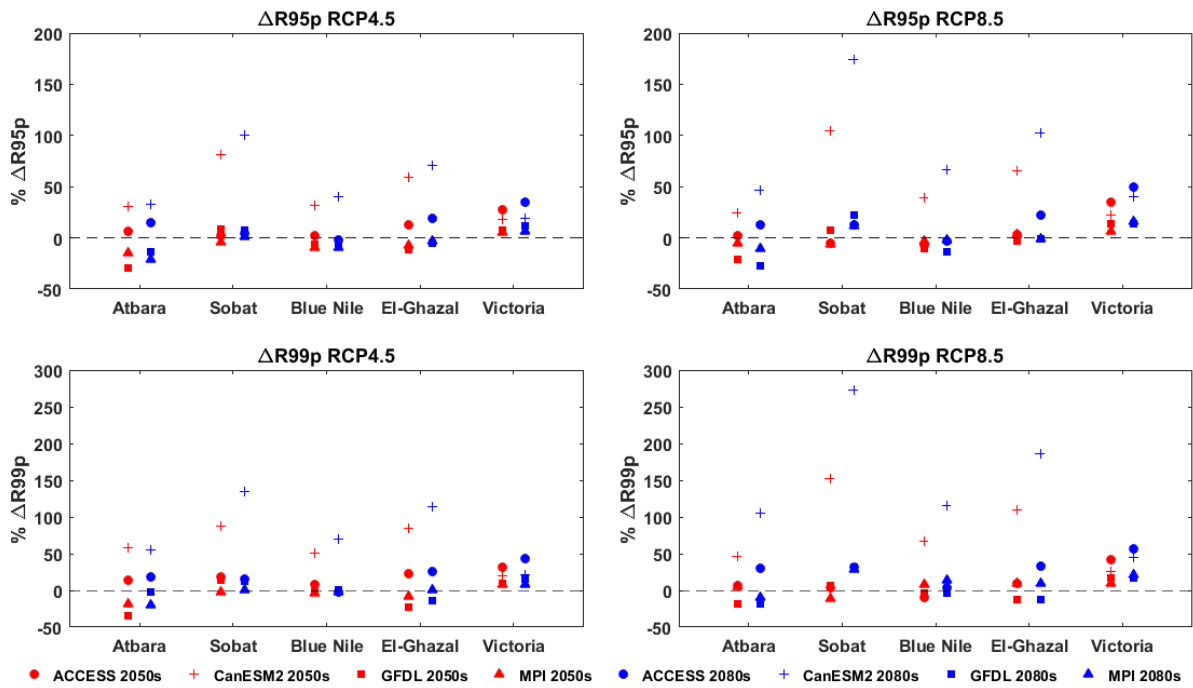
Figure 3.9: The projected changes to the R95p and R99p index of Atbara, Sobat, and Blue Nile river basin, and EL Ghazal and Lake Victoria regions with respect to the base period (1976-2005) derived from the projections of RCP4.5 and RCP8.5 climate scenarios of four GCMs downscaled by WRF.

c. RX1day and RX5day

RX1day and RX5day are indices that represent the maximum 1-day precipitation and maximum 5-day precipitation within a given period. Figure 3.10 and Table 3.2 show a predominantly projected increase in RX1day and RX5day in 2050s and 2080s relative to control period, as simulated by WRF driven with RCP4.5 and RCP8.5 climate scenarios of four GCMs, with an average range of 1 – 40% and -0.3 – 28% for all sub-basins, respectively.

The standard deviations of both indices for the sub-basins derived from downscaled climate scenarios of the GCMs show a large variation. Among the five sub-basins of NRB, the Lake Victoria region is projected to experience the largest increase in RX1day (20 – 40%) and RX5day (15 – 29%). This implies that with reference to the control period, more intensive extreme daily precipitation (maximum daily precipitation events) is projected over NRB in the mid- and late 21st century, especially in the Lake Victoria region.
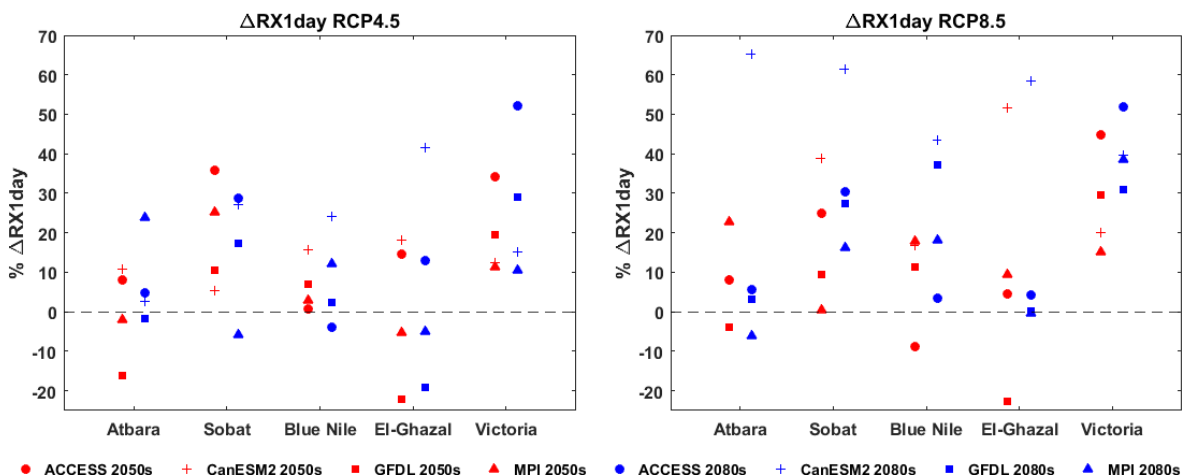
Figure 3.10: The projected changes to the RX1day index of Atbara, Sobat, and Blue Nile river basin, and El Ghazal and Lake Victoria regions with respect to the base period (1976-2005) derived from the projections of RCP4.5 and RCP 8.5 climate scenarios of four GCMs downscaled by WRF.

d. P30yr

The P30yr index is the daily rainfall intensity of 30-year return period for the base period, 2050s and 2080s (Chen and Knutson, 2008; Gizaw and Gan, 2015) estimated using a GEV distribution. The change in P30yr between the base period and that of 2050s and 2080s under

RCP4.5 and RCP8.5 scenarios represent how daily storm intensities are projected to change in NRB. Unlike other indices, all GCMs project a consistent increase in P30yr by 15 – 60% across all NRB sub-basins under RCP4.5 and RCP8.5 for 2050s and 2080s as shown in Table 3.2. This suggests that the daily rainfall intensity for future storm events of 30-year return period over the NRB is projected to increase. Again, the Lake Victoria region is projected with the largest increase in P30yr than other sub-basins.

Previous studies on climate change impact to extreme precipitation globally, NRB or its sub-basins also found an increase in observed and/or projected extreme precipitation indices, such as Alexander et al. (2006); Omondi et al. (2014); Sillmann et al. (2013a, &b) and Kharin et al. (2013). Alexander et al. (2006) investigated observed changes in daily temperature and precipitation extremes from a global station dataset for 1951-2003, detected a general increase in extreme precipitation indices such as RX1day, RX5day over the Northern Hemisphere and parts of Australia. However, their analysis did not include the NRB because of a lack of data. Contrary to the global results of Alexander et al. (2006), Omondi et al. (2014) found that extreme precipitation indices over most stations of Greater Horn of Africa (GHA) have decreased, but these trends are not statistically significant over 1961-2010. In a few cases, they detected increasing trends in precipitation indices that are statistically significant. Sillmann et al. (2013b) analyzed projected changes of CMIP5 GCMs in climate extremes indices on global and regional scales for the late 21st century relative to the reference period, 1981-2000. They found that the global land average RX5day is projected to increase by 20%, 10% and 6% according to RCP8.5, RCP2.6 and RCP4.5 climate scenarios, respectively. For

East Africa, based on RCP8.5, RX5day is projected to increase by 20-30%, and R10mm and R95p are also projected to increase which means East Africa is projected to become wetter in the future. In the CMIP5 multi-model analysis, Kharin et al. (2013) also found that the global average annual precipitation of 20-year return period is projected to increase by about 6% under RCP2.6, 10% under RCP4.5 and more than 20% under RCP8.5 by the end of the 21st century, respectively.

3.3.4. Change in temperature extremes

a)   *TN10p and TX10p indices*

TN10p and TX10p indices represent the % of days with T_{min} and T_{max} that are less than the historical 10th percentile value, respectively. All NRB sub-basins are projected to experience substantial decrease in TN10p and TX10p for both RCP4.5 and RCP8.5 climate scenarios in 2050s and 2080s as shown in Table 3.3. Again, for both TN10p and TX10p, the largest changes are projected to occur over the Lake Victoria region, such that the 10th percentile TN and TX observed over 1976-2005 is projected to decrease to less than 1% (e.g., almost no cold night or days), while relatively small changes are projected for Atbara river basin and El Ghazal regions. The projected decrease in the % of days is more pronounced for TN10p than for TX10p, for RCP8.5 than RCP4.5, and for 2080s than 2050s. This implies that NRB is expected to experience warmer cool nights and days in the future than observed during the control period. The standard deviations of both indices are much smaller than the projected change for the sub-basins, which demonstrate that NRB is consistently projected to become warmer, with relatively minor variations between projections of GCMs.

Table 3.3: The mean and standard deviation (STD) based on four GCMs ensemble, temperature extreme indicators over the sub-basins of Nile River, the percent of days above 90th or below 10th percentile of 1976-2005, historical and the projected change for 2041-2070 and 2071-2100 under RCP4.5 and RCP8.5 scenarios. All units are in %days/year, WSDI and CSDI are in days/year

	Atabra		Baro		Blue Nile		El Ghazal		Lake Victoria	
TN10p	Mean	STD	Mean	STD	Mean	STD	Mean	STD	Mean	STD
Historical	9.9	0.0	9.8	0.0	9.9	0.0	9.9	0.0	9.9	0.014
RCP4.5_2050	1.3	0.4	0.6	0.1	0.8	0.2	1.3	0.3	0.4	0.1
RCP4.5_2080	1.0	0.3	0.4	0.1	0.5	0.2	1.0	0.3	0.2	0.1
RCP8.5_2050	0.9	0.3	0.5	0.4	0.6	0.3	0.8	0.3	0.1	0.1
RCP8.5_2080	0.2	0.1	0.1	0.0	0.1	0.0	0.2	0.1	0.0	0.0
TX10p										
Historical	9.8	0.0	9.8	0.0	9.8	0.0	9.8	0.0	9.9	0.0
RCP4.5_2050	2.3	0.4	2.2	0.6	2.0	0.6	2.4	0.5	1.2	0.5
RCP4.5_2080	1.6	0.3	1.6	0.4	1.3	0.4	1.8	0.4	0.8	0.3
RCP8.5_2050	1.5	0.5	1.2	0.3	1.1	0.4	1.4	0.3	0.6	0.3
RCP8.5_2080	0.4	0.1	0.4	0.1	0.3	0.1	0.4	0.1	0.1	0.1
TN90P										
Historical	9.7	0.0	9.9	0.0	9.8	0.0	9.8	0.0	9.9	0.01
RCP4.5_2050	55.9	4.5	68.1	6.3	63.1	5.2	58.3	2.2	71.4	7.03
RCP4.5_2080	63.4	5.3	76.6	6.1	71.0	5.2	63.2	1.9	79.6	7.24
RCP8.5_2050	69.9	3.4	82.7	3.6	76.7	3.1	69.4	1.4	85.6	4.07
RCP8.5_2080	86.6	1.8	95.3	1.0	91.7	0.9	83.0	0.7	97.8	1.29
TX90P										
Historical	9.8	0.0	9.8	0.0	9.8	0.0	9.8	0.0	9.8	0.0
RCP4.5_2050	45.2	2.0	52.8	9.2	48.0	5.4	43.6	4.2	54.5	4.9
RCP4.5_2080	52.0	2.2	59.9	11.3	56.4	5.2	50.1	5.0	61.9	7.0
RCP8.5_2050	58.8	2.7	68.1	9.8	64.1	5.4	58.1	5.3	68.6	5.8
RCP8.5_2080	78.7	2.3	86.7	5.4	84.5	3.0	79.0	3.9	87.8	4.6
WSDI										
Historical	1.0	0.1	1.2	0.1	1.0	0.1	1.1	0.1	1.0	0.1
RCP4.5_2050	8.8	0.2	9.4	1.2	9.1	0.8	8.6	0.7	8.9	1.1
RCP4.5_2080	9.5	0.2	9.7	0.9	9.8	0.5	9.7	0.8	9.4	1.3
RCP8.5_2050	9.9	0.3	9.7	0.4	10.0	0.3	10.4	0.6	9.2	1.2
RCP8.5_2080	8.8	0.6	7.8	1.5	8.3	1.1	9.4	1.1	6.7	0.7
CSDI										
Historical	0.89	0.06	0.72	0.06	0.83	0.07	0.84	0.05	0.65	0.08
RCP4.5_2050	0.06	0.04	0.02	0.01	0.04	0.01	0.08	0.04	0.01	0.01
RCP4.5_2080	0.03	0.03	0.01	0.01	0.02	0.01	0.06	0.03	0.00	0.00
RCP8.5_2050	0.06	0.08	0.05	0.08	0.05	0.07	0.05	0.04	0.00	0.00
RCP8.5_2080	0.00	0.00	0.00	0.00	0.00	0.00	0.00	0.00	0.00	0.00

b)   TN90p and TX90p indices

TN90p and TX90p indices, also referred to as warm nights and warm days, represent the % of days with T_{min} and T_{max} that are greater than the historical 90th percentile value, respectively. Warm nights and days are projected to generally increase in the mid and late 21st century for all sub-basins of NRB, as shown in Table 3.3. In all the sub-basins considered, at least 48% and 55% (or more) of the number of days in 2041-2070, and at least 50% and 80% (or more) of number of days in 2071-2100 are projected to have T_{max} and T_{min} that exceed the historical 90th percentile values, respectively. The projected increase is more pronounced for TN90p than TX90p.

The standard deviations of both indices are much smaller than the projected change for the sub-basins, which again shows that NRB is consistently projected to become warmer, with relatively minor variations between projections of GCMs. The projected increase in TN90p and TX90p show that NRB is expected to experience more warm nights and days in the mid- and late 21st century.

c)   WSDI and CSDI

WSDI and CSDI, the warm spell duration and the cold spell duration indices, are annual counts of at least six consecutive days with T_{max} greater than the historical 90th percentile value and with T_{min} less than the historical 10th percentile value, respectively. Table 3.3 shows that there will be virtually no cold spell expected at the end of the 21st century, but the warm spell is projected to increase compared with the historical 1976–2005 periods.

Previous studies on climate change impact to extreme temperature also found that observed and/or projected have increased or decreased in warm/cold temperature extremes indices, such as Alexander et al. (2006); Omondi et al. (2014); Sollimann (2013a, &b) and Kharin et al. (2013). Alexander et al. (2006) detected a global decrease in TN10p and TX10p, and an increase in TN90p and TX90p over 1951-2003. Omondi et al. (2014) found an increase in warm extreme and a decrease in cold extreme, temperature for GHA over 1961- 2010. Sillmann et al. (2013b) also found that the global land average cold spell duration is projected to decrease while the warm spell duration is projected to increase in all RCP climate scenarios. The TN10p are projected to decrease from about 10% in 1961-1990 to 3%, 1.5% and 0.3% by the end of 21st century under RCP2.6, RCP4.5 and RCP8.5, respectively. The TX10p are projected to decrease to 4%, 2% and 0.7% under RCP2.6, RCP4.5 and RCP8.5, respectively. The median in TN90p (median in TX90p) is projected to increase over the global land from about 10% in the baseline period to 69% (62%) under RCP8.5, and to 44% (39%) under RCP4.5 by the end of the 21st century, respectively. Kharin et al. (2013) also found that the projected global annual cold extremes (warm extremes) of 20-year return period will become warmer by 1.5 (0.8) ^{o}C, 2.4 (1.7) ^{o}C, and 4.9 (3.8) ^{o}C by the end of the 21st century under RCP2.6, RCP4.5 and RCP8.5, respectively.

Spatial distributions of some of the above extreme precipitation and temperature indices are presented in the Appendix 3.A. These plots show a projected higher increase in extreme precipitation indices, a projected higher decrease in cold or a higher increase in warm

temperature indices over southern NRB (headwater of NRB) than over northern NRB, but the projected changes vary between four GCMs of CMIP5.

3.3.5. Changes in air temperature and precipitable water

According to the Clausius–Clapeyron relationship, the saturation vapor pressure will increase by about 7% for every 1°K rise in temperature (Boer, 1993). Therefore as climate warms, a warmer atmosphere will have a larger capacity to hold more water vapour, which fuel more evaporation, and generate more precipitation (Houghton, 2009). In other words, global warming can potentially cause future extreme storm events to occur more frequently and in greater severity. Therefore in this section, we will discuss how precipitable water will change in response to temperature change.

Figure 3.11 shows spatially averaged, 2m annual air temperature anomaly time series for BNRB based on the RCP4.5 and RCP8.5 climate scenarios dynamically downscaled by WRF. Shaded blue and red plots represent the range of temperature/precipitable water projected for 2041-2100 by WRF driven by four GCMs based on RCP4.5 and RCP8.5 scenarios, respectively. The temperature anomaly time series simulated shows consistent increasing trends, which imply that BNRB is projected to become increasingly warmer over the mid and late 21st Century. In 2041-2100, under RCP4.5 climate scenarios of the four GCMs, the projected rates of increase in air temperature for BNRB estimated from the Theil-Sen estimator (Sen, 1968) ranges between 0.006 and 0.017°C/year, with an average of 0.012 °C/year, and between 0.041 and 0.06 °C/year, with an average of 0.052 °C/year under RCP8.5 climate scenarios. Initially RCP4.5 and RCP8.5 scenarios project similar range of temperature

increase in the BNRB, but in the 2080s, the RCP8.5 projects a higher increase in air temperature than RCP4.5. Based on the Mann-Kendall trend test at a 0.05 significance level, the increasing trends of 2m air temperature anomaly time series over 2041-2100 are statistically significant.
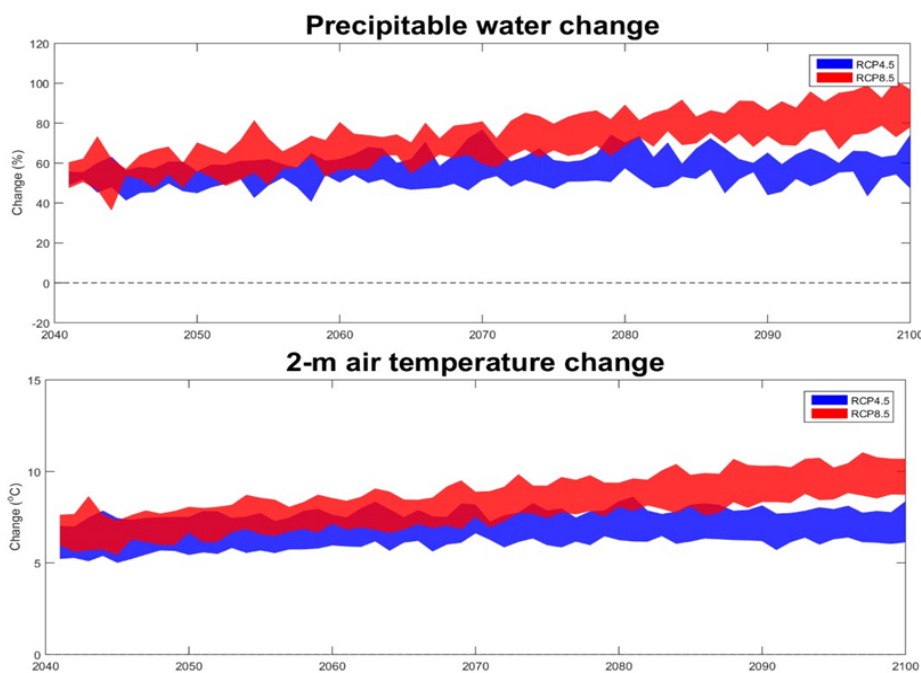
Figure 3.11: The projected changes to the precipitable water and 2m surface air temperature for Blue Nile river basin with respect to the base period (1976-2005) derived from the projections of RCP4.5 and RCP 8.5 scenarios of four GCMs downscaled by WRF.

The precipitable water is the depth of water vapour integrated over the entire column of the atmosphere. The spatially averaged annual precipitable water anomaly time series projected for BNRB also consistently show increasing trends similar to the projected 2m air temperature trends, as shown in Figure 3.11. In 2041-2100, under RCP4.5, the projected rate of increase in precipitable water ranges from 0.04 to 0.155 %/year, with an average increase of 0.11 %/year,

and under RCP8.5, a projected increase of 0.428 – 0.658 %/year, with an average increase of 0.561 %/year. The increasing trends of precipitable water over 2041-2100 are also statistically significant based on the Mann-Kendall's test at a 0.05 significance level. A similar increasing trend, but of different rate of increase for temperature and precipitable water are projected for other sub-basins of NRB considered in this study.

3.4.   Summary and conclusions

The potential impact of climate change on the future mean annual and extreme precipitation, and temperature of the Nile river basin in the 2050 and 2080s was investigated using RCP4.5 and RCP8.5 climate scenarios of four GCMs of CMIP5 dynamically downscaled by a regional climate model called WRF. As expected, precipitation projections using downscaled RCP scenarios of four GCMs for NRB exhibit wide range of possible changes as compared with temperature projections. Under downscaled RCP4.5 and RCP8.5 climate scenarios, the annual precipitation of BNRB, *Atbara*, and Sobat river basin, *El Ghazal* and Lake Victoria sub-basins of NRB are projected to change by about [-7, 14.2], [-19, 25.3], [-7, 39], [-5.9, 23], and [3.6, 27] % in the 2050s, and [-14, 25], [-22.5, 39], [-4.7, 60.4], [-11, 31], and [11.8, 41] % in the 2080s, respectively. Between downscaled projections of GCMs for air temperature, the five sub-basin of NRB are projected to become warmer by about $1.67 – 2^{o}C$ in the 2050s and $2 – 2.5^{o}C$ in the 2080s under RCP4.5 climate scenarios, and by about $2.5 – 3^{o}C$ in the 2050s and $3.9 – 4.6^{o}C$ in the 2080s under RCP8.5 climate scenarios. The precipitable water of these sub-basins of NRB is also projected to increase because according to the Clausius-Clapeyron equation, the atmospheric water vapor is expected to increase with air temperature.

Besides, extreme precipitation indices derived from precipitation projections of the four GCMs for NRB also exhibit wide range of possible changes. For example, R20mm, R95p, R99p and P30yr indices estimated for 2050s and 2080s are projected to mostly increase for all sub-basins of NRB. The R20mm index is projected to increase by 2.5–77.5% for all sub-basins except for the Atbara river basin which is projected to decrease by 0.8–1.9% in 2050s, but then to increase by 0.9–1.4% in 2080s. The range of mean projected changes in R95p and R99p indices for all sub-basins is 0.75–55% and -13–90%, respectively. The P30yr index is also projected to increase by 15–60% for all sub-basins of NRB under RCP4.5 and RCP8.5 scenarios for 2050s and 2080s. The predominantly projected increase in extreme precipitation indices implies that NRB is expected to experience more severe extreme wet precipitation and more frequently in 2050s and 2080s. Similarly, RX1day and RX5day indices are projected to increase in 2050s and 2080s by about 1–40% and -0.3–28% for all sub-basins, which implies that flood causing precipitation events over the NRB could occur more frequently in the future. Among the sub-basins of NRB considered, the Lake Victoria region is projected to experience the largest increase in all extreme precipitation indices possibly because under a warmer climate, Lake Victoria's contribution to the atmospheric moisture will be enhanced, leading to occurrences of more severe extreme precipitation.

On the basis of extreme temperature indices derived from temperature projections of the four GCMs, NRB is projected to experience a large decrease in cold extremes (i.e., cool nights (TN10p) and cool days (TX10p)) but increase in warm extremes (i.e., warm nights (TN90p) and warm days (TX90p)), such that the number of days that exceed the historical 90th

percentile values of T_{min} (TN90p) and T_{max} (TX90p) over the NRB could be at least equal to or greater than 48% and 55% in the 2050s periods, and at least equal to or greater than 50% and 80% in the 2080s, respectively. Correspondingly, the number of days that T_{min} (TN10p) and T_{max} (TX10p) will fall below the historical 10th percentile values are projected to decrease to less than 1%, e.g., almost no cold night or days is expected to occur, in the 2050s and 2080s. The indices for warm and cold spells also project an increase in warm spells but a decrease in cold spells in NRB.

On a whole, results from the downscaled RCP climate scenarios of four GCMs project that NRB is expected to experience warmer climate, and extreme precipitation events, and extreme temperature are expected to occur more frequently and in greater severity in the mid and late 21st century, which could have significant impact to the future water resources of NRB. It will be crucial for countries relying on the water resources of NRB to seriously consider implementing adaptation strategies and mitigation measures to combat the potential impact of climate change to NRB.

References

Alemseged TH, and Tom R (2015) Evaluation of regional climate model simulations of rainfall over the Upper Blue Nile basin. Atmos. Res. 161–162, pp. 57–64.

Alexander LV et al (2006) Global observed changes in daily climate extremes of temperature and precipitation. J. Geophys. Res., 111, D05109, doi:10.1029/2005JD006290.

Anyah RO, Semazzi FHM (2007) Variability of East African rainfall based on multiyear RegCM3 simulations. Int J Climatol 27:357–371.

Anyah RO, Semazzi FHM, Xie L (2006) Simulated physical mechanisms associated with multiscale climate variability over Lake Victoria Basin in East Africa. Mon Weather Rev 134:3588–3609.

Anyamba, A., J. L. Small, S. C. Britch, C. J. Tucker, E. W. Pak, C. A. Reynolds, J. Crutchfield, and K. J. Linthicum, (2014) Recent Weather Extremes and Impacts on Agricultural Production and Vector-Borne Disease Outbreak Patterns. PLoS ONE 9 (3), doi: https://doi.org/10.1371/journal.pone.0092538.

Beyene T, Lettenmaier D.P, Kabat P (2010) Hydrologic impacts of climate change on the Nile River Basin: implications of the 2007 IPCC scenarios. Climatic Change 100: pp. 433-461. doi:10.1007/s10584-009-9693-0.

Bhattacharjee P.S, and Zaitchik B.F. (2015) Perspectives on CMIP5 model performance in the Nile River headwaters regions. Int. J. Climatol., 35: 4262–4275. doi:10.1002/joc.4284.

Block P., and Rajagopalan B. (2007) Interannual Variability and Ensemble Forecast of Upper Blue Nile Basin Kiremt Season Precipitation. J. Hydrometeorol., 8 (3), pp. 327–343, DOI: 10.1175/JHM580.1.

Boer, G. J. (1993) Climate change and the regulation of the surface moisture and energy budgets. Climate Dynamics 8, 225-239. doi:10.1007/BF00198617.

Boko M, Niang I, Nyong A, Vogel C, Githeko A, Medany M, Osman-Elasha B, Tabo R and Yanda P. (2007) Africa. Climate Change 2007: Impacts, Adaptation and Vulnerability. Contribution of Working Group II to the Fourth Assessment Report of the Intergovernmental Panel on Climate Change, Parry M L, Canziani O F, Palutikof J P, van

der Linden P J and Hanson C E (eds). Cambridge University Press, Cambridge UK, 433 – 467.

Chen C.T, and Knutson T. (2008) On the verification and comparison of extreme rainfall indices from climate models. Amer. Meteor. Soc. 21: 1605–1621, doi: 10.1175/2007JCLI1494.1.

Diem J. E., Ryan S. J, Hartter J, and Palace M.W. (2014) Satellite-based rainfall data reveal a recent drying trend in central equatorial Africa. Climate Change, 126: 263–272, doi:10.1007/s10584-014-1217-x.

Diro, G. T., Grimes D., and Black E. (2012) Dynamical downscaling of ECMWF Ensemble seasonal forecasts over East Africa with RegCM3. J Geophys Res 117:D16103. doi: 10.1029/2011JD016997.

Dodo, MK. (2014) Examining the Potential Impacts of Climate Change on International Security: EU-Africa Partnership on Climate Change. SpringerPlus 3. https://doi.org/10.1186/2193-1801-3-194.

Dudhia J. (1989) Numerical study of convection observed during the winter experiment using a mesoscale two-dimensional model. J. Atmos. Sci., 46:3077–3107. doi:10.1175/1520-0469(1989)046<3077:NSOCOD>2.0.CO;2.

Ek, M., and Mahrt L. (1991) OSU 1-D PBL model user's guide, version 1.04. Department of Atmospheric Sciences, Oregon State University, 120 pp.

Eltahir E. A. B. (1996) El Niño and the Natural Variability in the Flow of the Nile River, Water Resour. Res., 32(1), 131–137, doi:10.1029/95WR02968.

Elshamy, M. E, Seierstad I. A, and Sorteberg A. (2009) Impacts of climate change on Blue Nile flows using bias-corrected GCM scenarios, Hydrol. Earth Syst. Sci., 13, 551-565, doi:10.5194/hess-13-551-2009.

Endris H.S, Omondi P, Jain S, et al (2013) Assessment of the Performance of CORDEX Regional Climate Models in Simulating East African Rainfall. J. Climate, DOI: 10.1175/JCLI-D-12-00708.1.

Fowler H.J, Blenkinsop S, and Tebaldi C. (2007) Review Linking climate change modelling to impacts studies: recent advances in downscaling techniques for hydrological modelling. Int. J. Climatol. 27: 1547–1578. doi:10.1002/joc.1556.

Frich P., Alexander L.V, Della-Marta P, Gleason B, Haylock M, Klein Tank A.M.G, and Peterson T. (2002) Observed coherent changes in climatic extremes during the second half of the twentieth century. Climate Res.19, 193–212. doi:10.3354/cr019193.

Funk C.C, Peterson P.J, Landsfeld M.F, Pedreros D.H, Verdin J.P, Rowland J.D, Romero B.E, Husak G.J, Michaelsen J.C, and Verdin A.P (2014) A quasi-global precipitation time series for drought monitoring: U.S. Geological Survey Data Series 832, 4 p., http://dx.doi.org/110.3133/ds832.

Gan, T. Y., Mari Ito, S Huelsmann, X Qin, X Lu, S. Y Liong, P Rutschman, M Disse & H Koivosalo, (2015) Possible climate change/variability and human impacts, vulnerability of African drought prone regions, its water resources and capacity building, Hydrological Sciences Journal, DOI: 10.1080/02626667.2015.1057143.

Giorgi F, Jones C, and Asrar G. R (2009) Addressing climate information needs at the regional level: The CORDEX framework. WMO Bull., 58, 175–183.

Gizaw, M., and Gan, T. Y. (2016) Impact of Climate Change and El Niño Episodes on Droughts in sub-Saharan Africa, Climate Dynamics, 49:665, DOI: 10.1007/s00382-016-3366-2.

Gizaw M, and Gan T.Y (2015) Possible Impact of climate change on future extreme precipitation of the Oldman, Bow and Red Deer River Basins of Alberta. Int. Journal Climatology, 36(1), 208-224. DOI:10.1002/joc.4338.

Harris I, Jones P.D, Osborn T.J, and Lister D.H (2014) Updated high-resolution grids of monthly climatic observations–the CRU TS3.10 Dataset. Int. J. Climatol., 34, 623–642. doi: 10.1002/joc.3711.

Hong, S.Y., Dudhia J., and Chen S. H. (2004) A revised approach to ice microphysical processes for the bulk parameterization of clouds and precipitation. Mon. Wea. Rev., 132, 103–120, doi: 10.1175/1520-0493(2004)132<0103:ARATIM>2.0.CO;2.

Houghton J. (2009) Global Warming the complete briefing, 4th Edition, 438 pg., Cambridge Univ. Press.

Indeje M, Semazzi H.M.F, and Ogallo J.L (2000) ENSO signal in East African rainfall seasons. Int. J. Climatol., 20, 19–46.

IPCC (2007) Climate Change 2007: The Physical Science Basis. Contribution of Working Group I to the Fourth Assessment Report of the Intergovernmental Panel on Climate Change, Solomon S, Qin D, Manning M, Chen Z, Marquis M, Averyt KB, Tignor M, Miller HL (eds). Cambridge University Press: Cambridge, UK and New York, NY, pp. 849-925.

IPCC (2013) Climate Change 2013: The Physical Science Basis. Contribution of Working Group I to the Fifth Assessment Report of the Intergovernmental Panel on Climate Change [Stocker, T.F., D. Qin, G.-K. Plattner, M. Tignor, S.K. Allen, J. Boschung, A. Nauels, Y. Xia, V. Bex and P.M. Midgley (eds.)]. Cambridge University Press, Cambridge, United Kingdom and New York, NY, USA, 1535 pp.

IPCC (2014) Climate Change 2014: Impacts, Adaptation, and Vulnerability. Part B: Regional Aspects. Contribution of Working Group II to the Fifth Assessment Report of the Intergovernmental Panel on Climate Change [Barros, V.R., C.B. Field, D.J. Dokken, M.D. Mastrandrea, K.J. Mach, T.E. Bilir, M. Chatterjee, K.L. Ebi, Y.O. Estrada, R.C. Genova, B. Girma, E.S. Kissel, A.N. Levy, S. MacCracken, P.R. Mastrandrea, and L.L. White (eds.)]. Cambridge University Press, Cambridge, United Kingdom and New York, NY, USA, pp. 1199-1265.

Janjic Z.I. (1994) The step-mountain eta coordinate model: further developments of the convection, viscous sublayer, and turbulence closure schemes. Mon. Wea. Rev.,122,927–945, doi: 10.1175/1520-0493(1994)122<0927:TSMECM>2.0.CO;2.

Kain J.S. (2004) The Kain–Fritsch Convective Parameterization: An Update. J Appl. Meteor., 43,170–181, doi: 10.1175/1520-0450(2004)043<0170:TKCPAU>2.0.CO;2.

Kerkhoven, E., Gan, T.Y., Shiiba, M., G. Reuter, and Tanaka, K., (2006) A comparison of cumulus parameterization schemes in a numerical weather prediction model for a monsoon rainfall event, *Hydro. Processes*, 20(9), 1961-1978. DOI: 10.1002/hyp.5967.

Kharin, V. V., Zwiers, F. W., Zhang, X., & Wehner, M. (2013) Changes in temperature and precipitation extremes in the CMIP5 ensemble. Climatic Change, 119, 345–357. doi:10.1007/s10584-013-0705-8.

Kim U. and Kaluarachchi J. J (2009) Climate Change Impacts on Water Resources in the Upper Blue Nile River Basin, Ethiopia. JAWRA Journal of the American Water Resources Association, 45: 1361–1378. doi:10.1111/j.1752-1688.2009.00369.x.

Klein Tank AMG, Zwiers FW, and Zhang X (2009) Guidelines on analysis of extremes in changing climate in support of informed decision for adaption. World Meteorological Organization, Climate Data and Monitoring, WCDMP-No. 72. WMO: Geneva, Switzerland.

Lucas-Picher P, Caya D, de Elia R, Laprise R (2008) Investigation of regional climate models' internal variability with a ten-member ensemble of 10-year simulations over a large domain. Climate Dyn. 31:927–940.

Mariotti L, Coppola E, Sylla M. B, Giorgi F, and Piani C (2011) Regional climate model simulation of projected 21st century climate change over an all-Africa domain: Comparison analysis of nested and driving model results. J. Geophys. Res., 116, D15111, doi:10.1029/2010JD015068.

Mariotti L, Diallo I, Coppola E, et al (2014) Seasonal and intraseasonal changes of African monsoon climates in 21st century CORDEX projections. Climatic Change 125: 53. doi:10.1007/s10584-014-1097-0.

McSweeney C.F, Jones R.G, Lee R.W, et al (2015) Selecting CMIP5 GCMs for downscaling over multiple regions. Climate Dyn. 44: 3237-3260, doi:10.1007/s00382-014-2418-8.

Mlawer E.J., Taubman S.J., Brown P.D., Iacono M.J., and Clough S.A., (1997) Radiative transfer for inhomogeneous atmosphere: RRTM, a validated correlated-k model for the long-wave. J. Geophys. Res., 102, 16663–16682, doi:10.1029/97JD00237.

Mohamed Y. A, van den Hurk B, Savenije H. H. G, and Bastiaanssen W. G. M (2005) Hydroclimatology of the Nile: results from a regional climate model. Hydrology and Earth System Sciences, 9, 263–278. doi:10.5194/hess-9-263-2005.

Mwale D, and Gan T.Y (2005) Wavelet analysis on variability, teleconnectivity and predictability of September-November East African Rainfall. J. of App. Met., 44,256-269.

Ntale, H. K., and Gan, T.Y., Mwale, D. (2003) Prediction of East African Seasonal Rainfall Using Canonical Correlation Analysis, J. of Climate, 16(12), 2105-2112. DOI: http://dx.doi.org/10.1175/1520-0442(2003)016<2105:POEASR>2.0.CO;2.

Ntale H. K, and Gan T.Y (2004) East African Rainfall Anomaly Patterns in Association with El Niño/Southern Oscillation. J. Hydrologic Eng., ASCE, 9(4), 257-268.

Omondi, P. A., Awange, J. L., Forootan, E., Ogallo, L. A., Barakiza, R., Girmaw, G. B., Fesseha, I., Kululetera, V., Kilembe, C., Mbati, M. M., Kilavi, M., King'uyu, S. M., Omeny, P. A., Njogu, A., Badr, E. M., Musa, T. A., Muchiri, P., Bamanya, D. and Komutunga, E. (2014) Changes in temperature and precipitation extremes over the Greater Horn of Africa region from 1961 to 2010. Int. J. Climatol., 34: 1262–1277. doi:10.1002/joc.3763.

Patz, J. A., D. Campbell-Lendrum, T. Holloway, and J. A. Foley (2005) Impact of Regional Climate Change on Human Health. Nature, 438, pp. 310-317, doi:10.1038/nature04188.

Rosenberg, E. A., P. W. Keys, D. B. Booth, D. Hartley, J. Burkey, A. C. Steinemann, D. P. Lettenmaier, (2010) Precipitation Extremes and the Impacts of Climate Change on Stormwater Infrastructure in Washington State. Clim. Change 102: 319–349, doi:10.1007/s10584-010-9847-0.

Schneider T., Bischoff T., and Haug, G. H. (2014) Migrations and dynamics of the intertropical convergence zone, Nature, 513, 45-53, doi: https://doi.org/10.1038/nature13636.

Schneider U, Becker A, Finger P, Meyer-Christoffer A, Rudolf B, Ziese M (2011) GPCC Full Data Reanalysis Version 6.0 at 0.5°: Monthly Land-Surface Precipitation from Rain-

Gauges built on GTS-based and Historic Data. DOI: 10.5676/DWD_GPCC/FD_M_V6_050.

Segele Z.T and Lamb P. J. (2005) Characterization and variability of Kiremt rainy season over Ethiopia. Meteor. Atmos. Phys. 89: 153-180. doi:10.1007/s00703-005-0127-x.

Segele Z. T, Leslie L. M, and Lamb P. J (2009) Evaluation and adaptation of a regional climate model for the Horn of Africa: Rainfall climatology and interannual variability. Int. J. Climatol., 29, 47–65. doi:10.1002/joc.1681.

Sen, P.K. (1968) Estimates of the regression coefficient based on Kendall's tau. Journal of the American Statistical Association, 63 (324), 1379–1389. doi:10.2307/2285891.

Senay, G. B., N. M. Velpuri, S. Bohms, Y. Demissie, and M. Gebremichael (2014) Understanding the hydrologic sources and sinks in the Nile Basin using multisource climate and remote sensing data sets, Water Resour. Res., 50, 8625–8650, doi:10.1002/2013WR015231.

Shanahan TM, Overpeck JT, Anchukaitis KJ, Beck JW, Cole JE, Dettman DL, Peck JA, Scholz CA, King JW (2009) Atlantic forcing of persistent drought in West Africa. Science, 324:377–380.

Siam, M.S. and Eltahir, E.A. (2017) Climate change enhances interannual variability of the Nile river flow. Nature Climate Change, 7(5), pp.350-354. doi:10.1038/nclimate3273.

Sillmann J, Kharin VV, Zhang X, Zwiers FW, Bronaugh D. (2013a) Climate extremes indices in the CMIP5 multimodel ensemble: Part 1. Model evaluation in the present climate. J. Geophys. Res. Atmos., 118, 1716-1733. doi: 10.1002/jgrd.50203.

Sillmann, J., Kharin, V. V., Zwiers, F. W., Zhang, X., & Bronaugh, D. (2013b) Climate extremes indices in the CMIP5 multimodel ensemble: Part 2. Future climate projections, J. Geophys. Res. Atmos., 118, 2473–2493, doi:10.1002/jgrd.50188.

Skamarock WC, Klemp JB, Dudhia J, Gill DO, Barker DM, Duda M, Huang XY, Wang W, Powers JG (2008) A description of the advanced research WRF version 3. NCAR technical note, NCAR/TN-475+STR, 123 pp [http://www2.mmm.ucar.edu/wrf/users/docs/arw_v3.pdf].

Soliman E. S. A, Sayed M. A.-A, and Jeuland M. (2009) Impact assessment of future climate change for the Blue Nile basin using a RCM nested in a GCM. Nile Water Science & Engineering Special Issue on Water and Climate 2, 31–38.

Sun LQ, Semazzi F, Giorgi F, Ogallo L. (1999a) Application of the NCAR regional climate model to eastern Africa, 1. Simulation of the short rains of 1988. J. Geophys Res 104:6529–6548.

Swain, A. (2011) Challenges for Water Sharing in the Nile Basin: Changing Geo-Politics and Changing Climate. Hydrol. Sci. J. 56(4), 687–702. doi:10.1080/02626667.2011.577037.

Tariku, T.B, and Gan, T.Y (2017) Sensitivity of the Weather Research and Forecasting model to Parameterization Schemes for Regional Climate of Nile River Basin, *Climate Dynamics*, pp.1-17, doi: 10.1007/s00382-017-3870-z.

Teutschbein, C., and Seibert J. (2012) Bias correction of regional climate model simulations for hydrological climate-change impact studies: review and evaluation of different methods. J. Hydrol 456–457:12–29.

Vörösmarty C. J, Douglas E. M, Green P. A, and Revenga C (2005) Geospatial indicators of emerging water stress: an application to Africa. Ambio, 34, 230-236.

WWAP (World Water Assessment Programme) (2012) The United Nations World Water Development Report 4: Managing Water under Uncertainty and Risk. Paris, UNESCO.

Zaroug M. A. H., Giorgi F, Coppola E, Abdo G. M, and Eltahir E. A. B (2014) Simulating the connections of ENSO and the rainfall regime of East Africa and the upper Blue Nile region using a climate model of the Tropics. Hydrol. Earth Syst. Sci., 18, 4311-4323, doi:10.5194/hess-18-4311-2014.

Appendix 3.A

This appendix contains figures that show the spatial coverage of selected extreme climate indices analysed in this study for control period, 2050s and 2080s.
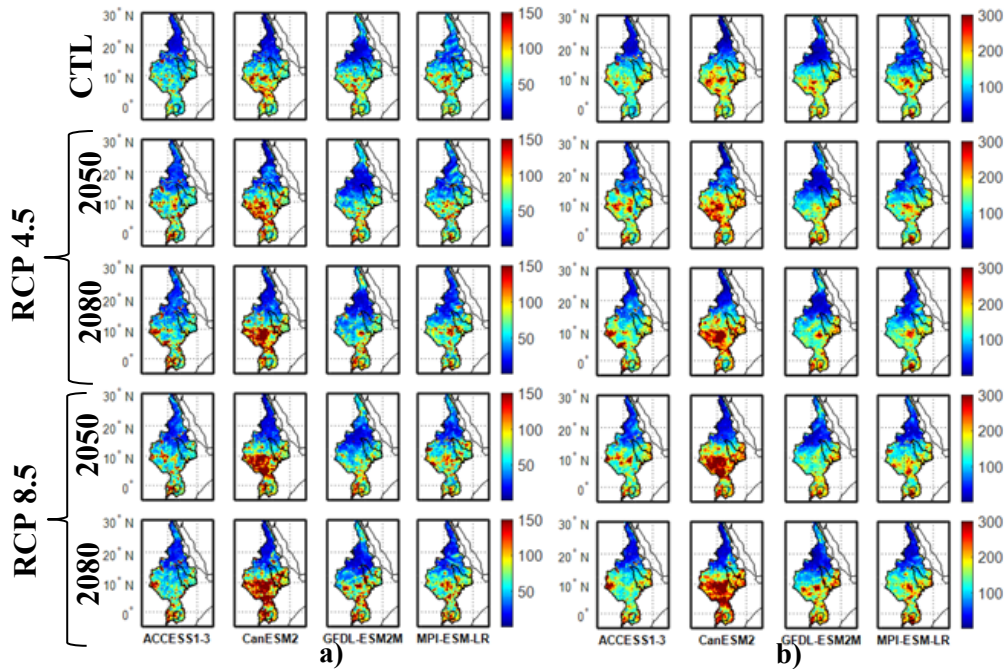
Figure 3.A1. (a) RX1day and (b) RX5day index over the NRB for control period, 2050s and 2080s of ACCESS1-3, CanESM2, GFDL-ESM2M and MPI-ESM-LR for RCP4.5 and RCP8.5 scenarios.
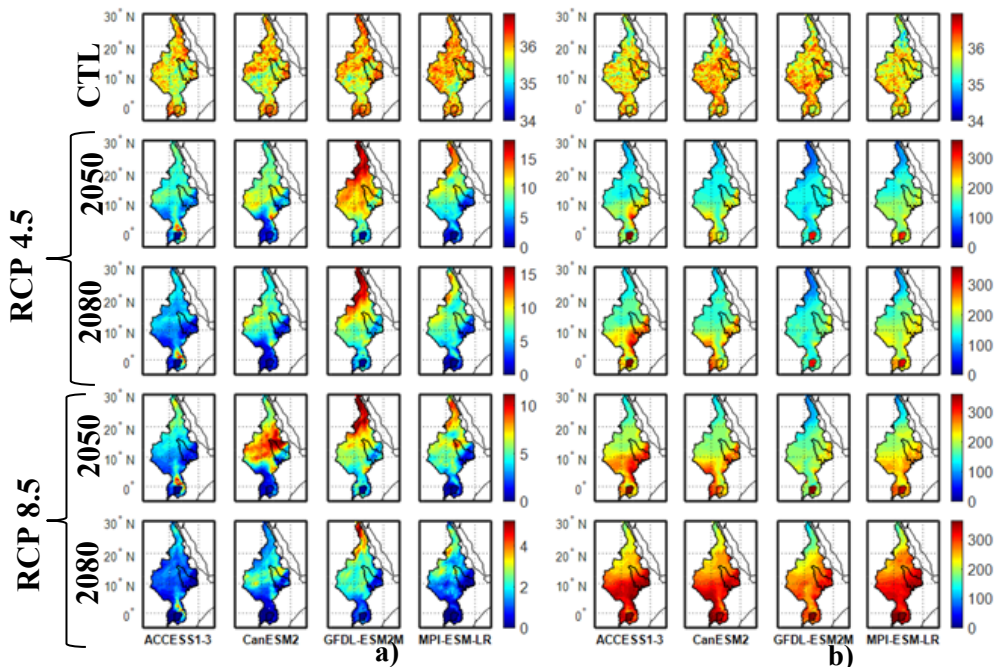
Figure 3.A2. (a) TX10p and (b) TX90 index over the NRB for control period, 2050s and 2080s of ACCESS1-3, CanESM2, GFDL-ESM2M and MPI-ESM-LR for RCP4.5 and RCP8.5 scenarios.

Chapter 4 Impact of Climate Change on Hydrology and Hydrologic Extremes of Upper Blue Nile River basin

4.1. Introduction

Water crises due to droughts and water pollution have affected many regions across the world, especially in developing countries (Vörösmarty et al., 2005). The potential hydrologic impact of climate change could lead to unforeseen water crises in future, especially to regions with semi-arid or arid climate. Since 1970s, observations show that hydrologic extremes (droughts and floods) have been occurring more frequently and in greater severity worldwide (Lemke et al., 2007). In the last decade, 90% of natural hazards have been related to water (Gopalakrishnan, 2013) and they could get worse in future, such as tsunamis, floods, droughts, and storm surges that could inflict costly damages to societies, such as the 2010 flood of Pakistan and the 2012 drought of USA (Grigg, 2014), which had been the worst in more than half a century, and which may be just a foretaste of more climatic extremes under a hotter and drier future in many places of the world. Many scientists and climatologists attribute the increase in occurrences of recent hydrologic extremes to the impact of climate change (e.g., Lemke et al., 2007; IPCC, 2013). The climate of Africa such as temperature and precipitation will likely continue to change in coming decades (e.g., Gizaw and Gan, 2016; Gizaw et al., 2017), but the pattern and magnitude of change will vary from region to region, and the change could severely compromise the future agricultural production and food security in many African countries (Boko et al., 2007).

Many recent studies on the potential impact of climate change indicate that global warming is expected to increase the frequency and magnitude of hydrologic extremes (e.g., Meehl, 2004; IPCC, 2013). According to IPCC (2013), the average air temperature has already increased by 0.5°C or more in the past century over most parts of Africa, and some regions have also experienced an increase in heavy precipitation ($> 95^{th}$ percentile) events at daily and sub-daily time scales since 1951. Furthermore, according to IPCC (2013), air temperature under RCP8.5 is projected to increase by $3 - 6^{\circ}$C across different parts of Africa by the late 21st century relative to the 1986-2005 baseline, which could have significant impact on extreme weathers. According to the Clausius–Clapeyron relationship, the saturation vapor pressure will increase by about 7% per $^{\circ}$C rise in temperature. As a result, a warmer atmosphere will have a larger capacity to hold more water vapour, giving rise to more extreme precipitation events. Therefore, global warming can potentially accelerate the hydrologic cycle, leading to more hydrologic extreme such as extreme floods and droughts.

The impact of climate change on the water resources of NRB or different sub-basins of NRB has been investigated using outputs of RCMs or GCMs (e.g. Beyene et al., 2010; Elshamy et al., 2009; Taye et al., 2011; and Liersch et al., 2016). Beyene et al. (2010) used the Variable Infiltration Capacity hydrological model driven by climate change scenarios (A2 and B1) of 11 GCMs of the 4th IPCC (2007) assessment report to assess the climate change impact on the NRB. The mean annual Nile River flow to the high Aswan dam is projected to increase by 11 (14) % in 2020s, but decrease by 8 (7) % in 2050s and 16 (13) % in 2080s for the A2 (B1) emission scenarios. Elshamy et al. (2009) used statistically downscaled precipitation and

potential evapotranspiration data of A1B emission scenarios of 17 GCMs of the 4th IPCC assessment report to drive the Nile Forecast System hydrological model to assess global warming impact on the Upper Blue Nile (UBN) river basin at El Diem over 2081-2098. They projected the ensemble mean annual flow of UBN at El Diem to decrease by about 15% in late 21st century. In contrary, Liersch et al. (2016) found an overall projected increase in the mean annual discharge of the UBN, but projected a decrease in discharge during June and July and an increase during August to November over the 21st century in both RCP4.5 and RCP8.5 climate scenarios.

However, only several studies have been conducted on the impact of climate change on hydrological extremes of the UBN river basin (e.g., Aich et al., 2014; Taye et al., 2011; Kim and Kaluarachchi, 2009). Using the hydrologic, SWIM model forced with RCP2.6 and RCP8.5 climate scenarios of five GCMs for the mid and late 21st century, Aich et al. (2014) projected an increase in the extreme flow of UBN, ranging from 10 to 50% for high streamflow (Q_{10}) and 40 to 60% for low streamflow (Q_{90}). Using SRES A2 climate scenarios of six GCMs, Kim and Kaluarachchi (2009) projected an increase or decrease in the extreme flow of UBN, Q_{90} by a range of -25 – 60% and Q_{10} by a range of -15 – 20% in 2050s. Using two conceptual hydrological models forced with A1B and B1 scenarios of 17 GCMs downscaled by a frequency perturbation approach, Taye et al., (2011) projected the streamflow of two catchments in NRB, the Nyando and Lake Tana catchments. They projected an increase in the mean runoff and extreme peak flows for Nyando in 2050s, but for

Lake Tana, they projected a wide range of changes in the mean volumes, high flows (-31 to 79%) and low flow (-61 to +56%).

Given a rather wide range of projected changes for the NRB was reported in a limited number of past studies based on RCP climate scenarios of GCMs without downscaling, or SRES climate scenarios that were statistically downscaled, the objective of this paper is to investigate the potential impact of climate change on the hydrology and hydrological extremes of the UBN river basin simulated by three hydrological models using RCP4.5 and RCP8.5 climate scenarios of four GCMs of CMIP5 dynamically downscaled by WRF for 2050s and 2080s. To partly address uncertainties associated with long-term, hydrologic projections of climate change impact, we compared the streamflow simulated by three hydrological models, of which two are distributed, partial physically based models while the 3rd is a lumped, conceptual model.

The chapter is organized as follows: the study area and data are given in Section 4.2, research methodology in Section 4.3, the results and discussions in Section 4.4 and conclusions in Section 4.5.

4.2. Study area and data

4.2.1. Description of the study area

The study area is the upper Blue Nile river basin, the primary sub-basin of NRB located in the highland region of Ethiopia. The drainage area of UBN upstream of the El Diem station is about 176,000 km^2, which contributes about 60% of the average annual streamflow of the Nile

River. The first tributary of the UBN river originates from Gish Abbay is called the Gilgel Abbay River which flows northwards into Lake Tana (3,200 km^2) of Ethiopia, then it flows pass the Sudanese Border downstream to meet the White Nile River at Khartoum, Sudan. Based on the GPCC and CRU data for 1976 – 2005, the mean annual rainfall of UBN varies from about 875 to 1900 mm per year, its mean annual temperature varies from 14 to 28°C, respectively, which means the climate of UBN varies from semi-arid to humid. UNB has a wet (June-September) and a dry (October-March) seasons caused by the northward and southward movement of ITCZ towards the area with the warmest surface temperature resulted from most solar heating. UBN also has a complex terrain with a surface elevation varying from 487 m to 4176 m as shown in Figure 4.1. The soil of UBN is mostly dominated by clay, and its land use is dominated by savannah, dryland and cropland.
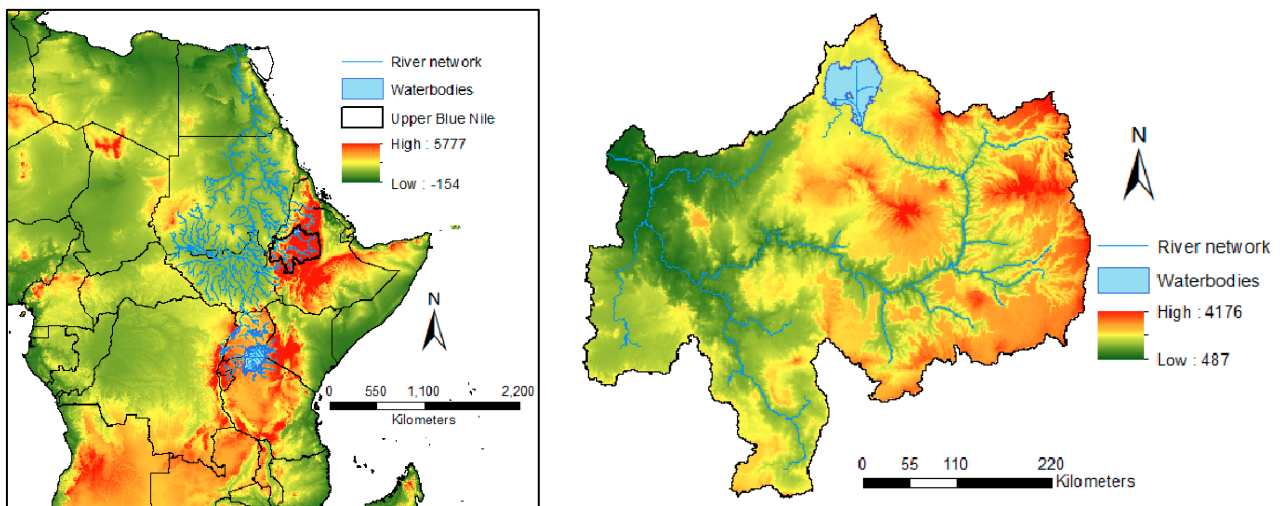
Figure 4.1: Topography (m) and stream network for Nile river basin (left) and the upper Blue Nile river basin (right).

4.2.2.   Data

The daily precipitation, and climate data used to estimate potential evapotranspiration (ETo) using maximum, minimum and mean temperature, wind speed, surface pressure for 1980-2001 were taken from the ERA-Interim reanalysis data downscaled by WRF (Tariku and Gan, 2017). The observed discharge at the El Diem station near the Sudanese-Ethiopian border for 1981-1991 was used to calibrate the three hydrological models selected for this study, and the calibrated models were validated using the 1992-1997 data independent of the calibration experience.

The hydrologic impact of climate change on UBN was assessed using climate variables of RCP4.5 and RCP8.5 climate scenarios of four GCMs (CanESM2, GFDL-ESM2M, MPI-ESM-LR and ACCESS1-3) of IPCC (2013) dynamically downscaled by WRF at 36 km resolution over a domain of 2^oE to 57^oE, 20^oS to 37^oN that covers the entire NRB. Using ERA-Interim data, WRF was first configured and fine-tuned with various parameterization schemes until it could simulate representative regional climate of NRB (Tariku and Gan, 2017). Then WRF was used to downscale the historical data of four GCMs for the baseline period (1976-2005), and RCP4.5 and RCP8.5 climate scenarios for 2050s (2041-2070) and 2080s (2071-2100) (Tariku and Gan, 2018). WRF's simulated precipitation and temperature data for the base period were validated against the data of Global Precipitation Climatology Centre (GPCC version 6, 1901-2010; Schneider et.al, 2011) and the Climate Research Unit data of the University of East Anglia (CRU version 3.22, 1901-2013; Harris et.al, 2014), respectively.

The flow direction and other catchment characteristics of UBN were generated using the Shuttle Radar Topographic Mission (STRM) digital elevation model at a grid resolution of 90m (Jarvis et al., 2008). The Global Land Cover Characterization (GLCC) data was used as the land use/cover classification of UBN.

4.3. Research Methodology

4.3.1. Hydrological modelling

The hydrologic models used for simulating the streamflow of UBN are the Variable Infiltration Capacity (VIC), Watflood and NAM models. The three hydrologic models are chosen because they are different structurally as an effort to investigate uncertainties related to hydrological modeling in climate change impact studies.

VIC is a semi-distributed, macroscale hydrological model that solves the water balance and surface energy budgets of a river basin at a grid cell level (Liang et al., 1996). The surface runoff and the baseflow output simulated for each land surface grid was routed to the outlet/gauge station of the basin using a routing model of Lohmann et al (1998). VIC has been successfully tested in many hydrologic studies at different places (e.g. Gao et al., 2010; Ashfaq et al., 2010; Beyene et al., 2010; Nijssen et al., 2001). The meteorological forcing data needed to drive the VIC model was daily precipitation, maximum and minimum temperature, and wind speed output of WRF at 36 km grid resolution; whereas other forcing variables such as short and longwave radiative fluxes were estimated from minimum and maximum temperature using methods described by Maurer et al. (2002). The soil and vegetation parameters of UBN were obtained from the global VIC input data at 0.5^o resolution (Nijssen

et al., 2001). Details of the soil and vegetation data required by VIC are given in Liang et al (1996). By a manual calibration approach, parameters for the variable infiltration curve parameter (b_infilt), fraction of the Dsmax parameter (Ds), fraction of soil moisture (Ws), maximum velocity of baseflow (Dsmax) and soil depth parameters were iteratively adjusted until a multi-objective function was optimized. In addition, routing parameters such as velocity, diffusivity, and the unit hydrograph were also manually calibrated.

Watflood is a distributed hydrologic model developed by Nicholas Kouwen at the University of Waterloo for flood forecasting and long-term hydrologic simulations (Kouwen et al., 1993). Watflood uses the Grouped Response Units (GRU) approach to calculate the overland flow, interflow and baseflow; and the Hargreaves, Preistley-Taylor (Priestley and Taylor, 1972) or pan evaporation methods to calculate the potential evapotranspiration. In this study, the Hargreaves method based on air temperature data was used to estimate ETo. The Watflood model accounts for canopy interception, infiltration, evaporation, snow accumulation and ablation, interflow, recharge, baseflow, overland and channel routing of river basins (Kouwen et al., 1993). Watflood has also been widely used at different places (e.g. Benoit et al. 2003; Pietroniro et al. 2006). The 6-hourly outputs of precipitation and surface air temperature of WRF were used to drive Watflood. The land use/cover data of UBN as input to Watflood was prepared from the GLCC and the STRM DEM data using the Green Kenue software. Watflood model parameters were calibrated by a combination of manual and auto-calibration methods such that the simulated streamflow agree with the observed streamflow data of UBN.

NAM is the Danish "Nedbør-Afstrømnings-Model", lumped, conceptual rainfall-runoff model developed at the Technical University of Denmark (DHI, 2008) which accounts for the soil moisture content in four different but mutually interrelated conceptual storages, which represent different physical storages of a catchment, such as: 1) snow storage, 2) surface storage, 3) lower root zone storage and 4) groundwater storage (DHI, 2008). In addition, NAM allows human interventions of the hydrological cycle, such as irrigation and groundwater pumping. The lower root zone reservoir plays a central role in NAM such that surface and subsurface flows simulated vary linearly with the relative soil moisture content of this lower zone storage. NAM simulates overland flow, interflow and baseflow as outputs using a linear reservoir model. ETo was estimated using the FAO Penman-Monteith method (Allen et al., 1998) which estimates radiation and relative humidity based on maximum and minimum temperature, locations and limited amount of input data. Other variables such as wind speed and surface air pressure are obtained from WRF. Different hydrologic processes modelled by NAM are conceptualised using empirical algorithms with model parameters that are manually calibrated, which is a trial-and-error approach against observed streamflow until the model parameters are optimized.

4.3.2. Bias correction

Between different bias correction methods such as linear scaling, local intensity scaling, power transformation and quantile mapping, Teutschbein and Seibert (2012) found that the quantile mapping method achieved the best bias correction of temperature and precipitation data of their study site. Because precipitation of UBN downscaled by WRF tends to be too

high compared to observed data, precipitation of UBN simulated by WRF was bias corrected at daily time scale based on monthly GPCC data using a linear scaling method, and at daily time scale based on the Climate Hazards Group Infrared Precipitation with Stations daily data (CHIRPS version 2.0, 1981-2005; Funk et al., 2014) using the quantile mapping method. WRF's simulated, daily temperature for UBN was bias corrected using a linear approach by adding the difference between the monthly long-term mean observed CRU temperature of 1976-2005 and the corresponding monthly mean of WRF's simulation. The four GCMs output downscaled by WRF are compared and bias corrected before applied to the hydrological models.

4.4. Results and discussions

4.4.1. Hydrological models calibration and validation

The calibration and validation results of three hydrological models versus observed daily streamflow of UBN are shown in Figure 4.2. Results of both Figure 4.2 and Table 4.1 show that all models generally captured the overall streamflow processes and dynamics in both calibration and validation periods. The Nash-Sutcliffe Efficiency (NSE), coefficient of correlation (R^2), the root mean square error (RMSE), the mean error (ME) statistics of all models obtained are encouraging, with NSE and R^2 above 0.6, small ME. The hydrologic models are further evaluated in terms of peak flow, low flow, and cumulative discharge. The cumulative discharge of VIC for the calibration and validation periods was over-simulated by about 8% while the other two models only marginally over simulated the cumulative discharge (< 2.5%). Overall, the performance of NAM model is the best.
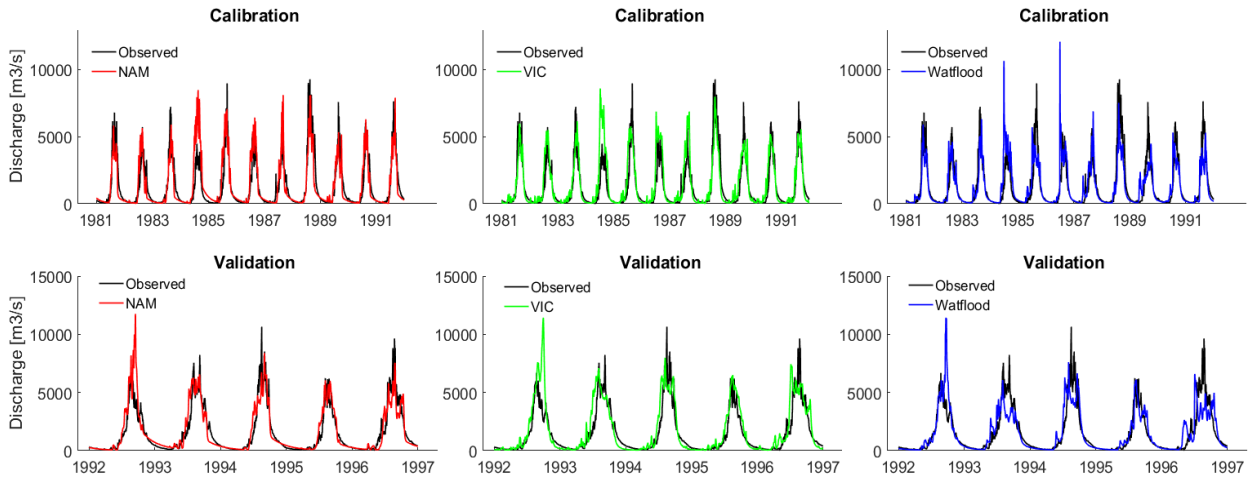
Figure 4.2: Calibration and validation time series plots using NAM, VIC and Watflood models for upper Blue Nile river basin.

Table 4.1: Performance of NAM, VIC and Watflood model in simulating the historical records for calibration and validation period.

	Model	NSE [-]	ME [m³/s]	RMSE [m³/s]	R² [-]
Calibration	NAM	0.74	10.87	889.1	0.76
	VIC	0.69	176.1	977.6	0.75
	Watflood	0.65	-31.5	1033	0.65
Validation	NAM	0.79	65.4	893.8	0.81
	VIC	0.64	245.6	1163	0.75
	Watflood	0.63	-12.3	1179	0.65

High and low flow extremes selected from the streamflow time series simulated by NAM, VIC and Watflood are compared with the high and low flow extremes observed for UBN using scatterplots shown in Figure 4.3 after re-distributing the data by Box-Cox transformation (Box and Cox, 1964; Willems, 2009) so that the data errors are homoscedastic.

Solid and dotted lines in the scatterplots represent the mean and the standard deviation of model residuals, respectively. Figure 4.3 shows that all NAM, VIC and Watflood have well captured the peak flows, especially the NAM model, with a mean peak flow residuals of - 0.007, -0.29 and -0.43 m^3/s respectively. The extreme low flows are also well simulated by VIC and NAM, but over-simulated by Watflood and under-simulated by VIC for the validation periods. The mean low flow residuals for NAM, VIC and Watflood are +0.16, - 0.59 and +0.61 m^3/s, respectively. The above results demonstrate that all NAM, VIC and Watflood models are well calibrated and therefore are adequate to assess the future hydrologic impact of climate change on UBN.
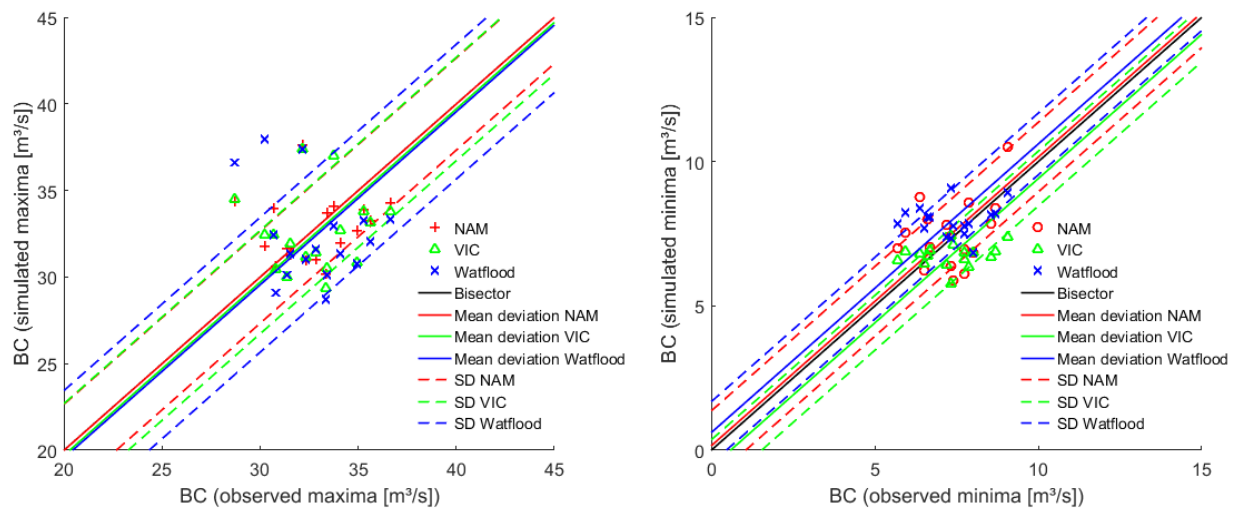
Figure 4.3: Scatterplots of Box-Cox transformed annual peak and low flow extremes at daily time step for the upper Blue Nile river basin between observed and simulations of NAM, VIC and Watflood models.

4.4.2.   Climate change impact on precipitation and temperature of UBN

The projected changes in annual precipitation, maximum and minimum temperature for RCP4.5 and RCP8.5 climate scenarios of four CMIP5 GCMs downscaled by WRF for 2050s and 2080s with respect to 1976-2005 (base period) are shown in Table 4.2. The maximum (minimum) temperature of UBN are projected to increase by about 1.35 – 2.38 (1.72 – 2.74) ^{o}C under RCP4.5, and 2.22 – 4.47 (2.5 – 5.1) ^{o}C under RCP8.5 climate scenarios for future periods with respect to the base period, respectively. As expected, projected changes in minimum temperature is higher than projected changes in maximum temperature. The results are consistent with that of previous studies, such as Elshamy et al. (2009) and Kim and Kaluarachchi (2009) who projected the mean annual temperature of UBN to increase by 2 – 5°C at the end of the 21st century under A1B scenario, and 1.4 – 2.6^{o}C for 2050s under A2 scenarios over the base period of 1961-1990, respectively. Based on RCP8.5 climate scenarios of four GCMs, the mean annual temperature of the BNRB is projected to increase by about 2.5 – 3°C (3.9 – 4.6^{o}C) in 2050s (2080s), respectively (Tariku and Gan, 2018). However, a projected change in precipitation varies widely, ranging from -10.3 to 19.4% for both RCP climate scenarios over 2050s and 2080s. The average annual precipitation is projected to increase (decrease) based on downscaled climate scenarios of CanESM2 (MPI-ESM-LR) in both future periods, respectively. On the other hand, the average annual precipitation is projected to decrease by both ACCESS1-3 and GFDL-ESM2M under RCP8.5 scenarios in both future periods, but increase in 2050s and decrease in 2080s under RCP4.5 scenarios. Previous climate change studies conducted for UBN or its sub-basins also show different

projected changes (increase or decrease) in precipitation by different GCMs, e.g., Kim and Kaluarachchi (2009), and Tariku and Gan (2018). Kim and Kaluarachchi (2009) found projected change in the mean annual precipitation over UBN to range between -11 to 44% for 2050s using six GCMs' output under A2 emission scenarios. Using four GCMs downscaled by WRF, Tariku and Gan (2018) found the projected change in the annual precipitation for Blue Nile river basin to range between -9 and 18.6 % under RCP4.5, and -14 to 25% under RCP8.5 climate scenario over 2050s and 2080s.

Table 4.2: The projected change in precipitation, minimum and maximum temperature of UBN under two RCP climate scenarios of four GCMs downscaled by WRF for 2050s and 2080s.

	ACCESS1-3		CanESM2		GFDL-ESM2M		MPI-ESM-LR	
	RCP4.5	RCP8.5	RCP4.5	RCP8.5	RCP4.5	RCP8.5	RCP4.5	RCP8.5
Relative change in precipitation (%)								
2050s	1.3	-6.5	11.2	10.4	2.6	-3.4	-6.6	-5.5
2080s	0.6	-6.9	12.0	19.4	-2.6	-4.6	-5.4	-10.3
Change in Maximum Temperature (^{o}C)								
2050s	1.86	2.95	1.68	2.4	1.35	2.22	1.82	2.5
2080s	2.38	4.47	2.02	3.86	1.79	3.6	2.1	4.38
Change in Minimum Temperature (^{o}C)								
2050s	2.20	3.03	2.27	3.1	1.72	2.51	1.69	2.5
2080s	2.68	4.82	2.74	5.1	2.02	3.86	2.06	4.4

Projected change in monthly precipitation of UBN based on RCP4.5 and RCP8.5 climate scenarios of four GCMs for 2050s and 2080s are shown in Figure 4.4. Precipitation is projected to decrease marginally in May - July, to increase marginally in March-April and in August-September. However, it is projected to increase significantly from October to January which is the dry season of UBN. Under both climate scenarios of CanESM2, monthly precipitation is projected to increase almost throughout the year. In contrast, projected

changes in monthly min/max temperature are consistent between the four GCMs and the months. On a whole, maximum temperature is projected to a larger increase during the rainy than the dry seasons, but the reverse is projected for minimum temperature of UBN, a larger increase in the dry than the rainy season.
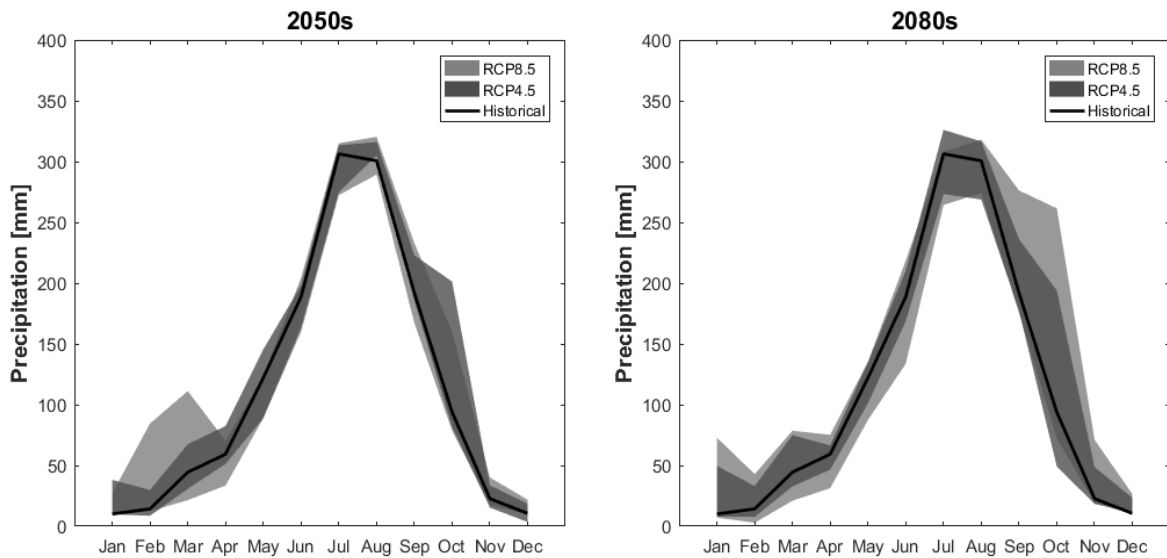
Figure 4.4: Projected monthly precipitation of four GCMs downscaled by WRF for UBN under RCP4.5 and RCP8.5 climate scenarios for 2050s and 2080s.

4.4.3. Projected Change to the Mean Annual streamflow

The hydrologic models are driven by RCP4.5 and RCP8.5 climate scenarios of four GCMs downscaled by WRF to project the future runoff of UBN, assuming the calibrated model parameters remain valid under climate scenarios in future periods. The projected changes in the streamflow of UBN for 2050s and 2080s were assessed against the base period of 1976-2005 to evaluate the hydrologic impact of climate change on UBN.

Projected changes in the future mean annual streamflow simulated by three models driven by two climate scenarios of four GCMs downscaled by WRF (see Table 4.3) vary widely due to the wide range of precipitation projected by the four GCMs. The mean annual streamflow of UBN is projected to decrease by all three hydrologic models driven by both RCP climate scenarios of all GCMs, except for CanESM2 that projected a significant increase in future precipitation, which led to a significant increase in the projected mean annual streamflow of UBN. Projected changes in the mean annual streamflow differ slightly between the three models, e.g., NAM projected the largest decrease in the mean annual streamflow under the climate scenarios of three GCMs but the largest increase under CanESM2. The change in the mean annual streamflow simulated by Watflood is similar to the precipitation change projected by the GCMs, which are predominantly negative except for CanESM2 as explained above. On a whole, Watflood simulated a smaller decrease in the mean annual streamflow of UBN than NAM and VIC partly because the latter models estimated higher ETo than Watflood. The future streamflow of UBN will either increase or decrease, depending on the net change in rainfall and evapotranspiration loss subjected to climate change impact. As expected, a larger change in the mean annual streamflow was projected under RCP8.5 than RCP4.5 climate scenarios. On a whole, forcing the three hydrological models using climate scenarios of four GCMs, the median of the mean annual streamflow of UBN are projected to change by -7.6% with a range of -19.7 to 17.7% in the 2050s and by -12.7% with a range of -26.8 to 31.6% in 2080s. Previous climate change studies on UBN also projected changes that range from an increase to a decrease in the future streamflow of UBN, depending mainly on

the projections of GCMs, e.g., Kim and Kaluarachchi (2009), and Elshamy et al. (2009). Using six GCMs' output under A2 emission scenarios, Kim and Kaluarachchi (2009) projected changes in the mean annual streamflow of UBN to range between -32 and 80% in 2050s. Elshamy et al. (2009) also projected the ensemble mean annual streamflow of UBN to decrease by 15%, with a range of -60% to +45% in 2081-2098 compared to the 1961-1990 baseline period.

Table 4.3 Percentage change in the mean annual flow projected by three hydrologic models driven by climate scenarios of four GCMs downscaled by WRF for 2050s and 2080s.

	NAM Model				Watflood				VIC model			
	RCP4.5		RCP8.5		RCP4.5		RCP8.5		RCP4.5		RCP8.5	
	2050	2080	2050	2080	2050	2080	2050	2080	2050	2080	2050	2080
ACCESS1-3	-1.9	-4.9	-24.9	-33.1	3.0	1.6	-8.7	-12.3	-5.24	-5.3	-19.7	-26.8
CanESM2	28.5	26.9	26.5	48.6	17.7	18.2	17.4	31.6	15.6	15.9	14.7	27.7
GFDL-ESM2M	-5.0	-19.4	-25.7	-34.2	3.6	-5.3	-7.9	-8.7	-1.2	-10.7	-13.4	-20.3
MPI-ESM-LR	-24.6	-22.1	-19.6	-40.7	-10.7	-8.7	-7.2	-13.7	-16.4	-14.7	-13.3	-25.5

Similar to projected changes to the mean monthly precipitation, projected changes to the mean monthly streamflow of UBN also differ from month to month (Figure 4.5). The mean monthly streamflow of UBN are projected to increase (decrease) by NAM driven by climate scenarios of CanESM2 (other GCMs). However, the median of projected changes in monthly streamflow by NAM is consistently a decrease compared to the base period. On the other hand, the mean monthly streamflow of UBN are always projected to increase by VIC and Watflood when the models are driven by climate scenarios of CanESM2, but to always decrease when they are driven by climate scenarios of MPI-ESM-LR. VIC and Watflood driven by climate scenarios of all four GCMs projected the median of the mean monthly

streamflow changes of UBN to increase over the dry season but to decrease over the rainy season, which is more or less similar to the monthly projected change in precipitation.
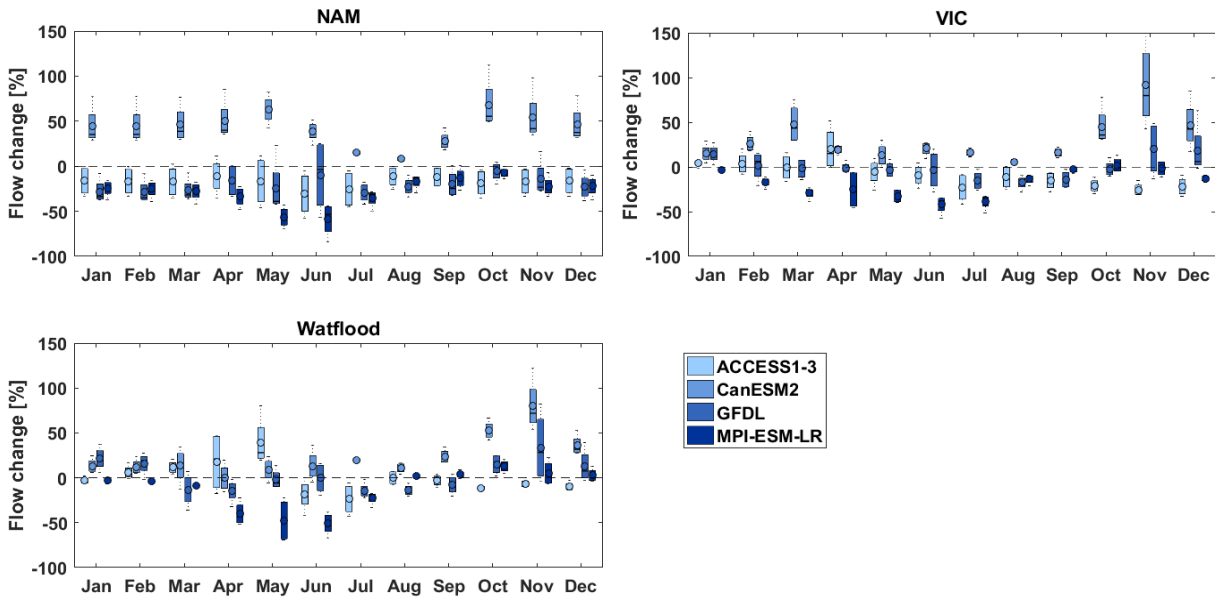
Figure 4.5: Monthly change in streamflow of UBN under four GCMs downscaled by WRF for RCP4.5 and RCP8.5 climate scenarios and both future periods.

Overall, the mean monthly streamflow of UBN projected by the three hydrological models differ from each other, partly because of different model structure. Sources of uncertainties associated with streamflow projections can be broadly classified under the structure of hydrologic models, climate data, GCMs and climate scenarios, which are related to future emissions of greenhouse gases and their radiative forcing (Kerkhoven and Gan, 2011). However, it is difficult to estimate the proportion of uncertainties attributed to these few sources accurately, partly because we have only conducted this study using four GCMs, three hydrologic models, and two RCP climate scenarios. Mathematical models are simplified

versions of nature, we expect uncertainties associated with models to be related to the structure and complexity of models. Given differences in the mean annual streamflow simulated by the three hydrologic models are larger than differences in the mean annual streamflow simulated by each hydrologic model driven by different GCMs, it seems that uncertainties attributed to hydrologic model structure are likely larger than uncertainties related to climate model structure and their climate scenarios. This could be partly because of significant differences in the structure between the three hydrologic models as explained above. Overall, median changes in the mean monthly streamflow of UBN are projected to increase in the dry season and to decrease in the rainy season by the three hydrologic models driven by two RCP scenarios of four GCMs in 2050s and 2080s with respect to the base period.

4.4.4.   Climate change impact on extremes

From 30 years of daily observed and projected streamflow time series of UBN, the annual maximum (minimum) streamflow are selected and ranked in descending order to estimate the return periods of 30 annual maxima (minima) streamflow. There are obvious differences between annual maxima and minima projected by the three models for 2050s and 2080s. The projected change in the annual maxima is larger for high than for lower return periods as shown in Table 4.4. Relative to the base period, annual maxima of high return period are projected to increase by a ratio of 1.08 to 1.13, while annual maxima of low return periods are projected to decrease by a ratio of about 0.85. On the other hand, annual minima of low return periods are projected to remain almost unchanged, but are projected to decrease under high

return periods, e.g., the ratio of the projected change of annual minima range from 1.0 to 0.73. This implies that UBN is likely to experience more frequent and/or more severe flooding and droughts in the future.

Table 4.4: Ensemble range and median of change between observed and projected daily peak/low flow extremes for UBN under two downscaled RCP climate scenarios of four GCMs for 2050s and 2080s.

Return period (years)	Peak flows		Low flows	
	Range of Change for Projected over observed	Median of Change	Range of Change for Projected over observed	Median of change
1	0.53 – 1.99	0.85	0.83-1.45	1.00
2	0.89 – 1.29	0.97	0.77-1.37	0.99
5	0.98 – 1.31	1.08	0.68-1.41	0.90
10	0.93 – 1.43	1.13	0.58-1.37	0.84
25	0.92 – 1.42	1.10	0.47-1.46	0.73

Under the same RCP climate scenarios for 2050s and 2080s, similar ranges of change for annual maxima are also projected by the three hydrological models. On a whole, there are larger differences between annual minima simulated by NAM, VIC and Watflood, e.g., NAM mostly simulated smaller annual minima of high return periods while Watflood simulated minimal change in the annual minima of UBN. This discrepancy between annual minima simulated by the three models is likely due to using different model structure for simulating baseflow. NAM uses the lumped approach and a simplified linear reservoir for modeling the baseflow, while VIC uses a distributed approach and routing schemes to compute the baseflow. The differences between annual minima simulated by the three models are larger

than differences simulated by the same hydrologic model driven by various downscaled climate change scenarios of the four GCMs.

Given the considerable decrease in annual minima projected by all three models, it seems that UBN could experience more frequent or severe droughts under climate change impact, which would affect different sectors, such as the municipal and agriculture sectors, and the future navigation in the Nile for both upstream and downstream countries of the Nile river basin. Similar changes to UBN are also projected in previous climate change impact studies for the UBN cited in the Introduction, except in Aich et al (2014) who projected an increase in the annual minima of UBN.

4.5. Summary and conclusions

The potential impact of climate change on the future mean and extreme streamflow of UBN in the 2050s and 2080s was projected by three hydrological models (NAM, VIC and Watflood models) driven with RCP4.5 and RCP8.5 climate scenarios of four GCMs dynamically downscaled by WRF. The mean daily maximum (minimum) temperature of UBN are projected to increase by about $1.35 - 2.38$ ($1.72 - 2.74$) ^{o}C under RCP4.5, and $2.22 - 4.47$ ($2.5 - 5.1$) ^{o}C under RCP8.5 climate scenarios for future periods with respect to the base period of 1976-2005. However, projected changes in the mean annual precipitation vary widely, ranging from -10.3 to 19.4%, but generally projected to decrease in the summer and increase in the winter, under both RCP climate scenarios over 2050s and 2080s.

Driven with gridded ERA-Interim data dynamically downscaled by WRF, the NAM, VIC and Watflood hydrologic models were calibrated and independently validated against observed

streamflow of the El-Diem gauging station. Almost all models have captured the overall streamflow dynamics of the UBN river basin accurately. At the calibration and validation stages, NSE and R^2 of simulated versus observed streamflow obtained are above 0.6, while the ME and RMSE are relatively low. On a whole, using three hydrological models driven by the RCP climate scenarios of four GCMs, the median of mean annual streamflow of UBN are projected to decrease by 7.6%, with a range of -19.7 to 17.7% in the 2050s, and by 12.7%, with a range of -26.8 to 31.6% in the 2080s. The mean streamflow of UBN is projected to increase in the winter, decrease in the summer, but on a whole, its mean annual streamflow is projected to decrease.

Both the annual maxima and minima of streamflow are projected to increase under climate scenarios of CanESM2 in both future periods compared with other GCMs. Annual maxima of high return periods are projected to increase by a ratio of 1.08 to 1.13, while annual maxima of low return periods are projected to decrease by a ratio of about 0.85. On the other hand, annual minima of low return periods are projected to remain almost unchanged, but are projected to decrease under high return periods, e.g., the ratio of the projected change of annual minima range from 1.0 to 0.73. This implies that UBN is likely to experience more frequent and/or more severe flooding and droughts in the future. This would affect different sectors of users, such as the municipal and agriculture sectors and future navigation in the Nile for both upstream and downstream countries of the Nile river basin.

Differences between the streamflow simulated by NAM, VIC and Watflood, especially for low flow, are larger than differences in the streamflow simulated by each hydrologic model

driven by RCP climate scenarios of different GCMs, partly because of significant differences in the structure between the three models, conceptual and lumped (NAM) versus partial physically based and distributed models (VIC and Watflood). Therefore, decision makers who plan to adapt water resources management to mitigate potential impact of climate change should be aware of uncertainties associated with streamflow projections, and sources of uncertainties, such as hydrologic or climate model structure, climate data, future emissions of greenhouse gases and their respective radiative forcing.

To overcome limitations of this study, such as using RCP climate scenarios of more GCMs (instead of only four GCMs) dynamically downscaled by a regional climate model such as WRF to resolutions of climate scenarios adequate to model basin scale hydrologic processes of UBN. Another limitation of this study is the possible effect of land use/cover change of UBN due to future developments of Ethiopia which could also exert significant impact on the future water resources of UBN.

References

Aich, V., Liersch, S., Vetter, T., Huang, S., Tecklenburg, J., Hoffmann, P., Koch, H., Fournet, S., Krysanova, V., Müller, E. N., and Hattermann, F. F. (2014) Comparing impacts of climate change on streamflow in four large African river basins. Hydrology and Earth System Sciences, 18(4), 1305–1321. doi: 10.5194/hess-18-1305-2014.

Allen, R.G., Pereira, L.S., Raes, D., and Smith, M. (1998) Crop evapotranspiration (guidelines for computing crop water requirements). Food and Agriculture Organization of the United Nations Irrigation and Drainage Paper 56, 328 pp.

Ashfaq, M., Bowling, L.C., Cherkauer, K., Pal, J.S., & Diffenbaugh, N.S. (2010) Influence of climate model biases and daily-scale temperature and precipitation events on hydrological impacts assessment: A case study of the United States. J. Geophys. Res., 115, D14116. doi.:10.1029/2009JD012965.

Beyene T, Lettenmaier D.P, Kabat P. (2010) Hydrologic impacts of climate change on the Nile River Basin: implications of the 2007 IPCC scenarios. Climatic Change 100: pp. 433-461. doi:10.1007/s10584-009-9693-0.

Benoit, R., Kouwen, N., Yu, W., Chamberland, S., & Pellerin, P. (2003) Hydrometeorological aspects of the Real-Time Ultrafinescale Forecast Support during the Special Observing Period of MAP. Hydrology and Earth System Sciences, 7(6), 877–889, doi: 10.5194/hess-7-877-2003.

Boko M, Niang I, Nyong A, Vogel C, Githeko A, Medany M, Osman-Elasha B, Tabo R and Yanda P. (2007) Africa Climate Change 2007: Impacts, Adaptation and Vulnerability. Contribution of Working Group II to the Fourth Assessment Report of the Intergovernmental Panel on Climate Change, Parry M L, Canziani O F, Palutikof J P, van der Linden P J and Hanson C E (eds). Cambridge University Press, Cambridge UK, 433 – 467.

Box, G.E.P., Cox, D.R. (1964) An analysis of transformations. J. Roy. Statist. Soc. 26, 211–243 (Discussion 244–252).

DHI, (2008) MIKE 11, a modelling system for rivers and channels, Reference manual. DHI Water & Environment, Horsholm, Denmark.

Elshamy, M. E, Seierstad I. A, and Sorteberg A (2009) Impacts of climate change on Blue Nile flows using bias-corrected GCM scenarios, Hydrol. Earth Syst. Sci., 13, 551-565, doi:10.5194/hess-13-551-2009.

Funk C.C, Peterson P.J, Landsfeld M.F, Pedreros D.H, Verdin J.P, Rowland J.D, Romero B.E, Husak G.J, Michaelsen J.C, and Verdin A.P (2014) A quasi-global precipitation time series for drought monitoring: U.S. Geological Survey Data Series 832, 4 p., http://dx.doi.org/110.3133/ds832.

Gao, H., Tang, Q., Ferguson, C. R., Wood, E. F., & Lettenmaier, D. P. (2010) Estimating the water budget of major US river basins via remote sensing. International Journal of Remote Sensing, 31:14, 3955-3978, DOI: 10.1080/01431161.2010.483488.

Gizaw, M., Biftu, G., Gan, T. Y., Moges, S., and Koivosalo, H. (2017) Potential Impact of climate change on streamflow of major Ethiopian rivers, Climatic Change, DOI: 10.1007/s10584-017ef-2021-1.

Gizaw, M., and Gan, T. Y., (2016) Impact of Climate Change and El Niño Episodes on Droughts in sub-Saharan Africa, Climate Dynamics, Springer, DOI: 10.1007/s00382-016-3366-2.

Gopalakrishnan C. (2013) Water and disasters: a review and analysis of policy aspects, International Journal of Water Resources Development, 29:2, 250-271, DOI:10.1080/07900627.2012.756133.

Grigg, N. S. (2014). The 2011–2012 drought in the United States: new lessons from a record event. International Journal of Water Resources Development, 30(2), 183–199. doi:10.1080/07900627.2013.847710.

Harris I, Jones P.D, Osborn T.J, and Lister D.H (2014) Updated high-resolution grids of monthly climatic observations–the CRU TS3.10 Dataset. Int. J. Climatol., 34, 623–642. doi: 10.1002/joc.3711.

IPCC (2013) Climate Change 2013: The Physical Science Basis. Contribution of Working Group I to the Fifth Assessment Report of the Intergovernmental Panel on Climate Change [Stocker, T.F., D. Qin, G.-K. Plattner, M. Tignor, S.K. Allen, J. Boschung, A. Nauels, Y. Xia, V. Bex and P.M. Midgley (eds.)]. Cambridge University Press, Cambridge, United Kingdom and New York, NY, USA, 1535 pp.

Jarvis, A., H.I. Reuter, A. Nelson, E. Guevara, (2008) Hole-filled SRTM for the globe Version 4, available from the CGIAR-CSI SRTM 90m Database (http://srtm.csi.cgiar.org).

Kerkhoven, E., and T.Y. Gan, (2011) Unconditional uncertainties of historical and simulated river flows subjected to climate change, *J. of Hydrology*, *396*(1-2), 113-127. DOI:10.1016/j.jhydrol.2010.10.042.

Kim, U., & Kaluarachchi, J. J. (2009). Climate Change Impacts on Water Resources in the Upper Blue Nile River Basin, Ethiopia. JAWRA Journal of the American Water Resources Association, 45(6), 1361–1378. doi:10.1111/j.1752-1688.2009.00369.x.

Kouwen, N., E.D. Soulis, A. Pietroniro, J. Donald, and R.A. Harrinton (1993) Grouping Response Unit for Distributed Hydrologic Modelling, ASCE Journal of Water Resources Management and Planning, 119(3): 289-305, doi:10.1061/(ASCE)0733-9496(1993)119:3(289).

Lemke, et al., (2007) Observations: Changes in Snow, Ice and Frozen Ground. Climate Change 2007: The Physical Science Basis. Working Group I to the 4th Assessment Rept of IPCC, Cambridge University Press.

Liang, X., Wood, E. F., & Lettenmaier, D. P. (1996) Surface soil moisture parameterization of the VIC-2L model: Evaluation and modification. Global and Planetary Change, 13, 195–206.

Liersch, S., Tecklenburg, J., Rust, H., Dobler, A., Fischer, M., Kruschke, T. and Koch, H., Hattermann, F. (2016) Are we using the right fuel to drive hydrological models? A climate impact study in the Upper Blue Nile. Hydrol. Earth Syst. Sci. Discuss. doi:10.5194/hess-2016-422.

Lohmann, D., E. Raschke, B. Nijssen and D. P. Lettenmaier (1998) Regional scale hydrology: I. Formulation of the VIC-2L model coupled to a routing model, Hydrol. Sci. J., 43(1), 131-141.

Maurer EP, Wood AW, Adam JC, Lettenmaier DP, Nijssen B (2002) A long-term hydrologically- based data set of land surface fluxes and states for the conterminous United States. J Climate 15:3237–3251.

Meehl, G. A. (2004) More Intense, More Frequent, and Longer Lasting Heat Waves in the 21st Century. Science, 305(5686), 994–997. https://doi.org/10.1126/science.1098704

Nijssen, B.N., G.M. O'Donnell, D.P. Lettenmaier and E.F. Wood, 2001: Predicting the discharge of global rivers, J. Clim., 14(15), 3307-3323, doi: 10.1175/1520-0442(2001)014<3307:PTDOGR>2.0.CO;2.

Pietroniro, A., Leconte, R., Toth, B., Peters, D. L., Kouwen, N., Conly, F. M., & Prowse, T. (2006) Modelling climate change impacts in the Peace and Athabasca catchment and delta: III—integrated model assessment. Hydrological Processes, 20(19), 4231–4245. doi:10.1002/hyp.6428.

Priestley, C. H. B., and R. J. Taylor (1972) On the assessment of surface heat flux and evaporation using large-scale parameters. Mon. Wea. Rev., 100, 81–92.

Schneider U, Becker A, Finger P, Meyer-Christoffer A, Rudolf B, Ziese M (2011) GPCC Full Data Reanalysis Version 6.0 at 0.5°: Monthly Land-Surface Precipitation from Rain-Gauges built on GTS-based and Historic Data. DOI: 10.5676/DWD_GPCC/FD_M_V6_050.

Tariku, T.B, and Gan, T.Y (2017) Sensitivity of the Weather Research and Forecasting model to Parameterization Schemes for Regional Climate of Nile River Basin, Climate Dynamics, pp.1-17, doi: 10.1007/s00382-017-3870-z.

Tariku, T.B, and Gan, T.Y (2018) Regional Climate Change Impact on Extreme Precipitation and Temperature of the Nile River Basin, Climate Dynamics, pp. 1-20, doi: 10.1007/s00382-018-4092-8.

Taye, M. T., Ntegeka, V., Ogiramoi, N. P., & Willems, P. (2011) Assessment of climate change impact on hydrological extremes in two source regions of the Nile River Basin. Hydrology and Earth System Sciences, 15(1), 209–222. doi:10.5194/hess-15-209-2011.

Teutschbein, C., and Seibert J. (2012) Bias correction of regional climate model simulations for hydrological climate-change impact studies: review and evaluation of different methods. J. Hydrol 456–457:12–29.

Vörösmarty C. J, Douglas E. M, Green P. A, and Revenga C (2005) Geospatial indicators of emerging water stress: an application to Africa. Ambio, 34, 230-236.

Willems, P., (2009) A time series tool to support the multi-criteria performance evaluation of rainfall-runoff models. Environmental Modelling & Software, 24, 311–321.

Chapter 5 Optimal Operation of a Multipurpose Multireservoir system in the Blue Nile River Basin under climate change

5.1. Introduction

The Sub-Saharan Africa is the world's largest consumer of biomass energy because only one person in four in Africa has access to electricity (WWAP, 2012) even though the Nile River Basin (NRB) has enough hydropower potential to meet the entire basin's electricity needs. However, the hydropower potential of NRB is far from fully developed because of economic and political reasons (NBI, 2015). Furthermore, the amount of water withdrawn from the river is unevenly distributed among eleven riparian countries located in NRB (Goor et.al, 2010), such that Egypt and Sudan are the two largest consumers, which according to their agreement in 1959, get 55.5 billion m^3 and 18.5 billion m^3 of water per year, respectively. However, this agreement neglects upstream countries such as Ethiopia even though 85% of the Nile water comes from Ethiopian highlands. The Nile Basin Initiative launched in February 1999 by the Council of Ministers of Water Affairs of Nile Basin States has helped to develop the river in a more cooperative manner, to share socio-economic benefits from the river more equitably, and to promote regional peace and security (NBI, 2015). Currently, certain Nile riparian countries are developing their water resources to meet increasing food and energy demand due to population growth. For example, to boost hydropower production and food security, Ethiopia has started constructing one of four proposed reservoirs (Karadobi, Beko-Abo, Mendaya and Border), hydropower stations and irrigation areas in the Blue Nile River Basin (BNRB), based on studies conducted by the United States Bureau of Reclamation (USBR) in

1964 (Goor et.al, 2010; Block, 2007; Block and Strzepek, 2010). Given upstream developments will have both positive and negative impact on the downstream users, a proper overall planning and management of the whole NRB is recommended.

In the past, various water resources management models have been developed to assess the hydropower and agricultural irrigation potential within Ethiopia and for the entire NRB (Guariso and Whittington 1987; Levy and Baecher 1999; Geogakakos 2006; Whittington et al. 2005). Digna et al. (2016) provided a detailed review on past studies on the water resources management of NRB. These studies have provided insight to develop and to manage viable hydropower and irrigation projects for NRB, which will potentially have significant hydrologic and economic implications for the entire river basin. For example, Guariso and Whittington (1987) developed a linear programming model to predict long-term consequences of the proposed water resources development program of Ethiopia over the Blue Nile to Egypt and Sudan. They showed that developing the four reservoirs by Ethiopia would benefit downstream countries by effectively ending the annual Nile flood; by increasing the amount of water available for agriculture because the river could be more easily regulated downstream, thus reducing storage requirements in Sudan and evaporation losses from the Aswan High Dam Reservoir.

Whittington et al. (2005) developed an economic model to optimize the water resources of the entire NRB. They used a non-linear, constrained optimization algorithm to determine the annual pattern of water use that will maximize the sum of economic benefits from irrigated agriculture and hydropower generation in the Nile basin. However, their study did not

consider the stochastic nature, possible climate change impact and climate variability of the Nile River. Goor et al. (2010) developed a stochastic, hydro-economic model for the Eastern Nile River Basin to assess the impacts of upstream development in the Blue Nile basin on the allocation decisions, reservoirs operating strategies, and the economic value of reservoirs in Ethiopia. They found that storage by upstream reservoirs in Ethiopia will generate positive benefits to both Ethiopia and Sudan. For example, by developing four proposed reservoirs, the hydropower production is projected to increase by 40TWh. Sudan will also benefit from increasing the irrigation water withdrawals by about 5.5%. Even though they concluded that the four proposed reservoirs in Ethiopia would not affect the reliability of water supply to Egypt, their study has not considered the possible hydrologic impact of climate change to future streamflow of the NRB. From a deterministic, reservoir optimization model developed to assess the implications and the feasibility of the proposed reservoirs over the 21st century, Block and Strzepek (2010) analyzed transient conditions associated with the period of filling the proposed reservoirs in Ethiopia, under the possible impact of climate variability and climate change impact. In their study, they found that neglecting the transition period of filling the reservoirs will result in over-estimating the total benefits by as much as $6 billion and the downstream flows by 170%. They also found that climate change and climate variability have considerable impact on the potential benefits of the proposed reservoirs but their results are based on raw climate change scenarios of global climate models, which are generally too coarse for the basin-scale, climate change impact study of the NRB.

.

Various water resources management models have been developed to assess the impact of certain proposed reservoirs over the upper Blue Nile on countries downstream of Egypt and Sudan. Most of the past studies have not used climate change scenarios that are downscaled to assess climate change impact to the reservoir operations of BNRB. In this study, selected Representative Concentration Pathway (RCP) climate scenarios of IPCC (2013) were dynamically downscaled by a regional climate model, the Weather and Research Forecasting (WRF) (Skamarock et al., 2008) before they are used to drive a physically-based hydrologic model, VIC, to project the future streamflow of BNRB under climate change impact. Next, the projected streamflow data are used to drive a stochastic dynamic programing model to investigate the potential impact of climate change on the water resources management and reservoir operations of the BNRB, with the objective of optimizing the hydropower production and optimal allocation of water for irrigation projects of the BNRB under future development plans. This will be enable policy makers to execute informed, prudent decisions on the future planning, design and management of water resources of the BNRB.

The chapter is organized as follows: a brief description of the study area, climate scenarios, stochastic dual dynamic programming formulations, and model parameters and assumptions are presented in Section 5.2, results and discussions in Section 5.3, and summary and conclusions are in Section 5.4.

5.2. Materials and Methods

5.2.1. Study Site

The study site is the BNRB with an approximate drainage area of 210,000 km^2, which contributes about 60% of the average annual flow of the Nile River. The NRB covers an area of about 3.35 x 10^6 km^2 which is 10% of Africa's landmass. NRB countries have the fastest growing population, with about 54% of their total population living within the NRB (Swain, 2011). The water resource of the NRB distributes unevenly between the NRB countries. A number of dams have already been constructed across the Nile River for hydropower generation, flood control, irrigation and domestic water supply, and for navigation. However, the BNRB is still unregulated, even though there is an increasing pressure to construct a new dam across the Blue Nile River for hydropower production and irrigation. Among the four major hydroelectric dams along the Blue Nile proposed by USBR in 1964, the Grand Ethiopian Renaissance Dam (GERD) is currently under construction based on a revised version of the original design of this dam. Given the runoff of the Blue Nile River is much higher than the White Nile River, this development over the Blue Nile would have significant impact on the downstream countries. Furthermore, possible hydrologic impact of climate change, such as rising temperature, increase or decrease in precipitation, and higher evaporation loss over the NRB would also affect its future water management. The proposed and existing reservoirs in the Blue Nile River basin are shown in Figure 5.1 and Table 5.1.

Table 5.1: List constructed and proposed reservoirs across the Blue Nile river basin

Fig. Symbol	Name	Country	Live storage (hm^3)	Hydropower Capacity (MW)
RR1	Tis Abbay I and II	Ethiopia	Run-of-river	86
RR2	Tana-Beles	Ethiopia	Run-of-river	270
R2	Karadobi*	Ethiopia	17000	1600
R3	Beko-Abo*	Ethiopia	20000	2100
R5	Mandaya*	Ethiopia	24000	1620
R6	GERD**	Ethiopia	75000	6500
R7	Roseires	Sudan	6900	275
R8	Sennar	Sudan	480	15

*=planned, **=under construction. Sources: ENTRO (2009) and Goor et al. (2010).
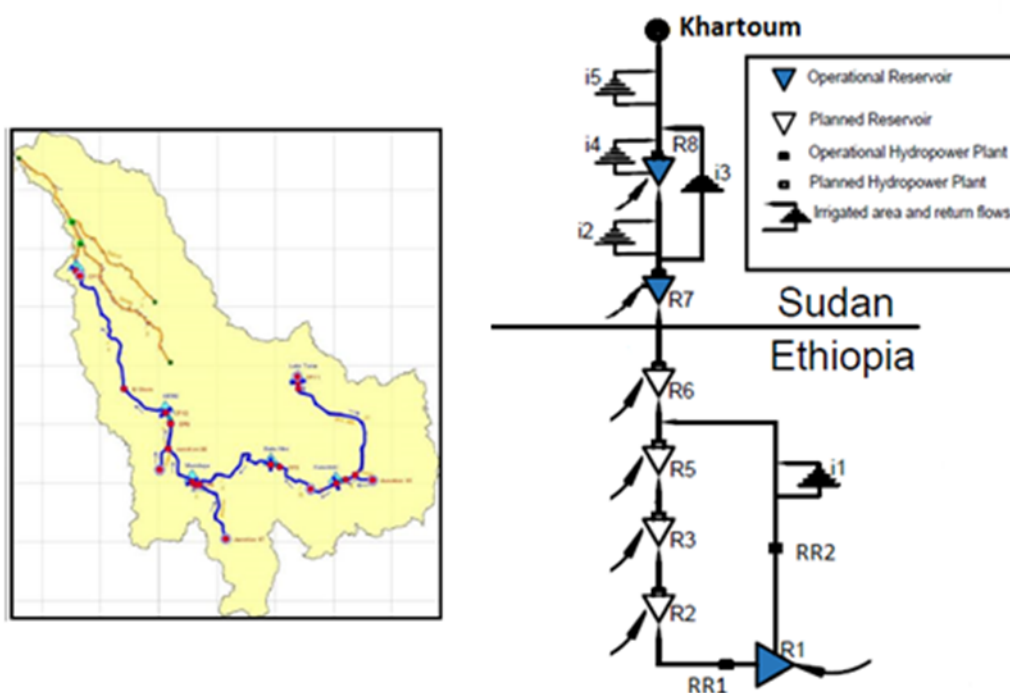
Figure 5.1: Existing and planned reservoir layout of the Blue Nile River basin; i1 up to i5 represent the irrigation sites, while R1 to R8 represent the reservoir sites over the BNRB.

5.2.2. Climate Change Scenarios

The Reginal climate model, WRF was set up for NRB (2°E to 57°E, 20°S to 37°N). The hydrologic impact of climate change on BNRB was assessed using climate variables of RCP4.5 and RCP8.5 climate scenarios of four GCMs (CanESM2, GFDL-ESM2M, MPI-ESM-LR and ACCESS1-3) of IPCC (2013) dynamically downscaled by WRF at 36 km resolution over a one-domain framework that covers the entire NRB (Tariku and Gan, 2017 and 2018; Tariku et al., 2018). Using the ERA-Interim reanalysis data, WRF was first configured and fine-tuned with various parameterization schemes until it could simulate representative regional climate of NRB (Tariku and Gan, 2017). Then WRF was used to downscale the historical data of four GCMs for the baseline period (1976-2005), and RCP4.5 and RCP8.5 climate scenarios for 2050s (2041-2070) and 2080s (2071-2100) (Tariku and Gan, 2018). The VIC macroscale hydrological model was used to simulate the water and surface energy fluxes of the BNRB in a fully distributed approach (Liang et al., 1996). Daily precipitation, maximum and minimum temperature, and wind speed simulated by WRF at 36 km grid resolution, and the specific humidity, short and longwave radiative fluxes estimated from minimum and maximum temperature using methods described by Maurer et al. (2002) were used to force the VIC model to simulate the inflow upstream and the lateral inflow at each reservoir location. The Lohmann et al. (1998) routing model is used to route the surface runoff and the baseflow output simulated by VIC for each land surface grid to the outlet/gauge station of the BNRB.

5.2.3. Stochastic dual dynamic programming (SDDP)

Stochastic dynamic programming (SDP) is one of the most commonly used optimization algorithms in reservoir network management studies for it accounts for uncertainties associated with reservoir operations based on projected hydrologic inflows, and the economic use of water (Loucks and van Beek 2005). However, SDP suffers from the curse of dimensionality because computational and memory requirements grow exponentially as the dimension of the state vector increases (Powell, 2011). Various strategies have been developed to circumvent this curse of dimensionality in SDP, such as using coarse grid/interpolation techniques, dynamic programming successive approximations, incremental dynamic programming or discrete differential dynamic programming (Labadie, 2004). The Stochastic Dual Dynamic Programming (SDDP) used in this study has been developed to remove the computational burden of discrete SDP by constructing a piecewise linear approximation of the objective function at time step $(t+1)$, F_{t+1}. SDDP was first developed by Pereira (1989) and Pereira and Pinto (1991) for operating power plants of Brazil.

In SDDP, the reservoir operation problem will be solved using certain recursive stochastic dynamic programming equations which maximize an objective function, F_t, represented by the total, present $f_t (.)$ and expected future F_{t+1} benefits obtained from the reservoir operation (Goor et al, 2010; Tilmant and Kelman, 2007; and Tilmant et al., 2008; 2009). The problem is set up as below:

$$F_t(s_t, q_t, y_t) = max_{r_t} \left\{ f_t(s_t, q_t, r_t, y_t) + E_{q_{t+1}|q_t}[F_{t+1}(s_{t+1}, q_t, y_{t+1})] \right\} \qquad (5.1)$$

Where s_t is the volume of water stored in the system at the beginning of period t and q_t is the current or forecasted inflows to the system. r_t is a vector of decision variables (outflow or reservoir release) and y_t is the volume of water stored for irrigation water requirement at the beginning of period t and $E[.]$ is the expectation operator for the forecasted inflow q_{t+1} given the current inflow of q_t.

The optimization of reservoir operations is subjected to several physical constraints: (a) the reservoir storage is bounded by lower ($\underline{s}_{t+1}$) and upper ($\bar{s}_{t+1}$) storage levels; (b) the maximum release ($\bar{r}_t$) is constrained by the turbine capacity of the hydropower station while the minimum release ($\underline{r}_t$) is to maintain a desired downstream minimum flow for environmental conservation, water quality, and navigation; and (c) the conservation of mass based on inflow, outflow and changes in reservoir storage.

$$\underline{s}_{t+1} \leq s_{t+1} \leq \bar{s}_{t+1}$$

$$\underline{r}_t \leq r_t \leq \bar{r}_t$$

$$s_{t+1} - C_R(r_t + l_t) = s_t + q_t - e_t(s_t) - i_t \tag{5.2}$$

For irrigation constraints: (a) irrigation water withdrawals are limited by the pumping station or channel capacity and crop water requirements; (b) throughout the growing season a continuity equation is used to keep track of the mass balance of "dummy" reservoirs of accumulated water for irrigation purposes; and (c) lower and upper bounds of "dummy" reservoirs.

$$\underline{i}_t \leq i_t \leq \bar{i}_t$$

$$y_{t+1} - \epsilon i_t \leq y_t$$

$$\underline{y}_{t+1} \leq y_{t+1} \leq \bar{y}_{t+1} \qquad (5.3)$$

Where l_t is the vector of spills; C_R is the system connectivity matrix ($C_R(j,k) = 1(-1)$) when reservoir j receives (releases) water from (to) reservoir k); e_t is the vector of evaporation losses; i_t is the vector of irrigation water withdrawals, ϵ is the vector of irrigation efficiencies, and y_{t+1} representing the end-of-period accumulated water into those "dummy" reservoirs.

The SDDP model will maximize net benefits from both irrigation and hydropower sectors by identifying optimal release $\mathbf{r_t}$ (j) and irrigation withdrawal $\mathbf{i_t}$ (j) decisions at each node **j** and for each time t step ϵ [1,…T], where T is the study or the planning period. The time step can be hourly, daily, weekly, monthly, or even seasonal, depending on the nature and scope of the reservoir system optimization problem (Labadie, 2004). A monthly time step was used for this study. The immediate benefit function $\mathbf{f_t}$ (.) is the sum of hydropower production ($\mathbf{HP_t}$), irrigated agriculture ($\mathbf{IR_t}$) and penalties for not meeting the target constraints.

$$f_t(s_t, q_t, R_t, y_t) = HP_t + IR_t - \xi_t x_t \qquad (5.4)$$

Where x_t is a vector of slack/surplus variables which incur a lost of benefits to the objective function estimated using an assumed rate of penalties ξ_t ($/unit of deficit or surplus) over x_t. The penalties represent the costs of not meeting the operational, physical, institutional, and/or legal constraints such as minimum flows, minimum storage volumes, minimum water withdrawals, etc.

1. **The net benefits from hydropower generation**

The benefit of hydropower from J number of hydropower plants will be calculated as follow:

$$HP_t = \tau_t \sum_{j=1}^{J} \left(\pi_t^h(j) - \theta^h(j) \right) \alpha(j) \widehat{P}_t(j) \tag{5.5}$$

Where τ is the number of hours in period t, $\widehat{P}_t$ is the power generated by hydropower plant j during period t (MW), $\pi^h(j)$ is the energy prices (\$/MWh); $\theta^h(j)$ is the variable cost (Operation and Maintenance) of hydropower plant j (\$/MWh) and α is a dimensionless adjustment coefficient. The power production of hydropower plant j is given as follow:

$$\widehat{P}_t = \gamma \eta(s_t, s_{t+1}, r_t) . h(s_t, s_{t+1}) . r_t \tag{5.6}$$

Where γ is specific weight of water (N/m^3); **h** is net hydraulic head of turbine (m), depending on the average storage (s_t, s_{t+1}) during period **t**; η is turbines/generators efficiency as a function of the average hydraulic head and the rate of discharge during period **t**; and r_t is the turbine outflow (m^3/s).

The hydropower production is a nonlinear function of the hydraulic head and the rate of release. There are many way to linearize this nonlinear function for SDDP. One approach is to assume that the hydropower production is dominated by the release term r_t but not by the hydraulic head approximated as a constant. Wallace and Fleten (2003) and Tilmant and Kerman (2007) defined a production coefficient c^h (MW/m^3/s) to characterize each hydropower station which only works when the difference between downstream and upstream water levels is small compared to the maximum level of the reservoir. The second method is proposed by Cunha et al. (1997) which approximates the hydropower function by linear and

concave functions of storage and total outflow of the power plant. The second method is used in this study, the detailed comparison of the two methods can be found in Goor et al, (2011).

2. The net benefits from irrigated agriculture

Tilmant et al. (2008) proposed to estimate net benefits from agricultural IR_t by considering "dummy" reservoirs as accumulated water allocated to irrigation sites at the end of crop harvest.

$$IR = \begin{cases} \sum_{d=1}^{D} \widehat{IR}_t^d[y_t(d)] & if\ t = t_f \\ 0 & if\ t \neq t_f \end{cases} \tag{5.7}$$

The benefits of agricultural water use at demand site **d** can be approximated by a piecewise linear function of accumulated water throughout the growing season. The overall benefits of agricultural sector IR are the sum of net benefits obtained from each irrigation sites (d=1,2, ..., D).

The benefit-to-go function F_{t+1} are dependent on the following constraints for L number of linear approximation functions:

$$\begin{cases} F_{t+1} - \varphi_{t+1}^1 s_{t+1} - \eta_{t+1}^1 y_{t+1} \leq \gamma_{t+1}^1 q_t + \beta_{t+1}^1 \\ \vdots \\ F_{t+1} - \varphi_{t+1}^L s_{t+1} - \eta_{t+1}^L y_{t+1} \leq \gamma_{t+1}^L q_t + \beta_{t+1}^L \end{cases} \tag{5.8}$$

Detailed explanations and derivations of the parameters, $\varphi_{t+1}^1, \eta_{t+1}^1, \gamma_{t+1}^1,$ and β_{t+1}^1, related to storage, irrigation demand, lateral inflow, and a physical constant for time step (*t+1*), respectively, are given in Tilmant and Kelman (2007), Tilmant et al. (2008) and Goor et al. (2011). The SDDP model is coded in MATLAB and relies on Gurobi linear programming solver.

5.2.4. Model parameters and assumptions

In this study, similar to Whittington et al. (2005) and Goor et al. (2010), the seasonal, short-run marginal cost (SRMC) are assumed to be 80 US$/MWh for the firm power and 50 US$/MWh for the secondary power for both Sudan and Ethiopia. The dominant crops cultivated over the Sudan and Ethiopia irrigation sites are wheat, sorghum, sugar cane, groundnuts, and vegetables, and their crop water requirements are estimated using the software CROPWAT. The flat demand curves for irrigation water withdrawals are assumed to have a net return of 0.05 US$/$m^3$ in this study (Goor et al., 2010 and Whittington et al., 2005).

We chose to work with a planning horizon of 10 years (T=120 month). Twenty backwards openings or trials (K=20) are set up and the forward simulation is carried out using 30 synthetic hydrological scenarios (M=30). The multisite, periodic autoregressive model of order p, *PAR(p)* are used to generate stochastic inflow to each reservoirs based on 43 years of historical streamflow (1954-1996). After obtaining optimal operation parameters of the reservoirs using a stochastic streamflow generator over the planning horizon, we re-run the full historical streamflow to evaluate the optimized results.

In this study, we assumed that the entire proposed hydropower project over the BNRB will be implemented in the 2050s and 2080s. Projected changes to the streamflow of BNR vary widely between the RCP4.5 and RCP8.5 climate scenarios of the four selected GCMs downscaled by WRF for 2050s and 2080s as shown in Figure 5.2. From the streamflow simulated by VIC driven with these climate scenarios, the minimum, median, and maximum projected change in streamflow for 2050s and 2080s are estimated. Next, these three sets of

projected change in streamflow (Δq) over the baseline period (1976-2005) are used to perturb the 43 years historical streamflow. The projected annual change in the streamflow at Lake Tana and GERD reservoir are shown in Figure 5.3, which shows that due to climate change impact, the mean annual streamflow of the BNRB are projected to decrease, but with a higher streamflow variability, in the mid and late 21th century.
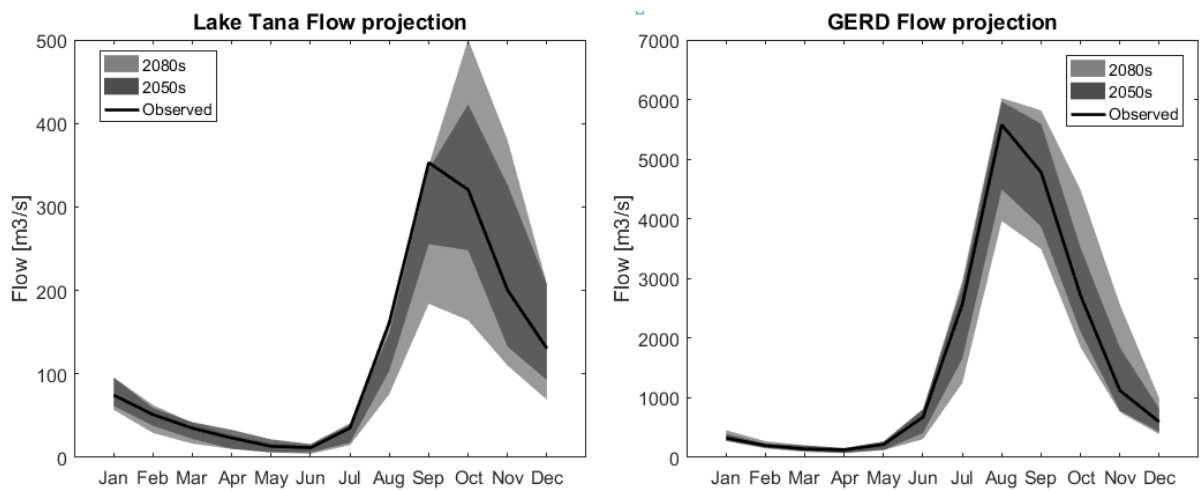
Figure 5.2: The projected change of BNRB streamflow at Lake Tana outlet and Boarder (GERD reservoir) using the climate scenarios of four GCMs dynamically downscaled by WRF for 2050s and 2080s.
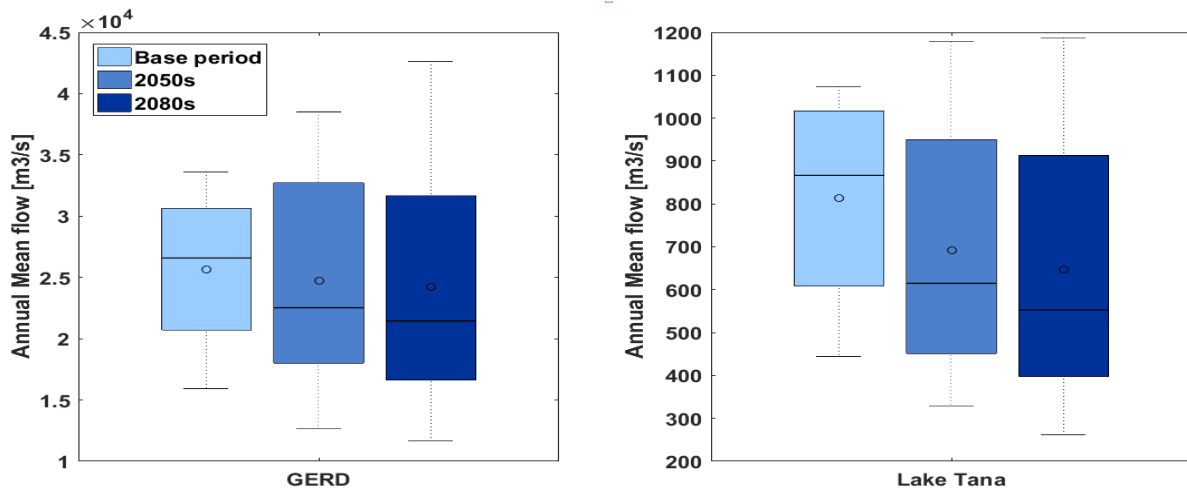
Figure 5.3: Boxplots of the historical and projected annual mean streamflow of BNRB at Lake Tana outlet and Boarder (GERD reservoir) using the climate scenarios of four GCMs dynamically downscaled by WRF for 2050s and 2080s.

5.3. Results and discussions

5.3.1. Drawdown-refill cycles

The drawdown-refill cycles for the GERD reservoir under historical, maximum, median and minimum projected change in streamflow of BNRB for 2050s and 2080s are shown in Figure 5.4. Overall, it seems the GERD reservoir will likely not operate at full storage level, because the streamflow of BNRB is assumed to be regulated by three upstream reservoirs (R2, R3 and R5 in Figure 5.1). Because of flow regulation by upstream reservoirs, the depletion during dry season and refilling during the high flow season for the GERD reservoir is expected to be small. On the other hand, if without the upstream reservoirs, the GERD reservoir will reach full storage capacity during the rainy season and mostly depleted during the dry season. Even with the upstream reservoirs, under the maximum projected change in streamflow, the GERD

reservoir is still projected to refill to a high storage capacity. Under median and minimum projected changes in the streamflow, the operating storage of the GERD reservoir is projected to decrease compared to reservoir storage under the historical condition. In addition, based on the three projected changes in streamflow, the levels of the GERD reservoir are projected to be lower in 2080s than in 2050s. Under climate change impact, similar changes are also projected in the other three proposed upstream reservoirs. However, due to their limited capacities, the downstream, Sennar and Roseires reservoirs are expected to always operate at the full reservoir capacity under all three projected changes in streamflow.

5.3.2. Evaporation losses

The evaporation losses from all the reservoirs is expected to increase in the future because the temperature of the BNRB is projected to increase by $1.67 – 3^oC$ in 2050s and by $2 – 4.6^oC$ in 2080s. Under historical climate, the average annual evaporation loss in the four proposed reservoirs in Ethiopia is estimated to be about 822 hm^3, which is projected to increase to 1190, 986 and 811 hm^3 under the maximum, median and minimum projected changes in streamflow for 2050s, respectively. The corresponding evaporation loss in Ethiopia is projected to increase to 1341, 1034 and 769 hm^3 in the 2080s. Apparently, the evaporation loss in Ethiopian reservoirs under the minimum projected streamflow change is projected to be smaller than under the historical condition because the amount of water stored in the reservoir is projected to be smaller. In 2080s, the annual evaporation loss from Sennar and Roseires reservoirs are projected to increase from 2472 to 2918, 2764 and 2631 hm^3 under the maximum, median and minimum projected change in streamflow, respectively. In 2050s, the

corresponding evaporation loss from Sennar and Roseires reservoirs are projected to increase to 2763, 2679 and 2599.7 hm^3, respectively. As the climate becomes warmer over the 21st century, the evaporation losses in all reservoirs are projected to be higher in the 2080s than in the 2050s. Further, the evaporation losses of Sudan reservoirs are expected to be higher than that of Ethiopian reservoirs because Sudan has higher temperature and lower precipitation. This means that Ethiopian reservoirs should generally store a larger amount of water compared to reservoirs in Sudan or in Egypt.
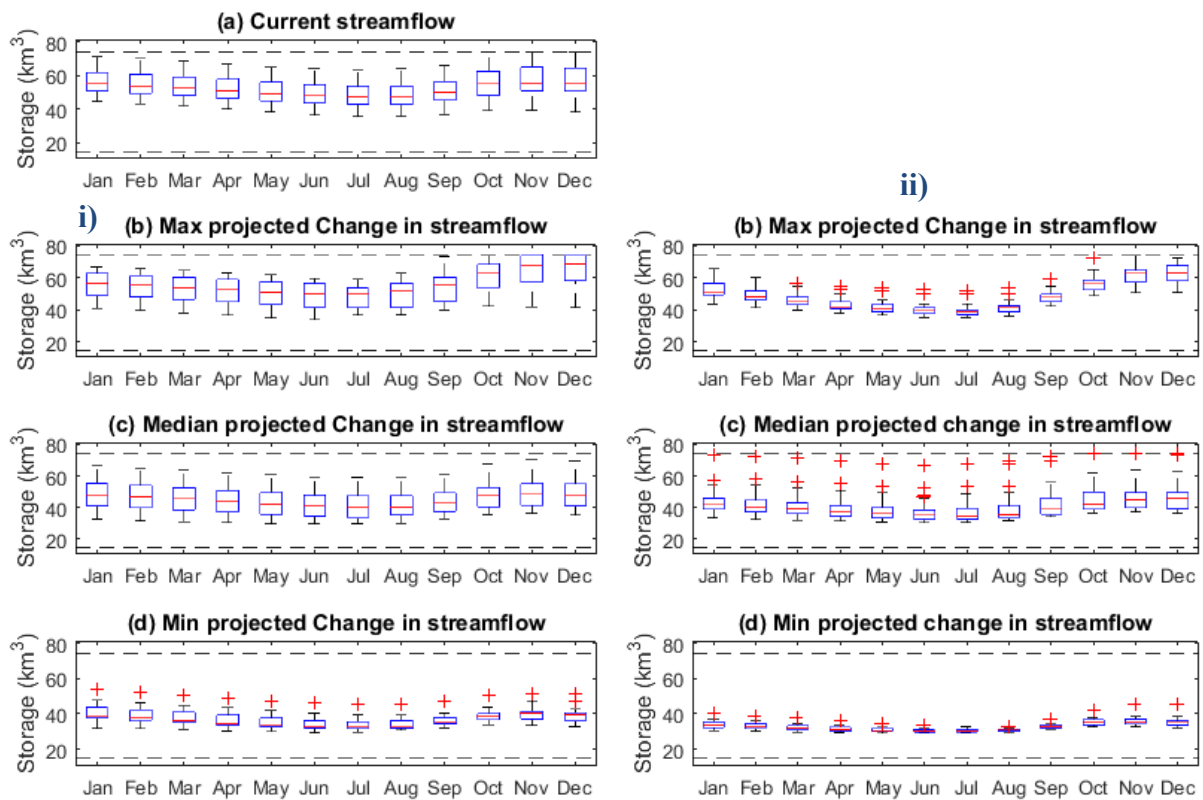
Figure 5.4: Simulated monthly storage of the GERD reservoir under current, maximum, median and minimum projected change in streamflow for (i) 2050s and (ii) 2080s. The dashed lines at the top and bottom of each graph mark the high and low storage levels, respectively.

5.3.3. Hydrological risk

The non-exceedance probability of annual outflows from the GERD reservoir under maximum, median and minimum projected change in streamflow are shown in Figure 5.5 for 2050s and 2080s. Based on the simulations of SDDP driven under historical climate and under the regulation effect of upstream reservoirs, the optimal annual outflow to be released at the GERD reservoir is estimated to be 47 km^3 y^{-1}, up to a non-exceedance probability of about 0.8. In 2050s, the median projected change in streamflow exhibits a similar, non-exceedance probability distribution with that under the historical climate, whereas under the minimum (maximum) projected changes in streamflow, the annual outflow is projected to be lower (higher) under the same non-exceedance probability. In contrast, by 2080s, under the median and minimum projected changes in streamflow, the annual outflow at GERD is projected to decrease while under the maximum projected change in streamflow, the annual outflow at GERD is projected to increase compared with the outflow under the historical climate.

In 2080s, under the maximum projected change in streamflow, the annual outflow of GERD that will exceed 60 km^3 y^{-1} will have an exceedance probability of 50% or higher, while under the median (minimum) projected change in streamflow, the corresponding annual outflow of GERD with 50% of exceedance probability or higher will only be about 43 (40) km^3 y^{-1}. The annual outflow of BNR at Khartoum is projected to decrease under median and minimum projected changes in streamflow for 2050s and 2080s, but it is projected to increase under the maximum projected change in streamflow. The annual outflow at Khartoum with a 50% exceedance probability or higher is projected to change from 32.5 km^3 y^{-1} under historical

climate to 35 (43), 31.5 (26.7) and 29.4 (23.2) km^3 y^{-1} under the maximum, median and minimum projected changes in streamflow for 2050s (2080s), respectively. This means that a higher risk of not meeting the future water demand of Egypt is projected under the median and minimum projected changes in streamflow, and under future development in Sudan.
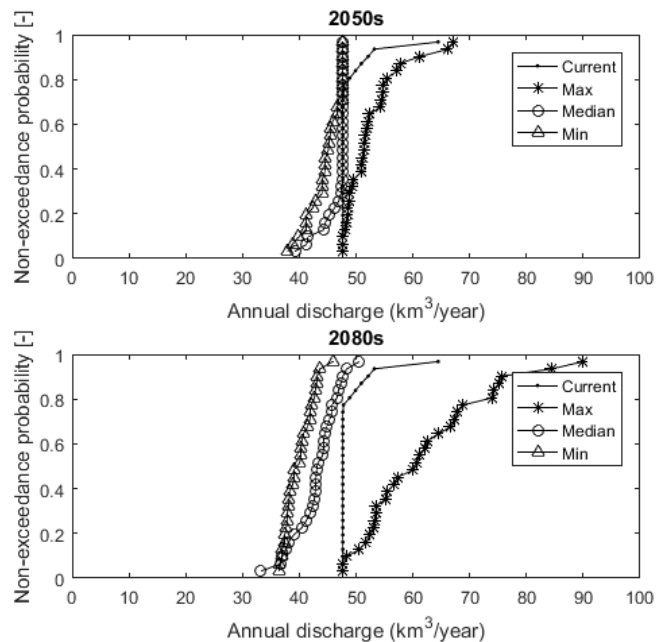
Figure 5.5: Empirical cumulative distribution functions of the projected annual discharge at GERD reservoir under maximum, median and minimum projected change in streamflow for 2050s and 2080s.

5.3.4. Hydropower generation

The projected annual hydropower production for the Blue Nile River in Ethiopia for 2050s and 2080s are presented in Table 5.2. At present, the hydropower production of Ethiopia over the BNRB is about 356MW, which is substantially smaller than the estimated full potential of 13GW. However, the hydropower production is expected to increase substantially because of the construction of GERD and the other three proposed reservoirs. The proposed future

development in Ethiopia will increase its future hydropower production to about 50TWh per year, assuming the climatic conditions remain more or less unchanged. However, after building the proposed reservoirs, the Beles hydropower will less likely to function much in the future because water passing the new reservoirs will be more productive economically than passing through the existing Beles hydropower plant. The hydropower production in Ethiopia is projected to increase under the maximum and decrease under the median and minimum projected changes in streamflow for both 2050s and 2080s (Table 5.2). In contrast, the hydropower production in Sudan is expected to remain unchanged because of flow regulation in Ethiopia.

Table 5.2: Projected annual energy production (TWh) in Ethiopian hydropower development for 2050s and 2080s

	Current	Max projection change in streamflow	Median projected change in streamflow	Min projected change in streamflow
2050s	50	57.5	48.6	45.1
2080s		63.5	45.6	42.6

5.3.5. Annual net benefits

The projected annual benefits from hydropower and irrigation production in Ethiopia and Sudan over the BNRB for 2050s and 2080s are shown in Table 5.3. The requirement in irrigation water for BNRB is projected to increase due to warmer air temperature and future irrigation expansions in Sudan. Almost under all projected changes in the streamflow of BNRB, the hydropower production of Sudan is not expected to change mainly because under flow regulations of upstream reservoirs, its reservoirs will operate at full capacity. However,

under climate change impact, agriculture production due to irrigation in Sudan will change marginally. Generally, the annual net benefit of Sudan is projected to increase by about 0.014 – 0.044, or decrease by about, 0.01 – 0.02 billion US$ under the maximum and minimum projected change in streamflow, respectively. In Ethiopia, the annual net benefit due to the development of the four proposed reservoirs will increase to about 3.95 billion US$/year, which could further increase by 0.41 – 0.72 billion US$, or it could decrease by 0.38 – 0.59 billion US$ under maximum and minimum projected change in streamflow, respectively.

Table 5.3: Projected annual net benefit (billion US$) in Ethiopian and Sudan under maximum, median and minimum projected change in streamflow for 2050s and 2080s.

		2050s			2080s		
	Current	Max	Median	Min	Max	Median	Min
Annual Hydropower benefit (billion US$)							
Ethiopia	3.802	4.192	3.714	3.501	4.497	3.522	3.322
Sudan	0.234	0.234	0.234	0.234	0.234	0.234	0.234
Annual Irrigation benefit (billion US$)							
Ethiopia	0.148	0.166	0.134	0.067	0.174	0.165	0.039
Sudan	0.747	0.761	0.745	0.730	0.791	0.762	0.736
Annual Net benefit (billion US$)							
Ethiopia	3.95	4.36	3.85	3.57	4.67	3.69	3.36
Sudan	0.981	0.995	0.979	0.963	1.02	0.996	0.969

5.4. Summary and conclusions

The water resource of the Blue Nile River basin (BNRB) is under pressure due to increasing demands from competing users, and global warming impact. From projected changes in the streamflow of BNRB simulated by the VIC hydrological model driven by the RCP4.5 and RCP8.5 climate change scenarios of four GCMs dynamically downscaled by WRF for 2050s and 2080s, the maximum, median and minimum projected changes in streamflow for BNRB were estimated. The potential impacts of climate change to future water allocations for hydropower production and irrigation water in BNRB were analyzed using a stochastic dual dynamic model (SDDP) driven by these three sets of projected changes in streamflow. The results show that the development of the four proposed reservoirs in Ethiopia will result in a consistent, controlled outflow for all seasons which will benefit Ethiopia, Sudan and Egypt. Under climate change impact, the outflow from the GERD reservoir, or the annual flow of BNR at Khartoum is projected to increase under maximum, but will decrease under median and minimum projected changes in streamflow for 2050s and 2080s.

The annual outflow at Khartoum with a 50% exceedance probability or higher is projected to change from 32.5 km^3 y^{-1} under historical climate to 35 (43), 31.5 (26.7) and 29.4 (23.2) km^3 y^{-1} under the maximum, median and minimum projected changes in streamflow for 2050s (2080s), respectively. As a result, the annual net benefit is projected to increase under the maximum projected change in streamflow, but decrease under the median and minimum projected changes in streamflow for the BNRB. Generally, the result shows that the

hydrologic impact of climate change to the BNRB will be significant, which should be incorporated in the future design and development of the water resources of the BNRB.

References

Beyene T, Lettenmaier D.P, Kabat P (2010) Hydrologic impacts of climate change on the Nile River Basin: implications of the 2007 IPCC scenarios. Climatic Change 100: pp. 433-461. doi:10.1007/s10584-009-9693-0.

Block, P. (2007) Integrated management of the Blue Nile Basin in Ethiopia: hydropower and irrigation modeling, International Food Policy Research Institute, Washington, DC, Discussion Paper 00700.

Block, P. and Strzepek, K. (2010) Economic analysis of large-scale upstream river basin development on the Blue Nile in Ethiopia considering transient conditions, climate variability, and climate change, J. Water Res. Pl.-ASCE, 136, 156–166.

Cunha, S., Prado, S., and da Costa, J. (1997) Modelagem da produtividade variável de usinas hidrelétricas com base na construção de uma função de produção energética. Proc., XII Simpósio Brasileiro de Recursos Hídricos, ABRH, anais 2, 391–397, Brazil, 16–20 (in Portuguese).

Digna R.F., Y. A. Mohamed, P. van der Zaag, S. Uhlenbrook & G. A. Corzo (2017) Nile River Basin modelling for water resources management – a literature review, International Journal of River Basin Management, 15:1, 39-52, DOI:10.1080/15715124.2016.1228656.

Georgakakos, A. (2006) Topics on system analysis and integrated water resources management, Chap. 6, A. Castelletti, and R. Soncini-Sessa, eds., Elsevier, Amsterdam.

Goor, Q., Kelman, R., and Tilmant, A. (2011) Optimal multipurpose multireservoir operation model with variable productivity of hydropower plants, J. Water Res. Plann. Manage., 137(3): 258-267.

Goor, Q., Halleux, C., Mohamed, Y., and Tilmant, A. (2010) Optimal operation of a multipurpose multireservoir system in the Eastern Nile River Basin, Hydrol. Earth Syst. Sci., 14, 1895-1908, https://doi.org/10.5194/hess-14-1895-2010.

Guariso, G. and Whittington, D. (1987) Implications of Ethiopian water development for Egypt and Sudan, Int. J. Water Resour. D., 3, 105–114.

Labadie, J. (2004) Optimal operation of multireservoir system: State-of-the-art review. J. Water Resour. Plann. Manage., 130(2), 93–111.

Levy, B., and Baecher, G. (1999) NileSim: A Windows-based hydrologic simulator of the Nile River Basin. J. Water Resour. Plann. Manage, 125(2), 100–106.

Liang, X., Wood, E.F. & Lettenmaier, D.P. (1996) Surface soil moisture parameterization of the VIC-2L model: Evaluation and modification. Global and Plan. Change 13, 195–206.

Lohmann, D., E. Raschke, B. Nijssen and D. P. Lettenmaier (1998) Regional scale hydrology: I. Formulation of the VIC-2L model coupled to a routing model, Hydrol. Sci. J., 43(1), 131-141.

Loucks, D., and van Beek, E. (2005) Water resources systems planning and management: An introduction to methods, models and applications, J. Stedinger, J. Dijkman, and M. Villars, eds., UNESCO Publishing/WL-Delft Hydraulics, Paris.

Maurer EP, Wood AW, Adam JC, Lettenmaier DP, Nijssen B (2002) A long-term hydrologically- based data set of land surface fluxes and states for the conterminous United States. J Climate 15:3237–3251.

NBI (Nile Basin Initiative) (2015) Nile Basin Initiative website, http://www.nilebasin.org (last access: September 2015).

Pereira, M. (1989) Optimal stochastic operations scheduling of large hydroelectric systems. Int. J. Electr. Power Energy Syst., 11(3), 161–169.

Pereira, M., and Pinto, L. (1991) Multi-stage stochastic optimization applied to energy planning. Math. Program., 52(1–3), 359–375.

Powell, W. B. (2011) Approximate Dynamic Programming: Solving the Curses of Dimensionality, John Wiley & Sons, Inc., ISBN-13: 9780470604458.

Skamarock WC, Klemp JB, Dudhia J, Gill DO, Barker DM, Duda M, Huang XY, Wang W, Powers JG (2008) A description of the advanced research WRF version 3. NCAR technical note, NCAR/TN\u2013475?STR, 123 pp

Swain, A. (2011) Challenges for Water Sharing in the Nile Basin: Changing Geo-Politics and Changing Climate. Hydrol. Sci. J. 56(4), 687–702. doi:10.1080/02626667.2011.577037.

Tariku, T.B, and Gan, T.Y (2017) Sensitivity of the Weather Research and Forecasting model to Parameterization Schemes for Regional Climate of Nile River Basin, *Climate Dynamics*, pp.1-17, doi: 10.1007/s00382-017-3870-z**.**

Tariku, T.B, and Gan, T.Y (2018) Regional Climate Change Impact on Extreme Precipitation and Temperature of the Nile River Basin, Climate Dynamics, pp. 1-20, doi: 10.1007/s00382-018-4092-8.

Tariku, T.B, Gan, T.Y, Li J., and Qin X., (2018) Impact of Climate Change on Hydrology and Hydrological Extremes of the upper Blue Nile River basin, Journal of Climate Change, under review.

Tilmant, A., Goor, Q., and Pinte, D. (2008) Assessing marginal water values in multipurpose multireservoir systems via stochastic programming. Water Resour. Res., 44, W12431.

Tilmant, A., and Kelman, R. (2007) A stochastic approach for analyzing trade-offs and risks associated with large-scale water resources systems. Water Resour. Res., 43, W06425.

Tilmant, A., Goor, Q., and Pinte, D. (2009) Agricultural-to-hydropower water transfers: sharing water and benefits in hydropower-irrigation systems, Hydrol. Earth Syst. Sci., 13, 1091–1101, doi:10.5194/hess-13-1091-2009.

Wallace, S., and Fleten, S. (2003). Stochastic programming models in energy. Chapter 10, Handbooks in operations research and management science, Vol. 10, A. Ruszczynski and A. Shapiro, eds. Elsevier Science, Amsterdam, The Netherlands.

Whittington, D., Wu, X., and Sadoff, C. (2005) Water resources management in the Nile Basin: The economic value of cooperation. Water Policy, 7(3), 227–252.

WWAP (World Water Assessment Programme) (2012) The United Nations World Water Development Report 4: Managing Water under Uncertainty and Risk. Paris, UNESCO.

Chapter 6 Summary, conclusions and recommendations

6.1. Summary and Conclusions

Climate change and climate variability will affect the food, water and energy security of African countries. Climate is a multifractal process, and hydrologic extremes are more than climate-driven, their patterns are difficult to pin down. The lack of good management and knowledge about the potential impact of climate change to the existing water resources could lead to unforeseen water crises in future. This needs a better understand of ongoing changes to the climatic and hydrologic regimes of the Nile. The objective of this research is to explore the potential impact of climate change to the water resources of the BNRB, and to optimize the management of water resources of BNRB subjected to the impact of climate change and future water system developments.

In Chapter 2, WRF model was carefully configured to select the best optimal combination of parameterization schemes to simulate representative climate of the NRB using ERA interim data as the boundary condition. As expected, no one parameterization scheme is consistently superior over other schemes under different evaluation criteria. Overall, with reference to NCEP reanalysis and CRU climate data, the T2 and LWRAD simulated are generally more accurate than precipitation and SWRAD data for all WRF parameterization schemes tested in this study. The simulation of rainfall is more sensitive to the choice of PBL, Cu and MP schemes than other schemes of WRF. T2 is more sensitive to LSM and Ra than to Cu, PBL and MP schemes selected for NRB. The surface air temperature simulated using Noah as the LSM agrees better with observed data (e.g., small negative bias) than that simulated using

RUC as the LSM which has a high positive bias. The SWRAD simulated by WRF is generally more dependent on MP and Ra schemes than Cu, LSM and PBL schemes. While most SWRAD simulated by WRF tends to have a positive bias, SWRAD simulated from combining the Morrison MP scheme with the Dudhia radiation scheme tends to be more accurate than other combination of schemes. Finally, LWRAD simulated by WRF is highly sensitive to LSM, Ra and PBL schemes, but less sensitivity to Cu and MP schemes. On a whole, RUC, RRTMG and YSU schemes tend to result in simulating LWRAD with a positive bias than other schemes. Furthermore, with a strong positive bias in SWRAD, WRF tends to simulate low rainfall and low longwave radiation, and vice versa. Therefore, a careful selection of the configuration and physical parameterization schemes for WRF is essential to simulate representative key climate variables such as T2, precipitation, SWRAD and LWRAD. From a tedious effort calibrating WRF with the objective of simulating representative regional climate of NRB, we found the following combination of schemes to be more comprising than other schemes: the Single-moment WSM3 microphysics, KF cumulus, MYJ PBL, RRTM longwave radiation scheme, Dudhia shortwave radiation scheme, and Noah LSM. In addition, these selected schemes are also efficient in terms of computation time as compared with other WRF parameterization schemes tested in this study. Lastly, the above configuration of WRF coupled to the Noah LSM has been shown to simulate representative regional climate of NRB over 1980-2001 which include a combination of wet and dry years of the NRB.

In Chapter 3, the potential impact of climate change on the future mean annual and extreme precipitation, and temperature of the Nile river basin in the 2050 and 2080s was investigated using RCP4.5 and RCP8.5 climate scenarios of four GCMs of CMIP5 dynamically downscaled by a regional climate model called WRF. As expected, precipitation projections using downscaled RCP scenarios of four GCMs for NRB exhibit wide range of possible changes as compared with temperature projections. Under downscaled RCP4.5 and RCP8.5 climate scenarios, the annual precipitation of BNRB, *Atbara*, and Sobat river basin, *El Ghazal* and Lake Victoria sub-basins of NRB are projected to change by about [-7, 14.2], [-19, 25.3], [-7, 39], [-5.9, 23], and [3.6, 27] % in the 2050s, and [-14, 25], [-22.5, 39], [-4.7, 60.4], [-11, 31], and [11.8, 41] % in the 2080s, respectively. Between downscaled projections of GCMs for air temperature, the five sub-basin of NRB are projected to become warmer by about 1.67 – 2°C in the 2050s and 2 – 2.5°C in the 2080s under RCP4.5 climate scenarios, and by about 2.5 – 3°C in the 2050s and 3.9 – 4.6°C in the 2080s under RCP8.5 climate scenarios.

Besides, extreme precipitation indices derived from precipitation projections of the four GCMs for NRB also exhibit wide range of possible changes. For example, R20mm, R95p, R99p and P30yr indices estimated for 2050s and 2080s are projected to mostly increase for all sub-basins of NRB. The R20mm index is projected to increase by 2.5–77.5% for all sub-basins except for the Atbara river basin which is projected to decrease by 0.8–1.9% in 2050s, but then to increase by 0.9–1.4% in 2080s. The range of mean projected changes in R95p and R99p indices for all sub-basins is 0.75–55% and -13–90%, respectively. The P30yr index is also projected to increase by 15–60% for all sub-basins of NRB under RCP4.5 and RCP8.5

scenarios for 2050s and 2080s. The predominantly projected increase in extreme precipitation indices implies that NRB is expected to experience more severe extreme wet precipitation and more frequently in 2050s and 2080s. Similarly, RX1day and RX5day indices are projected to increase in 2050s and 2080s by about 1–40% and -0.3–28% for all sub-basins, which implies that flood causing precipitation events over the NRB could occur more frequently in the future.

On the basis of extreme temperature indices derived from temperature projections of the four GCMs, NRB is projected to experience a large decrease in cold extremes (i.e., cool nights (TN10p) and cool days (TX10p)) but increase in warm extremes (i.e., warm nights (TN90p) and warm days (TX90p)), such that the number of days that exceed the historical 90th percentile values of T_{min} (TN90p) and T_{max} (TX90p) over the NRB could be at least equal to or greater than 48% and 55% in the 2050s periods, and at least equal to or greater than 50% and 80% in the 2080s, respectively. Correspondingly, the number of days that T_{min} (TN10p) and T_{max} (TX10p) will fall below the historical 10th percentile values are projected to decrease to less than 1%, e.g., almost no cold night or days is expected to occur, in the 2050s and 2080s. The indices for warm and cold spells also project an increase in warm spells but a decrease in cold spells in NRB.

On a whole, results from the downscaled RCP climate scenarios of four GCMs project that NRB is expected to experience warmer climate, and extreme precipitation events, and extreme temperature are expected to occur more frequently and in greater severity in the mid

and late 21st century, which could have significant impact to the future water resources of NRB.

In Chapter 4, the potential impact of climate change on the future mean and extreme streamflow of the UBN in the 2050s and 2080s was projected by three hydrological models (NAM, VIC and Watflood models) driven with RCP4.5 and RCP8.5 climate scenarios of four GCMs dynamically downscaled by WRF. The mean daily maximum (minimum) temperature of UBN are projected to increase by about 1.35 – 2.38 (1.72 – 2.74) ^{o}C under RCP4.5, and 2.22 – 4.47 (2.5 – 5.1) ^{o}C under RCP8.5 climate scenarios for future periods with respect to the base period of 1976-2005. However, projected changes in mean annual precipitation vary widely, ranging from -10.3 to 19.4%, but generally projected to decrease in the summer and increase in the winter, under both RCP climate scenarios over 2050s and 2080s.

Driven with gridded ERA-Interim data dynamically downscaled by WRF, the NAM, VIC and Watflood hydrologic models were calibrated and independently validated against observed streamflow of the El-Diem gauging station. Almost all models have captured the overall streamflow dynamics of the UBN river basin accurately. At the calibration and validation stages, NSE and R^{2} of simulated versus observed streamflow obtained are above 0.6, while the ME and RMSE are relatively low. On a whole, using three hydrological models driven by the RCP climate scenarios of four GCMs, the median of mean annual streamflow of UBN are projected to decrease by 7.6% with a range of -19.7 to 17.7% in the 2050s and by 12.7% with a range of -26.8 to 31.6% in the 2080s. The mean streamflow of UBN is projected to increase

in the winter, and decrease in the summer, but on a whole, its mean annual streamflow is projected to decrease.

Both the annual maxima and minima of streamflow are projected to increase under climate scenarios of CanESM2 in both future periods compared with other GCMs. Annual maxima of high return period are projected to increase by a ratio of 1.08 to 1.13, while annual maxima of low return periods are projected to decrease by a ratio of about 0.85. On the other hand, annual minima of low return periods are projected to remain almost unchanged, but are projected to decrease under high return periods, e.g., the ratio of the projected change of annual minima range from 1.0 to 0.73. This implies that UBN is likely to experience more frequent and/or more severe flooding and droughts in the future. This would affect different sectors of users, such as the municipal and agriculture sectors and future navigation in the Nile for both upstream and downstream countries of the NRB.

Chapter 5, from the projected changes in the streamflow of BNRB simulated by the VIC hydrological model driven by the RCP4.5 and RCP8.5 climate change scenarios of four GCMs dynamically downscaled by WRF for 2050s and 2080s, the maximum, median and minimum projected changes in streamflow for BNRB were identified. The potential impacts of climate change to future water allocations for hydropower production and irrigation water in BNRB were analyzed using a stochastic dual dynamic model (SDDP) driven by these three sets of projected changes in streamflow. The results show that the development of the four proposed reservoirs in Ethiopia will result in a consistent, controlled outflow for all seasons which will benefit Ethiopia, Sudan and Egypt. Under climate change impact, the outflow

from the GERD reservoir, or the annual flow of BNR at Khartoum is projected to increase under maximum, but will decrease under median and minimum projected changes in streamflow for 2050s and 2080s.

The annual outflow at Khartoum with a 50% exceedance probability or higher is projected to change from 32.5 km^3 y^{-1} under historical climate to 35 (43), 31.5 (26.7) and 29.4 (23.2) km^3 y^{-1} under the maximum, median and minimum projected changes in streamflow for 2050s (2080s), respectively. As a result, the annual net benefit is projected to increase under the maximum projected change in streamflow, but decrease under the median and minimum projected changes in streamflow for the BNRB. Generally, the result shows that the hydrologic impact of climate change to the BNRB will be significant, which should be incorporated in the future design and development of the water resources of the BNRB..

6.2. Recommendations

The climate of the NRB is likely to change in the 21st Century, which needs appropriate mitigation measure to reduce the climate change impact. If member countries of the NRB can better understand their vulnerability to potential climate change impact, they would better prepared to implement effective adaptation strategies to mitigate such impacts, and to establish effective warning systems that can issue reliable warnings of impending crisis of droughts or water shortfalls in a timely order.

If the water resource of the Nile River could be managed properly between riparian countries, the risk of facing water shortage problems in downstream countries will be minimized. The

strengthening of water management institutions and collaboration between basin countries, such as NBI and ENTRO are essential to promote sustainable water resource development and to avoid conflicts from competing users of the water resources of the NRB. The increase in water availability due to climate change impact will boost the irrigation and hydropower production over the BNRB, but a decrease in water resource will leads to more severe water shortages for different water sectors. The projected water shortages due to climate change impact could be mitigated by increasing the water-use efficiency and productivity, such as cultivating drought resistant crops, implement water efficient irrigation systems, promote wastewater recycling and climate change education to enhance the protection and sustainable use of the water resources of the NRB. The potential impact of projected increase of flooding events in the downstream countries could be minimized by a proper management of the upstream reservoirs. Overall, findings of this research will be useful to policy makers to execute informed prudent decisions on the future planning, design and management of the water resources of the BNRB. It will be crucial for countries relying on the water resources of NRB to seriously consider implementing adaptation strategies and mitigation measures to combat the potential impact of climate change to NRB.

Bibliography

Adeyewa ZD, Nakamura K. (2003) Validation of TRMM Radar Rainfall Data over Major Climatic Regions in Africa. J. Appl. Meteorol. 42: 331–347, doi: 10.1175/1520-0450(2003)042<0331:VOTRRD>2.0.CO;2.

Aich, V., Liersch, S., Vetter, T., Huang, S., Tecklenburg, J., Hoffmann, P., Koch, H., Fournet, S., Krysanova, V., Müller, E. N., and Hattermann, F. F. (2014) Comparing impacts of climate change on streamflow in four large African river basins. Hydrology and Earth System Sciences, 18(4), 1305–1321. doi: 10.5194/hess-18-1305-2014.

Alemseged TH, and Tom R. (2015) Evaluation of regional climate model simulations of rainfall over the Upper Blue Nile basin. Atmos. Res. 161–162, pp. 57–64.

Alexander LV et al (2006) Global observed changes in daily climate extremes of temperature and precipitation. J. Geophys. Res., 111, D05109, doi:10.1029/2005JD006290.

Allen, R.G., Pereira, L.S., Raes, D., and Smith, M. (1998) Crop evapotranspiration (guidelines for computing crop water requirements). Food and Agriculture Organization of the United Nations Irrigation and Drainage Paper 56, 328 pp.

Anyah R.O., and Semazzi F.H.M., (2006) Climate variability over the Greater Horn of Africa based on NCAR AGCM ensemble. Theor. Appl. Climatol., 86, 39-62, doi:10.1007/s00704-005-0203-7.

Anyah RO, Semazzi FHM (2007) Variability of East African rainfall based on multiyear RegCM3 simulations. Int J Climatol 27:357–371.

Anyah RO, Semazzi FHM, Xie L (2006) Simulated physical mechanisms associated with multiscale climate variability over Lake Victoria Basin in East Africa. Mon Weather Rev 134:3588–3609.

Anyamba, A., J. L. Small, S. C. Britch, C. J. Tucker, E. W. Pak, C. A. Reynolds, J. Crutchfield, and K. J. Linthicum, (2014), Recent Weather Extremes and Impacts on Agricultural Production and Vector-Borne Disease Outbreak Patterns. PLoS ONE 9 (3), doi: https://doi.org/10.1371/journal.pone.0092538.

Ashfaq, M., Bowling, L.C., Cherkauer, K., Pal, J.S., & Diffenbaugh, N.S. (2010) Influence of climate model biases and daily-scale temperature and precipitation events on hydrological impacts assessment: A case study of the United States. J. Geophys. Res., 115, D14116. doi.:10.1029/2009JD012965.

Beyene T, Lettenmaier D.P, Kabat P. (2010) Hydrologic impacts of climate change on the Nile River Basin: implications of the 2007 IPCC scenarios. Climatic Change 100: pp. 433-461. doi:10.1007/s10584-009-9693-0.

Benoit, R., Kouwen, N., Yu, W., Chamberland, S., & Pellerin, P. (2003) Hydrometeorological aspects of the Real-Time Ultrafinescale Forecast Support during the Special Observing Period of MAP. Hydrology and Earth System Sciences, 7(6), 877–889, doi: 10.5194/hess-7-877-2003.

Box, G.E.P., Cox, D.R. (1964) An analysis of transformations. J. Roy. Statist. Soc. 26, 211–243 (Discussion 244–252).

Bhattacharjee P.S, and Zaitchik B.F. (2015) Perspectives on CMIP5 model performance in the Nile River headwaters regions. Int. J. Climatol., 35: 4262–4275. doi:10.1002/joc.4284.

Block P., and Rajagopalan B, (2007) Interannual Variability and Ensemble Forecast of Upper Blue Nile Basin Kiremt Season Precipitation. J. Hydrometeorol., 8 (3), pp. 327–343, DOI: 10.1175/JHM580.1.

Block, P., (2007) Integrated management of the Blue Nile Basin in Ethiopia: hydropower and irrigation modeling, International Food Policy Research Institute, Washington, DC, Discussion Paper.

Block, P. and Strzepek, K., (2010) Economic analysis of large-scale upstream river basin development on the Blue Nile in Ethiopia considering transient conditions, climate variability, and climate change, J. Water Res. Pl.-ASCE, 136, 156–166.

Boer, G. J. (1993) Climate change and the regulation of the surface moisture and energy budgets. Climate Dynamics 8, 225-239. doi:10.1007/BF00198617.

Boko M, Niang I, Nyong A, Vogel C, Githeko A, Medany M, Osman-Elasha B, Tabo R and Yanda P. (2007) Africa. Climate Change 2007: Impacts, Adaptation and Vulnerability.

Contribution of Working Group II to the Fourth Assessment Report of the Intergovernmental Panel on Climate Change, Parry M L, Canziani O F, Palutikof J P, van der Linden P J and Hanson C E (eds). Cambridge University Press, Cambridge UK, 433 – 467.

Brown, A.R., (1996) Evaluation of parametrization schemes for the convective boundary layer using large-eddy simulation results. Bound.-Layer Meteor., 81, 167-200, doi:10.1007/BF00119064.

Chen C.T, Knutson T, (2008) On the verification and comparison of extreme rainfall indices from climate models. Amer. Meteor. Soc. 21: 1605–1621, doi: 10.1175/2007JCLI1494.1.

Chen C.-S., Lin Y.-L., Peng W.-C., Liu C.-L., (2010) Investigation of a heavy rainfall event over southwestern Taiwan associated with a subsynoptic cyclone during the 2003 Mei-Yu season. Atmos. Res., 95, 235–254, doi:10.1016/j.atmosres.2009.10.003.

Collins, W. D., et al., (2004) Description of the NCAR Community Atmosphere Model (CAM3.0). Technical Note TN-464+STR, National Center for Atmospheric Research, Boulder, CO, 214 pp.

Cunha, S., Prado, S., and da Costa, J. (1997) Modelagem da produtividade variável de usinas hidrelétricas com base na construção de uma função de produção energética. Proc., XII Simpósio Brasileiro de Recursos Hídricos, ABRH, anais 2, 391–397, Brazil, 16–20 (in Portuguese).

DHI, (2008) MIKE 11, a modelling system for rivers and channels, Reference manual. DHI Water & Environment, Horsholm, Denmark.

Diem J. E., Ryan S. J, Hartter J, and Palace M.W, (2014) Satellite-based rainfall data reveal a recent drying trend in central equatorial Africa. Climate Change, 126: 263–272, doi:10.1007/s10584-014-1217-x.

Diffenbaugh N.S., and Giorgi F., (2012) Climate change hotspots in the CMIP5 global climate model ensemble. Clim. Chang., 114, 813-822, DOI: 10.1007/s10584-012-0570-x.

Digna R.F., Y. A. Mohamed, P. van der Zaag, S. Uhlenbrook & G. A. Corzo (2017) Nile River Basin modelling for water resources management – a literature review, International Journal of River Basin Management, 15:1, 39-52, DOI:10.1080/15715124.2016.1228656.

Dinku T, Chidzambwa S, Ceccato P, Connor SJ, Ropelewski CF. (2008) Validation of high resolution satellite rainfall products over complex terrain. Int. J. Remote Sens. 29: 4097–4110.

Diro, G. T., Grimes D., and Black E. (2012) Dynamical downscaling of ECMWF Ensemble seasonal forecasts over East Africa with RegCM3. J Geophys Res 117:D16103. doi: 10.1029/2011JD016997.

Dodo, MK. (2014) Examining the Potential Impacts of Climate Change on International Security: EU-Africa Partnership on Climate Change. SpringerPlus 3. https://doi.org/10.1186/2193-1801-3-194.

Dudhia J., (1989) Numerical study of convection observed during the winter experiment using a mesoscale two-dimensional model. J. Atmos. Sci., 46, 3077–3107, doi: 10.1175/1520-0469(1989)046<3077:NSOCOD>2.0.CO;2.

Ek, M., and Mahrt L. (1991) OSU 1-D PBL model user's guide, version 1.04. Department of Atmospheric Sciences, Oregon State University, 120 pp.

Elshamy, M. E, Seierstad I. A, and Sorteberg A (2009) Impacts of climate change on Blue Nile flows using bias-corrected GCM scenarios, Hydrol. Earth Syst. Sci., 13, 551-565, doi:10.5194/hess-13-551-2009.

Eltahir E. A. B (1996) El Niño and the Natural Variability in the Flow of the Nile River, Water Resour. Res., 32(1), 131–137, doi:10.1029/95WR02968.

Endris H.S, Omondi P, Jain S, et al (2013) Assessment of the Performance of CORDEX Regional Climate Models in Simulating East African Rainfall. J. Climate, DOI: 10.1175/JCLI-D-12-00708.1.

Evans J.P., Ekström M. and Ji F. (2012) Evaluating the performance of a WRF physics ensemble over South-East Australia. Clim. Dynam., 39, 1241–1258, doi:10.1007/s00382-011-1244-5.

Flaounas E, Bastin S, and Janicot S. (2011) Regional climate modelling of the 2006 West African monsoon: sensitivity to convection and planetary boundary layer parameterisation using WRF. Clim. Dyn., 36, 1083-1105, doi:10.1007/s00382-010-0785-3.

Fowle M.A., Roebber P.J. (2003) Short-range (0-48 h) numerical prediction of convective occurrence, mode, and location. Wea. Forecasting, 18, 782–794, doi: 10.1175/1520-0434(2003)018<0782:SHNPOC>2.0.CO;2.

Fowler H.J, Blenkinsop S, and Tebaldi C. (2007) Review Linking climate change modelling to impacts studies: recent advances in downscaling techniques for hydrological modelling. Int. J. Climatol. 27: 1547–1578. doi:10.1002/joc.1556.

Frich P., Alexander L.V, Della-Marta P, Gleason B, Haylock M, Klein Tank A.M.G, and Peterson T. (2002) Observed coherent changes in climatic extremes during the second half of the twentieth century. Climate Res.19, 193–212. doi:10.3354/cr019193.

Fritsch J.M., Carbone R.E. (2004) Improving quantitative precipitation forecasts in the warm season: a USWRP research and development strategy. Bull. Amer. Meteor. Soc., 85, 955–965, doi: 10.1175/BAMS-85-7-955.

Funk C.C, Peterson P.J, Landsfeld M.F, Pedreros D.H, Verdin J.P, Rowland J.D, Romero B.E, Husak G.J, Michaelsen J.C, and Verdin A.P (2014) A quasi-global precipitation time series for drought monitoring: U.S. Geological Survey Data Series 832, 4 p., http://dx.doi.org/110.3133/ds832.

Gan, T. Y., Mari Ito, S Huelsmann, X Qin, X Lu, S. Y Liong, P Rutschman, M Disse & H Koivosalo (2015) Possible climate change/variability and human impacts, vulnerability of African drought prone regions, its water resources and capacity building, Hydrological Sciences Journal, DOI: 10.1080/02626667.2015.1057143.

Gao, H., Tang, Q., Ferguson, C. R., Wood, E. F., & Lettenmaier, D. P. (2010) Estimating the water budget of major US river basins via remote sensing. International Journal of Remote Sensing, 31:14, 3955-3978, DOI: 10.1080/01431161.2010.483488.

Georgakakos, A. (2006). Topics on system analysis and integrated water resources management, Chap. 6, A. Castelletti, and R. Soncini-Sessa, eds., Elsevier, Amsterdam.

Giorgi F, Jones C, and Asrar G. R (2009) Addressing climate information needs at the regional level: The CORDEX framework. WMO Bull., 58, 175–183.

Gizaw M, and Gan T.Y (2015) Possible Impact of climate change on future extreme precipitation of the Oldman, Bow and Red Deer River Basins of Alberta. Int. Journal Climatology, 36(1), 208-224. DOI:10.1002/joc.4338.

Gizaw, M., and Gan, T. Y. (2016) Impact of Climate Change and El Niño Episodes on Droughts in sub-Saharan Africa, Climate Dyn., 49:665, DOI: 10.1007/s00382-016-3366-2.

Gizaw, M., Biftu, G., Gan, T. Y., Moges, S., and Koivosalo, H. (2017) Potential Impact of climate change on streamflow of major Ethiopian rivers, Climatic Change, DOI: 10.1007/s10584-017ef-2021-1.

Goor, Q., Kelman, R., and Tilmant, A. (2011) Optimal multipurpose multireservoir operation model with variable productivity of hydropower plants, J. Water Res. Plann. Manage., 137(3): 258-267.

Goor, Q., Halleux, C., Mohamed, Y., and Tilmant, A. (2010) Optimal operation of a multipurpose multireservoir system in the Eastern Nile River Basin, Hydrol. Earth Syst. Sci., 14, 1895-1908, https://doi.org/10.5194/hess-14-1895-2010.

Gopalakrishnan C. (2013) Water and disasters: a review and analysis of policy aspects, International Journal of Water Resources Development, 29:2, 250-271, DOI:10.1080/07900627.2012.756133.

Grigg, N. S. (2014) The 2011–2012 drought in the United States: new lessons from a record event. International Journal of Water Resources Development, 30(2), 183–199. doi:10.1080/07900627.2013.847710.

Guariso, G. and Whittington, D. (1987) Implications of Ethiopian water development for Egypt and Sudan, Int. J. Water Resour. D., 3, 105–114.

Harris I, Jones P.D, Osborn T.J, and Lister D.H (2014) Updated high-resolution grids of monthly climatic observations–the CRU TS3.10 Dataset. Int. J. Climatol., 34, 623–642. doi: 10.1002/joc.3711.

Hong, S.Y., Dudhia J., and Chen S. H. (2004) A revised approach to ice microphysical processes for the bulk parameterization of clouds and precipitation. Mon. Wea. Rev., 132, 103–120, doi: 10.1175/1520-0493(2004)132<0103:ARATIM>2.0.CO;2.

Hong S.Y., and Lee J.W. (2009) Assessment of the WRF model in reproducing a flash-flood heavy rainfall event over Korea. Atmos. Res., 93, 818–831, doi:10.1016/j.atmosres.2009.03.015.

Hong, S.Y., Noh Y., and Dudhia J. (2006) A new vertical diffusion package with an explicit treatment of entrainment processes. Mon. Wea. Rev., 134, 2318–2341, doi: 10.1175/MWR3199.1.

Houghton J. (2009) Global Warming the complete briefing, 4th Edition, 438 pg., Cambridge Univ. Press.

Hu X.-M., Nielsen-Gammon J.W., and Zhang F. (2010) Evaluation of three planetary boundary layer schemes in the WRF model. J. Appl. Meteor. Climatol., 49, 1831–1844, doi: 10.1175/2010JAMC2432.1.

Iacono M.J., Delamere J.S., Mlawer E.J., Shephard M.W., Clough S.A., and Collins W.D. (2008) Radiative forcing by long-lived greenhouse gases: Calculations with the AER radiative transfer models. J. Geophys. Res., 113, D13103, doi:10.1029/2008JD009944.

Indeje, M., Semazzi H. M. F., and Ogallo J. L. (2000) ENSO signal in East African rainfall seasons. Int. J. Climatol., 20, 19–46, doi:10.1002/(SICI)1097-0088(200001)20:1<19::AID-JOC449>3.0.CO;2-0.

IPCC (2007) Climate Change 2007: The Physical Science Basis. Contribution of Working Group I to the Fourth Assessment Report of the Intergovernmental Panel on Climate Change, Solomon S, Qin D, Manning M, Chen Z, Marquis M, Averyt KB, Tignor M, Miller HL (eds). Cambridge University Press: Cambridge, UK and New York, NY, pp. 849-925.

IPCC (2013) Climate Change 2013: The Physical Science Basis. Contribution of Working Group I to the Fifth Assessment Report of the Intergovernmental Panel on Climate Change [Stocker, T.F., D. Qin, G.-K. Plattner, M. Tignor, S.K. Allen, J. Boschung, A. Nauels, Y.

Xia, V. Bex and P.M. Midgley (eds.)]. Cambridge University Press, Cambridge, United Kingdom and New York, NY, USA, 1535 pp.

IPCC (2014) Climate Change 2014: Impacts, Adaptation, and Vulnerability. Part B: Regional Aspects. Contribution of Working Group II to the Fifth Assessment Report of the Intergovernmental Panel on Climate Change [Barros, V.R., C.B. Field, D.J. Dokken, M.D. Mastrandrea, K.J. Mach, T.E. Bilir, M. Chatterjee, K.L. Ebi, Y.O. Estrada, R.C. Genova, B. Girma, E.S. Kissel, A.N. Levy, S. MacCracken, P.R. Mastrandrea, and L.L. White (eds.)]. Cambridge University Press, Cambridge, United Kingdom and New York, NY, USA, pp. 1199-1265.

IPCC-TGICA, (2007) General Guidelines on the Use of Scenario Data for Climate Impact and Adaptation Assessment. Version 2. Prepared by T.R. Carter on behalf of the Intergovernmental Panel on Climate Change, Task Group on Data and Scenario Support for Impact and Climate Assessment, 66 pp.

Janjic Z.I. (1994) The step-mountain eta coordinate model: further developments of the convection, viscous sublayer, and turbulence closure schemes. Mon. Wea. Rev.,122,927–945, doi: 10.1175/1520-0493(1994)122<0927:TSMECM>2.0.CO;2.

Jarvis, A., H.I. Reuter, A. Nelson, E. Guevara, (2008) Hole-filled SRTM for the globe Version 4, available from the CGIAR-CSI SRTM 90m Database (http://srtm.csi.cgiar.org).

Jones C. G., Samuelsson P. and Kjellström E. (2011) Regional climate modelling at the Rossby Centre. Tellus A, 63, 1–3. doi:10.1111/j.1600-0870.2010.00491.x.

Kain J.S. (2004) The Kain–Fritsch Convective Parameterization: An Update. J Appl. Meteor., 43,170–181, doi: 10.1175/1520-0450(2004)043<0170:TKCPAU>2.0.CO;2.

Katragkou E., Garcia-Diez M., Vautard R., Sobolowski S., Zanis P., Alexandri G., Cardoso R. M., Colette A., Fernandez J., Gobiet A., Goergen K., Karacostas T., Knist S., Mayer S., Soares P. M. M., Pytharoulis I., Tegoulias I., Tsikerdekis A., and Jacob D. (2015) Regional climate hindcast simulations with EURO-CORDEX: evaluation of a WRF multi-physics ensemble. Geosci. Model Dev., 8, 603-618, doi:10.5194/gmd-8-603-2015.

Kerkhoven, E., and Gan, T.Y. (2011) Unconditional uncertainties of historical and simulated river flows subjected to climate change, *J. of Hydrology*, *396*(1-2), 113-127. DOI:10.1016/j.jhydrol.2010.10.042.

Kerkhoven, E., Gan, T.Y., Shiiba, M., G. Reuter, and Tanaka, K. (2006) A comparison of cumulus parameterization schemes in a numerical weather prediction model for a monsoon rainfall event, *Hydro. Processes*, 20(9), 1961-1978. DOI: 10.1002/hyp.5967.

Kharin, V. V., Zwiers, F. W., Zhang, X., & Wehner, M. (2013) Changes in temperature and precipitation extremes in the CMIP5 ensemble. Climatic Change, 119, 345–357. doi:10.1007/s10584-013-0705-8.

Kim U. and Kaluarachchi J. J (2009) Climate Change Impacts on Water Resources in the Upper Blue Nile River Basin, Ethiopia[1]. JAWRA Journal of the American Water Resources Association, 45: 1361–1378. doi:10.1111/j.1752-1688.2009.00369.x.

Klein Tank AMG, Zwiers FW, and Zhang X (2009) Guidelines on analysis of extremes in changing climate in support of informed decision for adaption. World Meteorological Organization, Climate Data and Monitoring, WCDMP-No. 72. WMO: Geneva, Switzerland.

Koutsouris, A. J., Chen, D. and Lyon, S. W. (2016) Comparing global precipitation data sets in eastern Africa: a case study of Kilombero Valley, Tanzania. Int. J. Climatol., 36: 2000–2014. doi:10.1002/joc.4476.

Kouwen, N., E.D. Soulis, A. Pietroniro, J. Donald, and R.A. Harrinton (1993) Grouping Response Unit for Distributed Hydrologic Modelling, ASCE Journal of Water Resources Management and Planning, 119(3): 289-305, doi:10.1061/(ASCE)0733-9496(1993)119:3(289).

Labadie, J. (2004) Optimal operation of multireservoir system: State-of-the-art review. J. Water Resour. Plann. Manage., 130(2), 93–111.

Lemke, et al., (2007) Observations: Changes in Snow, Ice and Frozen Ground. Climate Change 2007: The Physical Science Basis. Working Group I to the 4th Assessment Rept of IPCC, Cambridge University Press.

Levy, B., and Baecher, G., (1999) NileSim: A Windows-based hydrologic simulator of the Nile River Basin. J. Water Resour. Plann. Manage., 125(2), 100–106.

Liang, X., Wood, E. F., & Lettenmaier, D. P. (1996) Surface soil moisture parameterization of the VIC-2L model: Evaluation and modification. Global and Plan. Change, 13, 195–206.

Liersch, S., Tecklenburg, J., Rust, H., Dobler, A., Fischer, M., Kruschke, T. and Koch, H., Hattermann, F. (2016) Are we using the right fuel to drive hydrological models? A climate impact study in the Upper Blue Nile. Hydrol. Earth Syst. Sci. Discuss. doi:10.5194/hess-2016-422.

Lin Y.L., Rarley R.D., Orville H.D. (1983) Bulk parameterization of the snowfield in a cloud model. J. Climate Appl. Meteor., 22, 1065–1092, doi: 10.1175/1520-0450(1983)022<1065:BPOTSF>2.0.CO;2.

Lim K.-S. S., and Hong S.-Y. (2010) Development of an Effective Double-Moment Cloud Microphysics Scheme with Prognostic Cloud Condensation Nuclei (CCN) for Weather and Climate Models. Mon. Wea. Rev., 138, 1587–1612, doi: 10.1175/2009MWR2968.1.

Lohmann, D., E. Raschke, B. Nijssen and D. P. Lettenmaier (1998) Regional scale hydrology: I. Formulation of the VIC-2L model coupled to a routing model, Hydrol. Sci. J., 43(1), 131-141.

Loucks, D., and van Beek, E. (2005) Water resources systems planning and management: An introduction to methods, models and applications, J. Stedinger, J. Dijkman, and M. Villars, eds., UNESCO Publishing/WL-Delft Hydraulics, Paris.

Lucas-Picher P, Caya D, de Elia R, Laprise R (2008) Investigation of regional climate models' internal variability with a ten-member ensemble of 10-year simulations over a large domain. Climate Dyn. 31:927–940.

Mariotti L, Coppola E, Sylla M. B, Giorgi F, and Piani C (2011) Regional climate model simulation of projected 21st century climate change over an all-Africa domain: Comparison analysis of nested and driving model results. J. Geophys. Res., 116, D15111, doi:10.1029/2010JD015068.

Mariotti L, Diallo I, Coppola E, et al (2014) Seasonal and intraseasonal changes of African monsoon climates in 21st century CORDEX projections. Climatic Change 125: 53. doi:10.1007/s10584-014-1097-0.

Mashingia F, Mtalo F, Bruen M. (2014) Validation of remotely sensed rainfall over major climatic regions in Northeast Tanzania. Phys. Chem. Earth, Parts 67–69: 55–63, doi: 10.1016/j.pce.2013.09.013.

Maurer EP, Wood AW, Adam JC, Lettenmaier DP, Nijssen B (2002) A long-term hydrologically- based data set of land surface fluxes and states for the conterminous United States. J Climate 15:3237–3251.

McSweeney C.F, Jones R.G, Lee R.W, et al (2015) Selecting CMIP5 GCMs for downscaling over multiple regions. Climate Dyn. 44: 3237-3260, doi:10.1007/s00382-014-2418-8.

Meehl, G. A. (2004) More Intense, More Frequent, and Longer Lasting Heat Waves in the 21st Century. Science, 305(5686), 994–997. https://doi.org/10.1126/science.1098704.

Mellor GL, Yamada T. (1982) Development of a turbulence closure model for geophysical fluid problems. Rev Geophys., 20,851–875, doi:10.1029/RG020i004p00851.

Mlawer E.J., Taubman S.J., Brown P.D., Iacono M.J., and Clough S.A. (1997) Radiative transfer for inhomogeneous atmosphere: RRTM, a validated correlated-k model for the long-wave. J. Geophys. Res., 102, 16663–16682, doi:10.1029/97JD00237.

Mohamed Y. A., van den Hurk B.J.J.M., Savenije H. H. G., and Bastiaanssen W. G. M. (2005) Hydroclimatology of the Nile: results from a regional climate model. Hydrol. Earth Syst. Sci., 9, 263–278, doi:10.5194/hess-9-263-2005.

Mooney P. A., Mulligan F. J., and Fealy R. (2011) Comparison of ERA-40, ERA-Interim and NCEP/NCAR reanalysis data with observed surface air temperatures over Ireland. Int. J. Climatol., 31, 545–557, doi:10.1002/joc.2098.

Mooney P.A., Mulligan F.J., and Fealy R. (2013) Evaluation of the sensitivity of the Weather Research and Forecasting Model to parameterization schemes for regional climates of Europe over the period 1990–1995. J. Climate, 26, 1002–1017, doi:10.1175/JCLI-D-11-00676.1.

Morrison H., Thompson G., and Tatarskii V. (2009) Impact of cloud microphysics on the development of trailing stratiform precipitation in a simulated squall line: comparison of one-and two moment schemes. Mon. Wea. Rev., 137, 991–1007, doi: 10.1175/2008MWR2556.1.

Mwale D, and Gan T.Y (2005) Wavelet analysis on variability, teleconnectivity and predictability of September-November East African Rainfall. J. of App. Met., 44,256-269.

Nair S, Srinivasan G, Nemani R. (2009) Evaluation of multi-satellite TRMM derived rainfall estimates over a western state of India. J. Meteorol. Soc. Jpn. 87: 927–939, doi: 10.2151/jmsj.87.927.

Nicholson SE, Some B, McCollum J, Nelkin E, Klotter D, Berte Y, Diallo BM, Gaye I, Kpabeba G, Ndiaye O, Noukpozounkou JN, Tanu MM, Thiam A, Toure AA, Traore AK. (2003a) Validation of TRMM and Other Rainfall Estimates with a High-Density Gauge Dataset for West Africa. Part I: Validation of GPCC Rainfall Product and Pre-TRMM Satellite and Blended Products. J. Appl. Meteorol. 42: 1337–1354, doi: 10.1175/1520-0450(2003)042<1337:VOTAOR>2.0.CO;2.

Nicholson SE, Some B, McCollum J, Nelkin E, Klotter D, Berte Y, Diallo BM, Gaye I, Kpabeba G, Ndiaye O, Noukpozounkou JN, Tanu MM, Thiam A, Toure AA, Traore AK. (2003b) Validation of TRMM and other rainfall estimates with a high-density gauge dataset for West Africa. Part II: validation of TRMM rainfall products. J. Appl. Meteorol. 42: 1355–1368, doi: 10.1175/1520-0450(2003)042<1355:VOTAOR>2.0.CO;2.

Nijssen, B.N., G.M. O'Donnell, D.P. Lettenmaier and E.F. Wood (2001) Predicting the discharge of global rivers, J. Clim., 14(15), 3307-3323, doi: 10.1175/1520-0442(2001)014<3307:PTDOGR>2.0.CO;2.

NBI (Nile Basin Initiative) (2015) Nile Basin Initiative website, http://www.nilebasin.org (last access: September 2015).

Ntale, H. K., and Gan, T.Y., Mwale, D. (2003) Prediction of East African Seasonal Rainfall Using Canonical Correlation Analysis, J. of Climate, 16(12), 2105-2112. DOI: http://dx.doi.org/10.1175/1520-0442(2003)016<2105:POEASR>2.0.CO;2.

Ntale H. K, and Gan T.Y (2004) East African Rainfall Anomaly Patterns in Association with El Niño/Southern Oscillation. J. Hydrologic Eng., ASCE, 9(4), 257-268.

Nyakwada, W. (2009) Predictability of East African seasonal rainfall with sea surface temperature gradient modes, Ph.D. dissertation, University of Nairobi, 265 pp.

Omondi, P. A., Awange, J. L., Forootan, E., Ogallo, L. A., Barakiza, R., Girmaw, G. B., Fesseha, I., Kululetera, V., Kilembe, C., Mbati, M. M., Kilavi, M., King'uyu, S. M., Omeny, P. A., Njogu, A., Badr, E. M., Musa, T. A., Muchiri, P., Bamanya, D. and Komutunga, E. (2014), Changes in temperature and precipitation extremes over the Greater Horn of Africa region from 1961 to 2010. Int. J. Climatol., 34: 1262–1277. doi:10.1002/joc.3763.

Patz, J. A., D. Campbell-Lendrum, T. Holloway, and J. A. Foley (2005) Impact of Regional Climate Change on Human Health. Nature, 438, pp. 310-317, doi:10.1038/nature04188.

Pereira, M. (1989) Optimal stochastic operations scheduling of large hydroelectric systems. Int. J. Electr. Power Energy Syst., 11(3), 161–169.

Pereira, M., and Pinto, L. (1991) Multi-stage stochastic optimization applied to energy planning. Math. Program, 52(1–3), 359–375.

Pietroniro, A., Leconte, R., Toth, B., Peters, D. L., Kouwen, N., Conly, F. M., & Prowse, T. (2006) Modelling climate change impacts in the Peace and Athabasca catchment and delta: III—integrated model assessment. Hydrological Processes, 20(19), 4231–4245. doi:10.1002/hyp.6428.

Pohl B., Cretat J., and Camberlin P. (2011) Testing WRF capability in simulating the atmospheric water cycle over Equatorial East Africa. Clim. Dyn., 37, 1357-1379, doi: 10.1007/s00382-011-1024-2.

Powell, W. B. (2011) Approximate Dynamic Programming: Solving the Curses of Dimensionality, John Wiley & Sons, Inc., ISBN-13: 9780470604458.

Priestley, C. H. B., and R. J. Taylor (1972) On the assessment of surface heat flux and evaporation using large-scale parameters. Mon. Wea. Rev., 100, 81–92.

Romilly TG, Gebremichael M. (2011) Evaluation of satellite rainfall estimates over Ethiopian river basins. Hydrol. Earth Syst. Sci. 15:1505–1514, doi: 10.5194/hess-15-1505-2011.

Rosenberg, E. A., P. W. Keys, D. B. Booth, D. Hartley, J. Burkey, A. C. Steinemann, D. P. Lettenmaier, (2010) Precipitation Extremes and the Impacts of Climate Change on Stormwater Infrastructure in Washington State. Clim. Change 102: 319–349, doi:10.1007/s10584-010-9847-0.

Saha, S., et al. (2010) NCEP Climate Forecast System Reanalysis (CFSR) 6-hourly Products, January 1979 to December 2010. Research Data Archive at the National Center for Atmospheric Research, Computational and Information Systems Laboratory. http://dx.doi.org/10.5065/D69K487J. Accessed† 20 Jul 2015.

Schneider T., Bischoff T., and Haug, G. H. (2014) Migrations and dynamics of the intertropical convergence zone, Nature, 513, 45-53, doi: https://doi.org/10.1038/nature13636.

Schneider U, Becker A, Finger P, Meyer-Christoffer A, Rudolf B, Ziese M (2011) GPCC Full Data Reanalysis Version 6.0 at 0.5°: Monthly Land-Surface Precipitation from Rain-Gauges built on GTS-based and Historic Data. DOI: 10.5676/DWD_GPCC/FD_M_V6_050.

Screen J. A., and Simmonds I. (2011) Erroneous Arctic temperature trends in the ERA-40 reanalysis: A Closer Look. J. Climate, 24, 2620–2627, doi: 10.1175/2010JCLI4054.1.

Segele Z.T and Lamb P. J (2005) Characterization and variability of Kiremt rainy season over Ethiopia. Meteor. Atmos. Phys. 89: 153-180. doi:10.1007/s00703-005-0127-x.

Segele Z. T, Leslie L. M, and Lamb P. J (2009) Evaluation and adaptation of a regional climate model for the Horn of Africa: Rainfall climatology and interannual variability. Int. J. Climatol., 29, 47–65. doi:10.1002/joc.1681.

Sen, P.K. (1968) Estimates of the regression coefficient based on Kendall's tau. Journal of the American Statistical Association, 63 (324), 1379–1389. doi:10.2307/2285891.

Senay, G. B., N. M. Velpuri, S. Bohms, Y. Demissie, and M. Gebremichael (2014) Understanding the hydrologic sources and sinks in the Nile Basin using multisource

climate and remote sensing data sets, Water Resour. Res., 50, 8625–8650, doi:10.1002/2013WR015231.

Shanahan TM, Overpeck JT, Anchukaitis KJ, Beck JW, Cole JE, Dettman DL, Peck JA, Scholz CA, King JW (2009) Atlantic forcing of persistent drought in West Africa. Science, 324:377–380.

Siam, M.S. and Eltahir, E.A. (2017) Climate change enhances interannual variability of the Nile river flow. Nature Climate Change, 7(5), pp.350-354. doi:10.1038/nclimate3273.

Sillmann J, Kharin VV, Zhang X, Zwiers FW, Bronaugh D (2013a) Climate extremes indices in the CMIP5 multimodel ensemble: Part 1. Model evaluation in the present climate. J. Geophys. Res. Atmos., 118, 1716-1733. doi: 10.1002/jgrd.50203.

Sillmann, J., Kharin, V. V., Zwiers, F. W., Zhang, X., & Bronaugh, D. (2013b) Climate extremes indices in the CMIP5 multimodel ensemble: Part 2. Future climate projections, J. Geophys. Res. Atmos., 118, 2473–2493, doi:10.1002/jgrd.50188.

Skamarock WC, Klemp JB, Dudhia J, Gill DO, Barker DM, Duda M, Huang XY, Wang W, Powers JG (2008) A description of the advanced research WRF version 3. NCAR technical note, NCAR/TN-475+STR, 123 pp [http://www2.mmm.ucar.edu/wrf/users/docs/arw_v3.pdf].

Smirnova, T. G., Brown J. M., and Benjamin S.G. (1997) Performance of different soil model configurations in simulating ground surface temperature and surface fluxes. Mon. Weather Rev., 125, 1870–1884, doi: 10.1175/1520-0493(1997)125<1870:PODSMC>2.0.CO;2.

Smirnova, T. G., Brown J. M., Benjamin S.G., and Kim D. (2000) Parameterization of cold season processes in the MAPS land surface scheme. J. Geophys. Res., 105, 4077–4086, doi:10.1029/1999JD901047.

Soliman E. S. A, Sayed M. A.-A, and Jeuland M (2009) Impact assessment of future climate change for the Blue Nile basin using a RCM nested in a GCM. Nile Water Science & Engineering Special Issue on Water and Climate 2, 31–38.

Sun LQ, Semazzi F, Giorgi F, Ogallo L (1999a) Application of the NCAR regional climate model to eastern Africa, 1. Simulation of the short rains of 1988. J. Geophys Res 104:6529–6548.

Swain, A. (2011) Challenges for Water Sharing in the Nile Basin: Changing Geo-Politics and Changing Climate. Hydrol. Sci. J. 56(4), 687–702. doi:10.1080/02626667.2011.577037.

Tariku, T.B, and Gan, T.Y (2017) Sensitivity of the Weather Research and Forecasting model to Parameterization Schemes for Regional Climate of Nile River Basin, *Climate Dynamics*, pp.1-17, doi: 10.1007/s00382-017-3870-z.

Tariku, T.B, and Gan, T.Y (2018) Regional Climate Change Impact on Extreme Precipitation and Temperature of the Nile River Basin, Climate Dynamics, pp. 1-20, doi: 10.1007/s00382-018-4092-8.

Tariku, T.B, Gan, T.Y, Li J., and Qin X., (2018) Impact of Climate Change on Hydrology and Hydrological Extremes of the upper Blue Nile River basin, Journal of Climate Change, under review.

Taye, M. T., Ntegeka, V., Ogiramoi, N. P., & Willems, P. (2011) Assessment of climate change impact on hydrological extremes in two source regions of the Nile River Basin. Hydrology and Earth System Sciences, 15(1), 209–222. doi:10.5194/hess-15-209-2011.

Teutschbein, C., and Seibert J. (2012) Bias correction of regional climate model simulations for hydrological climate-change impact studies: review and evaluation of different methods. J. Hydrol 456–457:12–29.

Tilmant, A., Goor, Q., and Pinte, D. (2008) Assessing marginal water values in multipurpose multireservoir systems via stochastic programming. Water Resour. Res., 44, W12431.

Tilmant, A., and Kelman, R. (2007) A stochastic approach for analyzing trade-offs and risks associated with large-scale water resources systems. Water Resour. Res., 43, W06425.

Tilmant, A., Goor, Q., and Pinte, D. (2009) Agricultural-to-hydropower water transfers: sharing water and benefits in hydropower-irrigation systems, Hydrol. Earth Syst. Sci., 13, 1091–1101, doi:10.5194/hess-13-1091-2009.

Touchan, R., K. J. Anchukaitis, D. M. Meko, S. Attalah, C. Baisan, and A. Aloui, (2008) Long term context for recent drought in northwestern Africa, Geophys. Res. Lett., 35, L13705, doi:10.1029/2008GL034264.

Troy, T. J., and Wood E. F. (2009) Comparison and validation of gridded radiation products across northern Eurasia. Environ. Res. Lett., 4, 045008, doi:10.1088/1748-9326/4/4/045008.

Vörösmarty C. J, Douglas E. M, Green P. A, and Revenga C (2005) Geospatial indicators of emerging water stress: an application to Africa. Ambio, 34, 230-236.

Wallace, S., and Fleten, S. (2003) Stochastic programming models in energy. Chapter 10, Handbooks in operations research and management science, Vol. 10, A. Ruszczynski and A. Shapiro, eds. Elsevier Science, Amsterdam, The Netherlands.

Whittington, D., Wu, X., and Sadoff, C. (2005) Water resources management in the Nile Basin: The economic value of cooperation. Water Policy, 7(3), 227–252.

Willems, P., (2009) A time series tool to support the multi-criteria performance evaluation of rainfall-runoff models. Environmental Modelling & Software, 24, 311–321.

WWAP (World Water Assessment Programme) (2012) The United Nations World Water Development Report 4: Managing Water under Uncertainty and Risk. Paris, UNESCO.

Zaroug M. A. H., Giorgi F, Coppola E, Abdo G. M, and Eltahir E. A. B (2014) Simulating the connections of ENSO and the rainfall regime of East Africa and the upper Blue Nile region using a climate model of the Tropics. Hydrol. Earth Syst. Sci., 18, 4311-4323, doi:10.5194/hess-18-4311-2014.

Zhang Q, Körnich H, Holmgren K. (2013) How well do reanalyses represent the southern African precipitation? Clim. Dyn. 40: 951. doi: 10.1007/s00382-012-1423-z.